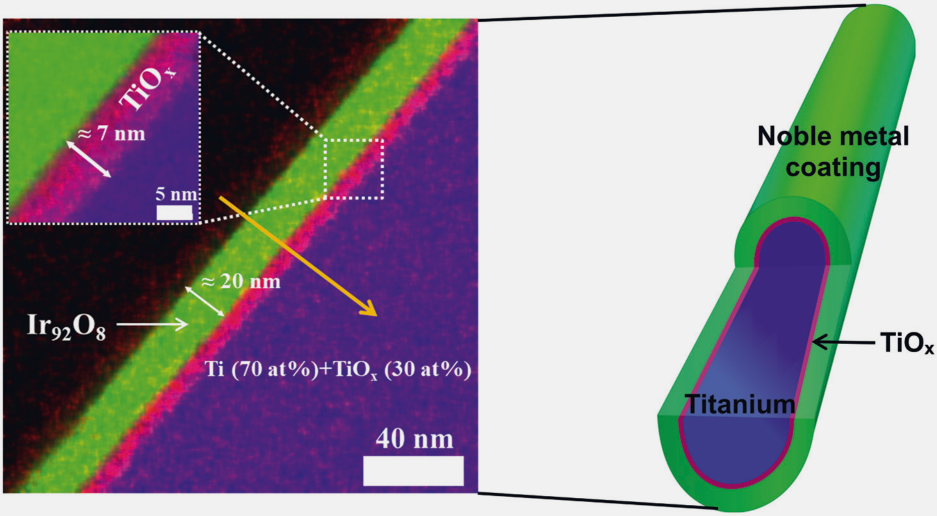

Noble Metal Coated Porous Transport Layers for Polymer Electrolyte Membrane Water Electrolysis

Chang Liu

Energie & Umwelt / Energy & Environment
Band / Volume 562
ISBN 978-3-95806-603-8

Mitglied der Helmholtz-Gemeinschaft

JÜLICH
Forschungszentrum

Schriften des Forschungszentrums Jülich
Reihe Energie & Umwelt / Energy & Environment Band / Volume 562

Forschungszentrum Jülich GmbH
Institut für Energie- und Klimaforschung
Elektrochemische Verfahrenstechnik (IEK-14)

Noble Metal Coated Porous Transport Layers for Polymer Electrolyte Membrane Water Electrolysis

Chang Liu

Schriften des Forschungszentrums Jülich
Reihe Energie & Umwelt / Energy & Environment Band / Volume 562

ISSN 1866-1793 ISBN 978-3-95806-603-8

Bibliografische Information der Deutschen Nationalbibliothek.
Die Deutsche Nationalbibliothek verzeichnet diese Publikation in der Deutschen Nationalbibliografie; detaillierte Bibliografische Daten sind im Internet über http://dnb.d-nb.de abrufbar.

Herausgeber und Vertrieb:	Forschungszentrum Jülich GmbH Zentralbibliothek, Verlag 52425 Jülich Tel.: +49 2461 61-5368 Fax: +49 2461 61-6103 zb-publikation@fz-juelich.de www.fz-juelich.de/zb
Umschlaggestaltung:	Grafische Medien, Forschungszentrum Jülich GmbH
Druck:	Grafische Medien, Forschungszentrum Jülich GmbH

Schriften des Forschungszentrums Jülich
Reihe Energie & Umwelt / Energy & Environment, Band / Volume 562

D 82 (Diss. RWTH Aachen University, 2021)

ISSN 1866-1793
ISBN 978-3-95806-603-8

Abstract

Polymer electrolyte membrane (PEM) water electrolyzers are electrochemical energy conversion devices that split water into its constituent elements of hydrogen and oxygen. Titanium-based porous transport layers (PTL) are widely used due to their good bulk conductivity, high corrosion resistivity, and excellent mechanical strength. However, titanium-based PTLs situated at the anode side of PEM electrolyzers are subjected to harsh oxidizing conditions such as high anode overpotential, low pH and oxygen evolution. Under these conditions, titanium (Ti^0) changes its oxidation state over time, which induces the formation of a thin but continuously growing layer of passivated titanium (TiO_x). Consequently, the contact resistance of titanium PTLs is adversely affected, critically decreasing cell performance and durability.

In this thesis, a very simple and scalable method is used to protect the titanium-based PTL from passivation by sputtering very thin layers of noble metal coatings such as Ir, Pt, or Au onto the PTLs. The 20 to 50 nm thick noble metal coatings on the titanium fibers significantly decreased interfacial contact resistance between the PTL and catalyst layer, and improved cell performance. The single cells assembled with Ir- or Pt-coated PTLs delivered higher cell performance than cells with Au-coated PTLs, and nearly identical cell performance as carbon paper, which is prone to carbon corrosion under these operating conditions.

The high cost of using noble metal coatings can be decreased by reducing the loading of the noble metals. The loading of Ir as a protective layer on the PTL has an impact on the cell performance. The amount of iridium on one side of the PTL was reduced to $0.025\ mg_{Ir}\cdot cm^{-2}$ and showed identical cell performance as Ir-coated PTLs with higher iridium loading, which effectively reduced the cost of the Ir. The total amount of iridium is 40 times less compared to what is usually used in an anode catalyst layer, and 20 times less than Au or Pt typically used as protective layers in contemporary and commercial electrolyzers.

The critical passivation of the bare titanium-based PTL is also one significant factor that restricts the durability of a PEM water electrolyzer. In order to investigate the durability of noble metal coatings (Ir, Pt, Au) on the PTLs, a series of long-term measurements were performed under 2 V and 80 °C on the single cells assembled with Ir-coated, Pt-coated and Au-coated PTLs, respectively. Compared to the cell without the coatings, the cell assembled with iridium and platinum coatings showed degradation rates close to zero, while the identical cell performance was observed after 4000 hours with a cell voltage of 2 V. These results demonstrate that iridium and platinum coatings on titanium-based PTLs are highly effective at protecting the PTL against passivation, ultimately improving cell performance and durability.

Kurzfassung

Polymerelektrolytmembran (PEM)-Wasserelektrolyseure sind elektrochemische Energiewandler, welche Wasser zu Wasserstoff und Sauerstoff aufzuspalten. Eine wesentliche Komponente dieser Elektrolysezellen sind Titan-basierte poröse Transportschichten (PTL). Diese weisen gute Bulkleitfähigkeit, hohe Korrosionsbeständigkeit und ausgezeichnete mechanische Festigkeit auf. Auf der Anodenseite von PEM-Elektrolyseuren sind sie korrosiven Bedingungen wie zum Beispiel hohen Überspannung, niedrigem pH-Wert und Sauerstoffentwicklung durch die Reaktion in der Elektrode ausgesetzt. Unter diesen Bedingungen ändert Titan (Ti^0) seinen Oxidationszustand im Laufe der Zeit. Eine dünne und kontinuierlich wachsende Schicht aus passiviertem Titan (TiO_x) wird gebildet. Infolgedessen wird der Kontaktwiderstand der Titan-PTLs negativ beeinflusst, was die Leistung und Haltbarkeit der Zelle verringert.

In dieser Arbeit wird eine sehr einfache und skalierbare Methode verwendet, um die titanbasierte PTL vor Passivierung zu schützen, indem sehr dünne Schichten von Edelmetall wie Ir, Pt oder Au auf die PTLs gesputtert werden. Die 20 bis 50 nm dicken Edelmetallbeschichtungen auf den Titanfasern verringern den Kontaktwiderstand zwischen PTL und Katalysatorschicht deutlich und verbessern die Zellleistung. Die Einzelzellen, die mit Ir- oder Pt-beschichteten PTLs betrieben wurden, lieferten eine höhere Zellleistung als Zellen mit Au-beschichteten PTLs und lieferten nahezu die gleiche Leistung wie Zellen mit kohlenstoffbasierten PTLs, die unter diesen Betriebsbedingungen anfällig für Kohlenstoffkorrosion sind.

Die hohen Kosten bei Verwendung von Edelmetallen als Schutzschichten können durch die Verringerung der Edelmetallbeladung reduziert werden. Die Iridiumbeladung der PTL wurde auf 0,025 $mg_{Ir}\cdot cm^{-2}$ reduziert und es zeigte sich eine identische Zellleistung wie bei Ir-beschichtete PTLs mit höherer Beladung. Die Gesamtbeladung von Iridium ist 40-mal geringer im Vergleich zu dem, was üblicherweise in einer Anodenkatalysatorschicht verwendet wird, und 20-mal geringer als von Au oder Pt, das typischerweise als Schutzschicht in derzeitigen und kommerziellen Elektrolyseuren verwendet wird.

Die Passivierung der Titan-basierten PTL ist ebenfalls ein wichtiger Faktor, der die Lebensdauer eines PEM-Wasserelektrolyseurs einschränkt. Langzeitmessungen bei 2 V und 80 °C an den mit Ir-, Pt- und Au-beschichteten PTLs montierten Einzelzellen wurden durchgeführt, um die Haltbarkeit der Edelmetallbeschichtungen zu untersuchen. Verglichen mit Zellen ohne Beschichtungen zeigten die mit Iridium- oder Platinbeschichtungen montierten Zellen Degradationsraten nahe Null während 4000 Stunden Betriebszeit. Diese Ergebnisse zeigen, dass Iridium- und Platinbeschichtungen auf titanbasierten PTLs hocheffektiv sind, um das PTL vor Passivierung zu schützen und letztendlich die Leistung und Lebensdauer der Zelle zu erhöhen.

Contents

1. Introduction and Goals of the work

1.1 Introduction

Hydrogen is one of the most promising energy carriers as a high specific energy, environmentally friendly fuel. However, hydrogen is essentially produced from fossil compounds, which results in high levels of pollution and greenhouse gas emissions [1, 2]. Our society is experiencing a rapid transition towards the use of sustainable energy conversion devices such as water electrolyzers for power-to-gas applications [3, 4]. In the near future, these electrochemical systems will be deployed worldwide and secure resilience in power generation for regions with access to renewable but stochastic energy sources [5].

Water electrolysis is the process of using electricity to split water into hydrogen and oxygen, which can produce sustainable hydrogen when coupled with renewable energy sources including wind and solar [6, 7]. Compared to traditional alkaline water electrolysis, polymer electrolyte membrane (PEM) water electrolysis offers several advantages including high hydrogen purity, fast dynamic response time, and a more compact design [8]. PEM water electrolyzer mainly consists of a catalyst coated membrane (CCM) sandwiched between two porous transport layers (PTLs) and two bipolar plates. The PTL situated at the anode side is a key component and works to transport water to the anode electrode, conduct electrons, and remove the produced oxygen. High corrosion resistance material titanium is typically used to construct cell and stack components such as PTLs and bipolar plates, due to the harsh acidic conditions such as high over potential, oxygen/water mixture at the anode side [9-13]. As a consequence, the high cost of raw titanium and complex/expensive machine labor accounts for 50% of overall stack costs [14]. However, the critical passivation of titanium-based components is one significant factor that restricts the development of PEM water electrolyzer because titanium (Ti^0) changes its oxidation state over time, which leads to drastic degradation of the PEM water electrolyzer cell [15, 16].

To circumvent this issue, the titanium-based PTLs in PEM water electrolyzers are typically coated with platinum [10, 11] or gold [12] to protect PTLs from passivation or even corrosion in long-term operation. However, it should be noted that loadings of these coatings are estimated to be at least 1 $mg_{metal} \cdot cm^{-2}$, which obviously increases the cost [17].

1.2 Goals of the work

The critical passivation of titanium-based PTLs that occurs under real cell conditions is a significant factor that restricts its application without a protective layer. In this study, iridium, platinum, and gold as protective layers on the surface of titanium-based PTLs were comprehensively investigated. The loadings of iridium coatings were minimized and investigated to further reduce the cost of the whole PEM water electrolyzer. In addition, the cell performance and durability of Ir-coated PTLs were compared with Pt-coated and Au-coated PTLs. In summary, the goals of this work are: 1) to compare the electrochemical cell performance and durability of Ir-coated PTL with uncoated, Pt-coated, and Au-coated titanium-based PTLs; 2) to minimize the Ir loading on the PTL; 3) to understand the PTL degradation mechanism and explore how the interface of a well-protected titanium fiber behaves against passivation after long-term operation under real electrolysis conditions.

1.3 Outline

Chapter 1 presents the introduction and goals of this work.

Chapter 2 presents the fundamental theory of water electrolysis, especially PEM water electrolysis. This chapter provides the principle and design of different components in a PEM water electrolyzer.

Chapter 3 introduces detailed information on experimental methods and setup.

Chapter 4 compares iridium, platinum, and gold as protective layers (coating) on titanium-based PTLs in short-term tests (polarization curve and impedance).

Chapter 5 investigates the effects of different loadings of iridium as a protective layer on titanium-based PTL.

Chapter 6 investigates the durability of Ir-coated and uncoated PTLs.

Chapter 7 compares the durability of Ir-coated PTL with Au-coated and Pt-coated PTLs.

Chapter 8 shows a partially coated PTL and explains the migration of the catalyst layer to the PTL.

Chapter 9 gives a comprehensive discussion of all the results.

Chapter 10 is the conclusion.

2. Theory and literature review

2.1 Category of water electrolysis cell

Water electrolyzers are electrochemical energy conversion devices that can split water into its constituent elements of hydrogen and oxygen, which was performed for the first time by Nicholson and Carlisle in 1800 [17]. Over the past decades, substantial research on this technology has been performed. Based on the type of electrolyte being used, water electrolysis can be divided into three categories: alkaline water electrolysis, solid oxide electrolysis (SOEC), and polymer electrolyte membrane (PEM) water electrolysis.

2.1.1 Alkaline water electrolysis

Alkaline water electrolysis is a well-matured technology for hydrogen production up to the megawatt range, which constitutes the most extended electrolytic technology at a commercial level worldwide [3, 18]. The traditional alkaline water electrolyzer consists of two electrodes separated by a diaphragm, which is immersed in an aqueous alkaline electrolyte at a level of 30-40 wt% KOH [6]. It is well known for its long lifetime and relatively low capital cost. For example, non-precious metal catalysts (e.g. Ni-based catalysts) are used for both anode and cathode, which significantly reduce the cost of the whole stack. However, drawbacks including corrosive liquid electrolyte, low current density, and low operating pressure restrain the further development of alkaline water electrolysis [3, 19].

Nowadays, a developing technology named anion exchange membrane (AEM) electrolysis emerges, which replaces the conventional diaphragm used in traditional alkaline electrolysis. It combines the advantages of traditional alkaline electrolysis and PEM electrolysis, including the use of platinum group metal (PGM) free catalysts without much performance loss, the use of distilled water or a low concentration of alkaline solution instead of concentrated and corrosive alkaline electrolytes, and use of less expensive membranes instead of perfluorinated membranes in PEM water electrolysis [20-22]. However, AEM electrolysis is still much less mature than liquid alkaline or PEM technology (e.g. durability, trade-offs between conductivity and water management), and it is presently suitable only for small-scale hydrogen production now [15]. More investigation should be done concerning these issues to make it more commercial and reliable.

2.1.2 Solid oxide electrolysis (SOEC)

Solid oxide electrolysis (SOEC) is a promising technology via high-temperature steam electrolysis and has attracted a great deal of interest due to its high energy efficiency [23]. The anode and cathode overpotential that cause the power loss is nearly negligible because SOEC is usually operated in the 800-1000 °C temperature range. Dönitz and Erdle demonstrated single cells operation during long-term periods with current densities of 0.3 $A \cdot cm^{-2}$ achieving 100% Faraday efficiency at a voltage as low as 1.07 V in the 1980s [24]. Additionally, SOEC can be used for CO_2 electrolysis due to the chemical flexibility of the devices and the high temperature of operation [6]. Up to date, though the initial performance of SOECs is promising, the long-term stability is of great concern. The critical operation adds some specific challenges to the materials, especially the corrosion issues due to the high operating temperature. The degradation of SOEC is a significant barrier to commercial viability [25, 26]. In contrast to alkaline and PEM water electrolysis, only limited long-term experience mainly based on single cells or short stacks (< 10 cells) is available for SOEC. Most of the durability tests reported in the literature are below 5000 h. The longest experiment reported so far in literature was more than 16000 h [18]. If the issues related to the durability of its components can be solved, SOEC could have a huge potential for the mass production of hydrogen in the future [6].

2.1.3 Polymer electrolyte membrane (PEM) water electrolysis

In order to overcome the drawbacks of alkaline electrolysis, the first PEM-based electrolyzer systems were developed in 1955 by General Electric [15]. The lifetime of PEM electrolysis reported so far in the literature is in the range of 60000 – 100000 h [18, 27]. PEM water electrolyzers use a proton exchange membrane (PEM) as the electrolyte, which permits proton transport from anode to cathode. Compared to the traditional alkaline water electrolyzer, PEM water electrolyzers have several advantages, including a faster dynamic response time, a much higher current density, higher hydrogen purity, and a more compact design [8]. PEM water electrolyzers can be operated under high pressures due to the compact system design and resistant structural properties. This brings the advantage of delivering hydrogen at a higher pressure and requires less energy to further compress and store hydrogen. However, the harsh acidic conditions, high cell overpotentials, and oxygen gas evolution at the anode not only demand the use of scarce and expensive materials such as noble catalysts (e.g. Pt and Ir), but also titanium-based porous transport layers (PTLs) and bipolar plates [6]. In the future, more effort is needed to reduce the high cost of these materials.

2.2 Basic theory of PEM electrolysis

2.2.1 Principle and design of PEMWE

PEM water electrolyzer is an electrochemical device that splits water into hydrogen and oxygen. The general schematic diagram of a PEM water electrolyzer is shown in Figure 2.1. Liquid water is introduced to the anode and split into protons, electrons, and oxygen (Equation 2.1). The produced protons from the oxygen evolution reaction (OER) transport through the proton exchange membrane to the cathode, and are reduced to molecule hydrogen in the hydrogen evolution reaction (HER) (Equation 2.2). The overall reaction is shown in equation 2.3.

Anode: $H_2O \rightarrow 2H^+ + \frac{1}{2} O_2 + 2e^-$ (Equation 2.1)

Cathode: $2H^+ + 2e^- \rightarrow H_2$ (Equation 2.2)

Overall: $H_2O \rightarrow H_2 + \frac{1}{2} O_2$ (Equation 2.3)

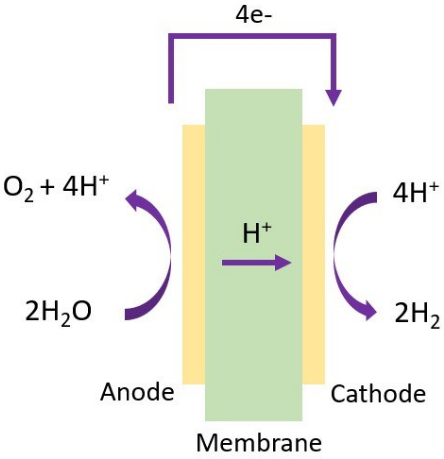

Figure 2.1 *Schematic diagram of the working principle of PEM water electrolyzer.*

2.2.2 Thermodynamics and kinetics of PEM water electrolyzer

2.2.2.1 Thermodynamics

In standard conditions (298 K, 1 bar), the water splitting reaction is as follows: H_2O (l) → H_2 (g) + ½ O_2 (g). Assuming that the reaction is a reversible path under isothermal conditions, the Gibbs free energy can be calculated as the following reaction:

$$\Delta G(T) = \Delta H(T) - T\Delta S(T) \qquad \text{(Equation 2.4)}$$

T in K is the absolute temperature. ΔG(T) in J/mol is the Gibbs free energy change, ΔG(T) represents the amount of electricity that must be supplied to the electrolysis cell in addition to the TΔS(T) amount of heat to split water (minimum electrical work needed for splitting water at the corresponding theoretical). ΔH(T) in J/mol is the enthalpy change associated with the reaction, which is the total amount of energy that must be supplied to the electrolysis cell to split water into H_2 and O_2. TΔS(T) in J/mol/K is the entropy change. In standard conditions (25 °C, 1bar), ΔG^0 = 237.23 kJ/mol, ΔH^0 = 285.83 kJ/mol, ΔS^0 = 0.163 kJ/mol/K. In standard conditions, the electrical work required for the electrolysis of 1 mol of water in standard conditions is:

$$\Delta G_T^0 = nFE^0 \qquad \text{(Equation 2.5)}$$

n is the number of electrons transferred in the reaction. F is Faraday's constant. E^0 is the standard thermodynamic voltage, for liquid water at 25 °C, E^0 = 1.23V. If there is no exchange of heat to the surroundings, the voltage required for water electrolysis to occur at constant temperature is called thermoneutral potential E^{th} = 1.48 V. In practical operation, the potential is higher for hydrogen production. During the electrolysis process, the excess energy in the form of overpotential is converted to heat and is necessary to manage well.

According to the Nernst Equation, the thermodynamic cell voltage required to split water into hydrogen and oxygen can be calculated in the following form:

$$E_{Nernst} = E^0 + \frac{RT}{2F}\ln\frac{P_{H_2}\cdot P_{O_2}^{1/2}}{a_{H_2O}} \qquad \text{(Equation 2.6)}$$

E_{Nernst} is a function of operating temperature, normalized partial pressures of reactants, and water activity in the electrolyte. R in J/mol/K is the absolute gas constant; T is the absolute temperature; P is the normalized partial pressure of the reaction products and a_{H_2O} is the activity of water in the electrolyte.

2.2.2.2 Kinetics

The cell voltage E_{cell} applied to the electrolysis cell must be higher than thermodynamic voltage [17]. The contribution to the total E_{cell} is shown in Equation 2.7:

$$E_{cell} = E_{Nernst} + \eta_{anode} + \eta_{cathode} + I \cdot R \qquad \text{(Equation 2.7)}$$

E_{Nernst} is the Nernst voltage, which is the theoretical voltage required by the electrolyzer. η_{anode} is the charge transfer overvoltage at anode/electrolyte interfaces and the resistivity of the electrolyte, which is associated with the oxygen evolution reaction (OER). $\eta_{cathode}$ is the charge transfer overvoltage, which is associated with hydrogen evolution reaction (HER). Both η_{anode} and $\eta_{cathode}$ are determined by operating current density according to the Butler-Volmer equation of charge transfer [17]. I is the current, R is the resistance. The transport of protons through the electrolyte and contact resistance between different components of cells contribute to the ohmic resistance to the cell. When the current applied to the cell is very high, the transport of reactants and products of the reaction at electrodes occurs very fast, and causes the mass limitation of the cell (not shown in Equation 2.7).

2.2.2.3 Polarization curve

Figure 2.3 shows an ideal curve of how cell voltage is depending on the current of a PEM water electrolysis cell, which is typically called polarization curve. The polarization curve consists of three parts, which are named by the main contributor. The low current density range is called activation overvoltage or charge transfer overvoltage, the increase of cell voltage is dominated by charge transfer kinetics of electrode. At the intermediate current density range, the ohmic resistance is predominant and the shape is almost linear. At the third range which is at the high current density, the increase of cell voltage is caused by the mass transport limitation of reactants and products from electrodes.

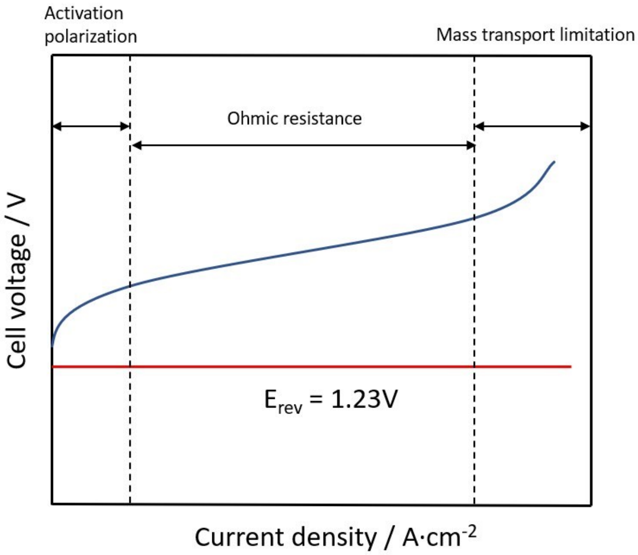

Figure 2.2 *Typical polarization curve of water electrolysis cell (blue) and ideal reversible voltage (red).*

The main components of a PEM water electrolyzer cell are presented in Figure 2.3. A PEM water electrolyzer consists of a catalyst coated membrane (CCM) sandwiched between two porous transport layers (PTLs) and two bipolar plates. Typically, Ir-based catalysts (e.g. IrO_2, $IrRuO_x$) are used at the anode, and Pt-based catalysts (e.g. Pt/C) are used at the cathode. At the anode side, water is split into molecular oxygen, protons, and electrons, which leads to a harsh operating environment for the components, such as the high cell overpotential, low pH, and oxygen gas evolution. This condition demands the use of high corrosion resistance PTLs and bipolar plates at the anode side. Therefore, these components are typically made of titanium due to the excellent chemical stability, good conductivity, and high corrosion resistivity [12, 15].

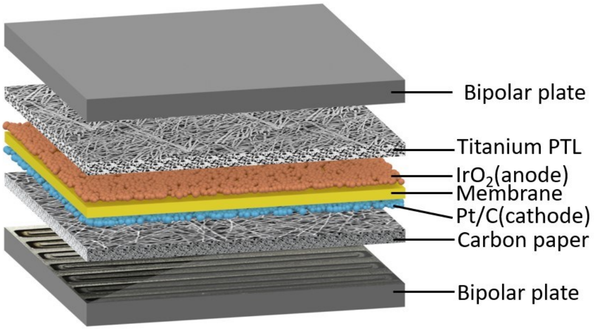

Figure 2.3 *Schematic illustration of the key components inside a PEM electrolyzer [28].*

2.3 Materials and Components

2.3.1 Catalyst coated membrane (CCM)

The catalyst coated membrane (CCM) is one of the key components of PEM water electrolyzer and the location of the actual chemical reactions. It consists of a solid polymer membrane (SPE), which is coated with electrode materials on both sides. The perfluorosulfonic acid (PFSA) membranes such as Nafion®, Flemion® or Aquivion® are used as a solid electrolyte [29]. Generally, the electrocatalysts with high activity and stability can only be selected from platinum group metals (PGM). At the cathode side, platinum black or carbon-supported platinum-based electrocatalysts are used for the HER. Studies have shown that a conventional Pt/C catalyst loading of 0.05 $mg{\cdot}cm^2$ is adequate to sustain current densities of 2 $A{\cdot}cm^2$ [15]. Further PGM reduction strategies include alloying Pt or structuring the catalyst using core-shell-type approaches to further reduce the PGM content [30, 31]. At the anode, due to the sluggish four-electron reaction, OER is the rate-limiting step in PEM water electrolysis. Iridium oxide, iridium black, or iridium-ruthenium oxide are well-performing electrocatalysts for OER. Ruthenium-based catalysts showed higher catalytic activity in the reaction of oxygen evolution, however, the rate of dissolution and corrosion is very high in PEM water electrolyzer [6, 32]. Currently, the most widely used electrocatalysts at anode are Ir black or Ir oxide with catalyst loadings ranging from 1 to 3 $mg{\cdot}cm^{-2}$. In order to increase efficiency at a fixed voltage and durability, and reduce the iridium loading, conductive support materials are often used to disperse precious metals or metal oxide catalysts. Carbon supports cannot be used at anode due to the high anodic potential of an operating PEM water electrolyzer (>1.5 V vs. reversible hydrogen electrode (RHE)) [33]. Less expensive oxides or ceramics materials such as Ta_2O_5 [34], Nb_2O_5 [35], SnO_2 [36], TaC [37], TiO_2 [38] antimony doped tin oxide (ATO) [39] have been reported to be used as catalyst supports at the anode. However, most of these supported catalysts are either not conductive enough or not stable enough to maintain conductivity over time. This weakness required the high loading of noble metal (1 to 2 $mg{\cdot}cm^{-2}$) to compensate the low electronic conductivity[15, 19]. In the future, it is of great importance to improve the conductivity of the supported catalysts or develop other well-performed catalysts with better structures.

2.3.2 Bipolar plate

Bipolar plates are used to transport reactants/products and conduct electrons and provide good mechanical support in PEM water electrolyzers. As a key example of the potential for cost reduction, the bipolar plate, or separator plate and associated flow fields, was originally the largest cost component of a PEM cell stack (64%) [15]. Currently, titanium, stainless steel, titanium, and graphite are the most widely used materials for bipolar plates in PEM fuel cells and electrolyzers. Graphite bipolar plates have been used frequently in the PEM fuel cell field due to their high conductivity. However, the low mechanical strength, high corrosion rates, difficulty of manufacture, and high cost restrict the applications in PEM water electrolyzer. Titanium has excellent mechanical strength, electrical conductivity, and corrosion resistance, but it is very expensive, and titanium corrodes and develops a passive oxide layer that significantly increases the contact resistance and reduces the surface conductivity especially at the anode side [40-42]. Stainless steel also showed good electrical conductivity and mechanical strength, although it also suffers from corrosion at the anode side [43-45].

Therefore, precious metals including Au [40-42] and Pt [13, 43], or some other non-noble metal such as Nb [44] have been used as protective and anticorrosion coatings on the surface of titanium or stainless steel bipolar plates in PEM water electrolyzer. These coatings greatly reduced the interfacial contact resistance between bipolar plates and PTL and improved the durability of the PEM water electrolyzer. In addition, to improve the efficiency and reduce the cost of the stacks, either simplifying the manufacturing process or using cheap materials like plastic materials could be effective [46, 47]. For example, additive manufacturing technology is an alternative to traditional manufacturing and is a revolutionary approach to fabricate bipolar plates with close to zero materials waste [42, 48]. Compared to the state-of-the-art components, the reported performance is promising, while it remains open in regards to whether the stability of these components is comparable to the pure metal components.

2.3.3 Porous transport layer (PTL)

The anode porous transport layer (PTL) is located between the catalyst layer and bipolar plate. It is a key component of a PEM water electrolyzer, and its function is to transport water to the anode electrode, conduct electrons, and remove the produced oxygen. In order to meet the primary requirement of a PEM water electrolyzer, PTL should be corrosion-stable, have good electrical conductivity, and be mechanically stable for operation at differential pressures [49].

High corrosion resistance material titanium is the most typically used to construct PTL at the anode side due to its excellent chemical stability, good conductivity, and high corrosion resistivity. Apart from titanium-based PTL, other different materials like carbon materials (carbon cloth or paper) and stainless steel were also investigated on PTL to minimize the whole cost of the stack [50, 51]. Carbon materials can be used at the cathode side, however, at the anode side, they can only be used for short tests or electrocatalysts characterization purposes, which do not represent the performance of a real PEM water electrolyzer at long-term operation [6]. Due to the high corrosive condition at the anode side, the high overvoltage at the anode side (~2 V) and high concentration of oxygen, water, and low pH (<2) will easily promote the oxidation of carbon materials to CO_2 [6]. Mo et al. investigated the corrosion mechanism of stainless steel mesh as an anodic PTL for PEM water electrolyzer. However, they observed a high corrosion rate with a high transport of iron and nickel from anode to cathode, which polluted the membrane and catalyst layers [51]. Therefore, titanium-based PTL is currently the most widely used and attracts more interest in PEM water electrolyzers.

Different types of titanium-based PTLs such as felt [52-55], mesh [56, 57], sheets [52, 58], and sintered titanium powders [59-61] are used at the anode side of PEM water electrolyzers. Figure 2.4 shows different varieties of PTLs. Over the last decades, several groups have investigated the effects of different parameters like thickness, particle size, pore diameter, or porosity of kinds of conventional PTLs. Grigoriev et al. optimized the microstructure of sintered titanium powder PTL. They pointed out that the optimum spherical particle sizes of titanium powders of PTLs are 50 - 75 µm and the optimum pore size value is 12 - 13 µm [59]. Ito et al. investigated an experimental study on the porosity and pore diameter on titanium felt PTLs. Their results showed that the electrolysis performance improved with the decrease of pore diameter when the mean pore diameter of the PTL was larger than 10 μm. They also pointed out that the porosity had no significant effect on the cell performance when the porosity is more than 0.5 [62]. Another study from this group showed that when the mean pore diameter of the anode PTL is less than 50 μm, the produced gas bubbles hinder the water supply to the electrode, the effect of the decrease in the water supply on the membrane resistance is limited [54]. Kang et al. investigated novel titanium-based PTLs with straight-through pores and well-defined pore morphologies. The impacts of the PTL porosity and pore size were precisely investigated and optimized. They found that porosity has a more significant impact on performance than pore size. In addition, their study showed that operating temperatures also have a large impact on the PEM water electrolyzer cell performance [58]. Lettenmeier et al. developed a novel type of PTL with a gradient in pore size distribution by vacuum plasma spraying method. The novel pore-graded PTLs achieved comparable cell performances to those of the state-of-the-art sintered titanium plates, and superior to those of titanium meshes. They pointed out that this method is a promising solution to reduce the cost of the whole stack [63].

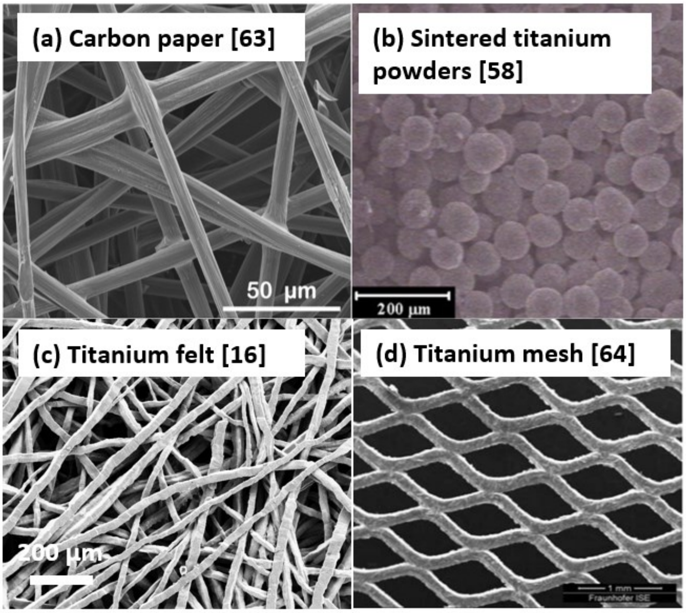

Figure 2.4 *Different types of PTLs in PEM electrolyzer.* ***(a)*** *Carbon paper [64];* ***(b)*** *Sintered titanium powders [59];* ***(c)****Titanium felt [16];* ***(d)*** *Titanium mesh [65].*

The effect of the thickness of PTLs was also investigated by several groups. Mo et al. investigated the effect of different parameters of titanium felt PTLs in a PEM water electrolyzer. They found that the thickness of PTLs has a significant impact on the cell performance, and the contribution of the thickness on the performance might be mainly due to the ohmic resistance [66]. Another group also found out that the cell performance of a PEM water electrolyzer decreases with the increasing thickness of the PTLs. A thinner carbon paper used as anode PTL will improve the cell performance by improving the gas diffusion property and electrical resistance [67].

Different state-of-the-art characterization technologies have been applied to study mechanical and physical-chemical properties of anode PTL. Previously, our group investigated the mechanical strength and stability of sintered titanium PTLs in the PEM water electrolyzer. We found that for a sintered PTL with a thickness of 500 μm and porosity above 25% to be able to withstand 50 bar different pressure in the cell, the maximum flow field width should be limited to 3 mm [61]. To understand the mass transport mechanism during operation in a PEM water electrolyzer cell, neutron spectroscopy was applied to visualize the water-gas distribution in the cell during operation. The results showed that more gas amasses in the PTL under the land than under the channel area, and the mass transport limitation in a polarization curve is caused by the insufficient moistening of the membrane [49]. One group used a high-speed and micro-scale visualization system (HMVS) to visualize the location of the electrochemical reactions. They found that the oxygen and hydrogen bubbles mainly occur on catalyst layers at the rim of pores of PTLs [68, 69]. To optimize and gain a better understanding of the governing parameters in electrolysis cells, Schuler et al. investigated the bulk properties (porosity, pore/solid size distributions, fiber orientation), surface parameters (roughness, membrane deformation, PTL surface area, and interfacial contact area), and mass transport properties (diffusivity, permeability, conductivities) by using X-ray tomographic microscopy (XTM) analysis [53, 55]. In addition, operando X-ray computed tomography (CT) and X-ray radiography were applied to visualize the morphology and oxygen transport in PEM water electrolyzers. Leonard et al. observed the non-homogeneous distribution of IrO_x electrocatalyst and correlated the polarization curves with the interface morphology by using X-ray CT. They also found that better morphological properties of titanium felt did not lead to better cell performance below 1 $A \cdot cm^{-2}$ compared to sintered titanium powder PTLs, because the X-ray radiography results showed that the oxygen residence time in the channels of both types of PTLs is similar [70].

Among all types of titanium PTLs including felt, mesh, foam, and sintered Ti powders, titanium meshes are the cheapest PTLs [63]. However, the cell performance of the electrolyzer with this type of PTL is not as high as with the felts or sintered structures, and the titanium felt (fiber) PTL showed higher porosity and lower tortuosity [70]. Therefore, in this study, we use a commerciallyavailable, off-the-shelf titanium felt PTL from Bekaert, which can be readily used for the conventional characterization of PEM water electrolysis components, as well as in the construction of stacks with large cell areas.

2.4 Degradation and mitigation strategies for titanium-based PTL

The durability and degradation of cell and stack components of PEM water electrolyzers have been discussed in the literature [19, 71]. From the studies related to this topic, the main phenomena of degradation for PEM water electrolyzer components include [19]:

i) Dissolution, deactivation, agglomeration, and catalyst support passivation of catalysts.

ii) Mechanical degradation, chemical degradation (radical attack, poisoning by foreign ions, e.g. ion impurities in the feed water), and thermal degradation of membranes.

iii) Corrosion and passivation of bipolar plates and porous transport layers (PTLs), especially at the anode side over time.

PTL is a key component in the PEM electrolyzer. Generally, the degradation of PTLs can be divided into two types: mechanical degradation and chemical degradation. Mechanical degradation is mainly due to compression force, dissolution, and erosion by the hydrothermal effect. However, chemical degradation is mainly due to passivation, corrosion, and hydrogen embrittlement.

2.4.1 Mechanical degradation

In the electrolysis cell, all components are pressed against each other with a certain pressure to prevent water/gas leakages and ensure good electrical conductivity. The contact resistance can be reduced by increasing the clamping pressure. However, the clamping pressure cannot be arbitrarily high and above a certain critical value, as too high a pressure could damage the components. It was shown that high contact pressures result in a reduced porosity of gas diffusion layer (GDL) and mass transport limitations in fuel cells [72-74]. Selamet et al. investigated the effect of bolt torque and contact resistance on the performance of the PEM water electrolysis cell with three different gasket materials. They pointed out that increasing the clamping pressure decreases the contact resistance, and an increase in compression pressure leads to high mass transport overpotential [75]. Borgardt et al. investigated the impact of clamping pressure and stress relaxation on the performance of PEM electrolysis cells. They tested three different cell designs with different PTLs (titanium meshes, carbon paper, sintered titanium sheets) and found that clamping pressure has a significant impact on cell performance, and the pressure above 2.5 MPa result in mass transport losses and reduced ohmic conductivity. In addition, their study also showed that mechanical degradation accounts for over 17% of total degradation with the present cell [57]. Another study showed that carbon paper can suffer from breakage or even displacement under compression, which changed the overall structure morphology and affect the permeability. The morphology change also leads to MEA deformation and reduced cell performance [76]. In conclusion, as the clamping pressure affects the performance of electrolyzers, the electrolysis cell should be operated in the optimal pressure range. A smooth surface of PTLs is essential to improve contact resistance and prevent degradation.

2.4.2 Chemical degradation

2.4.2.1 Passivation

Usually, the anode and cathode of a PEM water electrolyzer cell are operating at 1.8 to 2 V(RHE) and -0.2V(RHE) respectively at nominal current densities of 1 to 2 A·cm^{-2}. The feed water pumped through a PEM water electrolyzer cell is neutral, therefore most of the cell components are immerged in neutral water. Nevertheless, PTLs contact catalytic layers in a PEM water electrolyzer cell. The pH value within the cell can reach between 2 and 4, which is especially referring to the catalyst layer, which is in direct contact/combined with the Nafion ionomer [77]. According to the Pourbaix diagram of the titanium–water system (Figure 2.5), titanium is passivated at pH and potential conditions found in PEM water electrolysis cells [78]. The critical passivation of titanium-based components (bipolar plates and PTLs) is one significant factor that restricts the development of PEM water electrolyzer because titanium (Ti^0) changes its oxidation state over time, which leads to drastic degradation of the PEM water electrolyzer cell [15, 16].

According to the literature, the thickness of a naturally formed titanium passive layer can range from 3 to 7 nm under ambient conditions [79]. The whole surface of titanium PTLs in a PEM water electrolyzer is covered by a passivation oxide (hydroxide) layer. The passivation layer is very stable and compact, which protects the metal from further oxidation. The high corrosion resistance and excellent mechanical properties make titanium an indispensable material in the PEM water electrolyzer and many other fields. However, the composition of the passivation layer has an impact on its resistivity [80]. The passive layer is generally said to be TiO_2 (insulator), however, TiO_x with a ratio of O: Ti = 2 is only located primarily near the topmost sample surface. The passive layer TiO_x contains sub- and non-stoichiometric oxides (O: Ti < 2) and acts as an n-type semiconductor in the bulk [81, 82]. The oxygen content and average oxidation state of titanium decrease in the direction towards the metal phase. Therefore, the rising thickness of the passivation layer does not help to improve the corrosion resistance, and the ohmic resistance increases with the thickness of the passivation layer. The layer that functions as passivation protection is only the layer of actual anhydrous TiO_2. In summary, the passive layer has a high electrical resistivity, which greatly increases the contact resistance between PTLs and other components (bipolar plates and catalyst layers) [82]. Therefore, surface treatment such as introducing a protective coating is very necessary to protect titanium components from passivation.

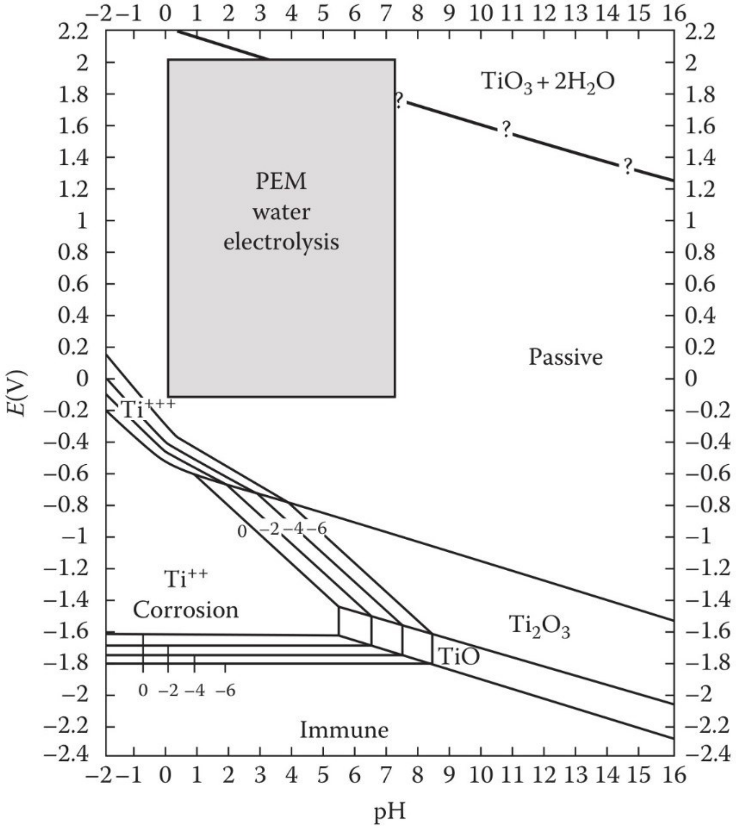

***Figure 2.5** Pourbaix diagram of the titanium–water system [78].*

2.4.2.2 Corrosion

After passivation, TiO_2 passive film can be corroded which gradually affects the performance of the electrolyzer due to the poisoning of the MEA and/or the loss of contact zone with the bipolar plates and MEA. Due to the deterioration of the perfluorinated ionomer electrolyte membrane, the fluoride ions are known to attack TiO_2 passive film, which results in the formation of $Ti\text{-}F^-$ compound. The corrosion reaction is shown in Equation 2.8 [83]. The corrosion of titanium depends not only on fluoride concentration but also on pH. The passive oxide film is easily destroyed by even low concentrations of F^- at a ppm level [84, 85].

$TiO_2 + 4H^+ + 6F_{aq}^- \rightarrow TiF_6^{2-} + 2H_2O$ (Equation 2.8)

2.4.2.3 Hydrogen embrittlement

At the cathode side of a PEM water electrolyzer, titanium components are saturated with hydrogen and may suffer from hydrogen embrittlement [78]. TiH_2 can form on the surface of titanium in the presence of hydrogen when the solubility limit of hydrogen exceeds (a few hundreds of ppm). Titanium components become brittle and lead to a risk of cracking under stress. The hydrogen content in titanium increases with pressure and time in the temperature range of the operation of PEM water electrolyzers. The risk of hydrogen embrittlement is considered severe when the hydrogen content in titanium is above 8000 ppm [86]. However, hydrogen embrittlement can be mitigated in the presence of moisture or passive layer TiO_2 [19]. It was found that hydrogen absorption does not occur in the presence of as little as 2% moisture in hydrogen gas, except in the condition of low pH and potentials more negative than -0.70 V(vs. SHE (standard hydrogen electrode)) [87]. The passive layer TiO_2 can act as an effective barrier. As aforementioned, the F^- originated from the deterioration of membranes can chemically attack TiO_2 passive film during the long-term operation of a PEM water electrolyzer, which makes the degradation process very complex. In addition, it should be noted that though there are few investigations about hydrogen embrittlement of titanium bipolar plate, this issue should not be ignored [45, 78]. However, it should be mentioned that this is beyond the topic of the thesis.

2.4.3 Mitigation strategies of degradation for PTLs

As mentioned, the degradation of titanium-based PTLs can originate from different aspects, while the critical passivation of titanium-based PTL that occurs under real cell conditions is the crucial factor that restricts the application of these PTLs in the absence of any surface modification. Different ways of surface modification such as applying noble metal coatings on the surface of PTL [10-12] and introducing an MPL [88-91] have been reported. The details will be introduced in the following sections.

2.4.3.1 Noble metal coatings

Noble metals such as platinum and gold are typically used to coat the components such as PTLs [10-12] and bipolar plates [40-43] in the PEM water electrolyzer. However, most of these studies focus on protecting the bipolar plate. For example, Gago et al. deposited Ti and then Ti with Pt coating (8 wt% Pt/Ti) on stainless steel bipolar plates by physical vapor deposition (PVD) magnetron sputtering for a PEM water electrolyzer cell. The conductive and corrosion-resistant coatings reduced the interfacial contact resistance and showed an average degradation rate of 26.5 µv h^{-1} in a 200 hour durability test. Another study showed that gold coating can serve as a barrier layer and inhibit the formation of the passive layer on the surface of titanium-based bipolar plates in both fuel cell and electrolyzer cells [40].

The use of protective coatings on titanium PTLs has rarely been reported and its degradation has yet to be fully quantified [10-12]. A novel titanium PTL modified with Au thin film achieved superior multifunctional performance and good short-term stability (100 h at 0.2 A·cm^{-2}, 80 °C) comparing to conventional titanium PTLs [12]. In our previous study, we observed that a PEM water electrolyzer cell with an uncoated titanium PTL at anode showed a degradation rate of 194 µv h^{-1} at a constant current density of 2 A·cm^{-2} in a 1000 h long-term test. We also concluded that 78% of the detectable degradation can be explained by an increase in ohmic resistance, which arose from the anodic titanium-based PTL. However, by using Pt coating on anodic PTL, the cell showed a degradation rate of only 12 µv h^{-1} [10]. Another similar study of our group showed that the cell with Pt coating on anodic PTL was stable at 2 A·cm^{-2}. Nevertheless, some detachment was observed at certain points and adhered to the anodic side of the catalyst coated membrane (CCM) under operation at elevated current densities, which caused obvious mass transport limitation [11]. Another study showed that electrodeposited IrO_2 coated on titanium mesh is not only a cost-effective catalyst layer for OER but also proposed to be a corrosion-protective film that suppresses the passivation of the titanium substrate in a high-temperature PEM system [92]. Nevertheless, the thickness of the coatings in these studies is very high (at least around 200 nm [11]). In other words, the amount of PGMs in these studies was very high (usually around or more than 1 mg·cm^{-2}), which significantly increased the investment cost of the PEM electrolyzer. Moreover, two challenges arise when using Pt or Au-based coatings on PTLs. First, very thick coatings of Pt and Au are required to extend the lifetime to values above 50,000 h. Secondly, under PEM water electrolysis conditions, the gold oxide cannot match the substantial electrical conductivity of iridium oxide and its concomitant, an acceptable degree of long-term stability [93, 94].

Iridium is the most resistant of all metals to corrosion, e.g. it does not dissolve in the aqua regia even at elevated temperatures [94-96]. Iridium has been applied in a wide range of fields such as a barrier layer on structural carbon materials [97, 98], protective coatings for some electrode materials [99], and anti-corrosive coatings for anodes in seawater electrolysis [100]. In our recent study, we reported a scalable and simple method by sputtering only 20 nm thick iridium layers to

PTLs, which effectively decreased the contact resistance and significantly improved cell performance. The total amount of iridium was only 0.1 $mg_{Ir} \cdot cm^{-2}$, which is around 10 times lower than Au or Pt protective layers applied than other studies and current commercial electrolyzers [16].

2.4.3.2 Micro porous layer (MPL)

The MPL between the catalyst layer and gas diffusion layer (GDL) at the cathode side is widely used in PEM fuel cells [101-104]. It can greatly increase the cell performance by reducing the ohmic losses, facilitating liquid water removal from the catalyst layer, and enhancing the chemical and mechanical stability of the catalyst layer and the membrane [104]. In PEM water electrolyzers, very little has yet been reported on the role of MPLs. Hwang attempted to fabricate MPLs by loading a Ti-felt with Ti powders, though the effects were limited as the powder covered only a small part of the pores and penetrated the porous electrode body [88]. Lettenmeier et al. developed a dense titanium layer as MPL to a commercially available powder sintered filters by using vacuum plasma spraying (VPS), resulting in a decrease in ohmic contact resistance of 20 $m\Omega \cdot cm^2$. However, the cells with the MPL showed almost identical performance as with the untreated PTL, which might be caused by the high bulk tortuosity [89]. Kang et al. fabricated MPLs both micro Ti particles (~5 μm) and nano Ti particles (30 to 50 nm) by spraying method. However, the microparticle coating resulted in only a moderate cell voltage decrease of 20 mV at 2 $A \cdot cm^{-2}$, and the nanoparticle coating induced higher overpotentials compared to the pristine PTLs [90]. Recently, another group developed a hierarchically structured MPL by titanium powders. The MPLs combine preferential surface properties with high open porosity and low tortuosity of sinter materials, which enable the use of thin membranes in combination with anodic titanium PTLs for the first time [91].

In addition to titanium-based MPL, some other materials to fabricate MPL such as antimony-doped tin oxide (ATO), nitride coatings have also been attempted and investigated. Polonsky et al. developed an MPL on Ti felt with ATO mixed with Nafion solution. However, their results showed that the MPL is only advantageous in a range of low current densities, while the ohmic resistance of the MPL significantly reduces the efficiency of electrolysis at higher current densities [105]. In another study, a titanium porous disc was coated with IrO_2/Ta_2O_5 composition as an MPL to prevent corrosion and oxidation. The MPL can effectively transform active oxygen species (such as oxygen atoms and hydroxyl free radicals) into harmless oxygen gas during water electrolysis [106].

2.4.3.3 Other methods

Thermal and plasma nitridation on the surface of PTLs and bipolar plates are of great interest due to the low cost, high conductivity, and good anticorrosion [66, 107]. Mo et al. introduced thermal nitride surface treatments to titanium felts, which improved the PEMEC performance to a certain extent. A chemical etching technique was also applied to reduce the contact resistance and mitigate the degradation of the PEM electrolyzer. Bystron et al. presented a chemical etching method to remove the titanium oxide layer of PTLs. The Ti hydride (TiH_x) on the surface of titanium reduced contact resistance and improved the cell performance compared to untreated PTL [28].

3. Experimental methods

3.1 Sample preparation

3.1.1 Titanium felt porous transport layers (PTL)

In chapters 4 and 5, Bekipor® ST Titanium Grade 1 felts with 68% porosity and 350 µm thicknesses from Bekaert (2GDL10-0.35) were used for the anode side. In chapters 6 and 7, Ti felt PTLs with a thickness of 250 µm and 56% nominal porosity (2GDL10-0.25) from Bekaert were used for the anode side. The porosity and thickness of PTLs are provided by Bekaert.

3.1.2 Cleaning procedure for the PTLs

The cleaning procedure aimed to remove organic substances and contaminants from titanium-based PTL fabrication before the sputtering step. The PTLs were immersed in deionized water (Milli-Q) (18.2 MΩ·cm) at 80 °C for 15 minutes, then immersed in 2-propanol and then acetone in an ultrasonic bath at ambient temperature for 15 minutes. This procedure was followed by rinsing the PTLs twice in deionized water at 80 °C for 15 minutes and finally air-dried at ambient temperature overnight.

3.1.3 Sputtering

A plasma sputtering instrument (Quorum Q150T) was used to deposit iridium, platinum, or gold layers on the PTLs. The sputtering procedure was carried out for both sides of the PTLs individually, using a current of 30 mA and 0.7 Pa under Ar, with metallic iridium, platinum, and gold targets for 360s. The total loading and thickness of iridium, platinum, and gold were calculated by weighing the PTLs before and after sputtering, and the results are shown in Table 3.1. The thickness of the iridium coating was also examined from their cross-section, using a focused ion beam (FIB). In chapter 5, the loading and thickness of the Iridium coating were controlled by varying sputtering time (30, 90, 180, and 360 seconds, respectively). It should be noted that the variation of loadings of different coatings is due to the sputtering device, which can't control the growth rate precisely. The loadings here are the noble metal loading on one side of the PTL.

Table 3.1 Parameters of iridium, platinum and gold coated PTL.

Sample	Sputtering time (s)	Loading ($mg\cdot cm^{-2}$)	Thickness of coating (nm)
Ir-coated PTL	360s	0.05	≈ 25
Pt-coated PTL	360s	0.08	≈ 37
Au-coated PTL	360s	0.09	≈ 45

3.1.4 Manufacturing catalyst-coated membrane (CCM)

The CCM samples were manufactured using a combination of the doctor blade and decal methods using a Nafion® 117 membrane as the polymer electrolyte. The fabrication method of CCM was published in our previous work [16]. 60% Pt/C (HiSPEC 9100, Johnson & Matthey) and iridium oxide (Alfa Aesar, Premion, 99.99%) were used as the cathode and anode catalyst, respectively. Catalyst powder and ionomer solution (10% Nafion® for anode and 15% Nafion® for cathode) were dispersed in appropriate mixtures of water and 2-Butanol to prepare the catalytic slurries. The mixtures were agitated in an ultrasonic homogenizer for 5 minutes and then coated onto inert decal substrates by automated bar coating (Coatmaster 509 MCI, Erichsen GmbH & Co. KG). The membrane was then sandwiched between the two dried catalyst coated decals (anode and cathode) and hot-pressed at a temperature of 130°C for 3 min. The final catalyst loadings were ~0.8 ± 3% $mg_{Pt}\cdot cm^{-2}$ Pt at the cathode and ~2.2 ± 10% $mg_{Ir}\cdot cm^{-2}$ IrO_2 at the anode.

3.2 Electrochemical characterizations

3.2.1 Basic information of the single cells and test rig

In chapters 4 and 5, Ti felt PTLs with a thickness of 350 μm and 68% nominal porosity (2GDL10-0.35) were used for the anode side. TGP-H 120 Toray® paper with a 350 μm thickness was used as the cathodic PTL for the test. At the anode, in-house Pt-coated bipolar plates with pin-type flow fields were used. The cathode was additionally gold-plated against hydrogen embrittlement. The image of the pin-type flow fields used in this work is shown in Figure 12.1a in the appendix. The cells were then compressed using PTFE gaskets with a thickness of 0.3 mm at both sides, at a torque of 8 Nm on each of the 6 bolts. The thickness of the CCM we used in this study is 200 ± 10 µm. The active area was 25 cm^2. The electrolyzer cell design used in the study of these two chapters is presented in Figure 3.1.

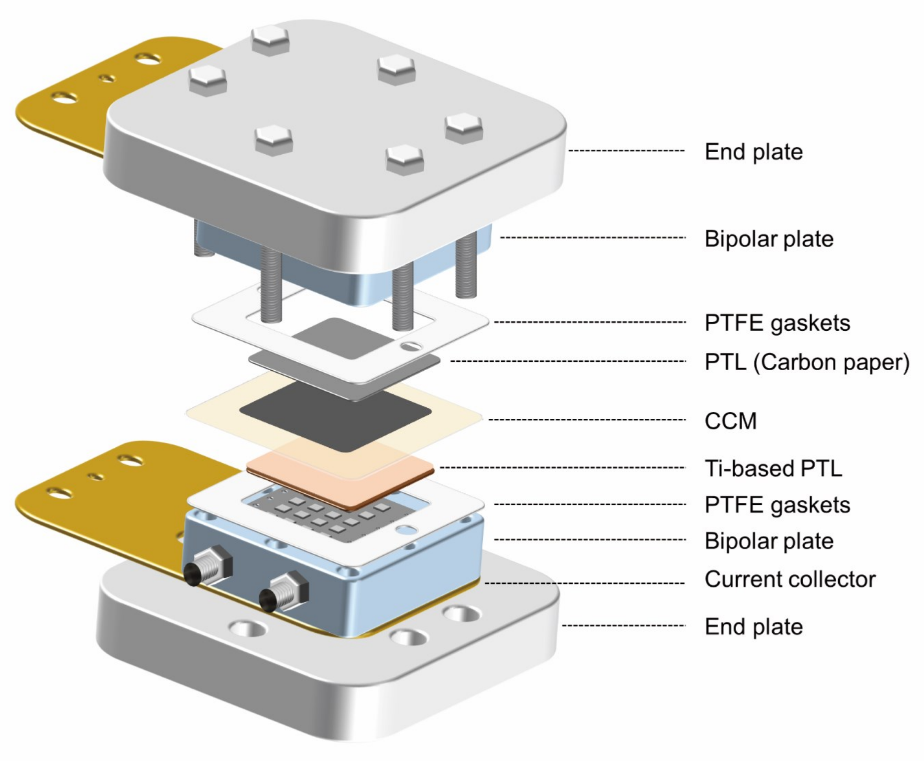

Figure 3.1 *Schematic illustration of the 25 cm^2 PEM water electrolysis cell [108].*

In chapters 6, 7, and 8, Ti felt PTLs with a thickness of 250 µm and 56% nominal porosity (2GDL10-0.25) from Bekaert were used for the anode side. TGP-H 120 Toray® paper with a 350 µm thickness was used as the cathodic PTL for the test. Platinum-coated bipolar plates with single serpentine flow fields were used on both sides, that of the cathode being additionally gold-plated against hydrogen embrittlement. The image of the single serpentine flow fields used in this work is shown in Figure 12.1b in the appendix. The cells were compressed using PTFE gaskets with a thickness of 0.3 mm at the cathode and 0.2 mm at the anode, at a torque of 8 Nm on each of the 8 bolts. The thickness of the CCM we used in this study is 200 ± 10 µm. The active area was 17.64 cm^2. The parameters of the single cell components are shown in Table 3.2.

Table 3.2 Parameters of characteristics and conditions of PEM water electrolyzers.

Characteristics	**Chapter 4 and 5**	**Chapter 6, 7 and 8**
Cathode catalyst (Pt/C)	~ 0.8 ± 3% $mg_{Pt}\cdot cm^{-2}$	~ 0.8 ± 3% $mg_{Pt}\cdot cm^{-2}$
Anode catalyst (IrO_2)	~ 2.2 ±10% $mg_{Ir}\cdot cm^{-2}$	~ 2.2 ±10% $mg_{Ir}\cdot cm^{-2}$
Cathode PTL	TGP-H 120 Toray® paper	TGP-H 120 Toray® paper
Anode PTL	2GDL10-0.35, Ti felt from Bekaert	2GDL10-0.25, Ti felt from Bekaert
Thickness of anodic Ti PTL	0.35 mm	0.25 mm
Porosity	68%	56%
Electrode area	25 cm^2	17.64 cm^2
Flow field	pin-type (see Fig. 12.1a in the appendix)	single serpentine type (see Fig. 12.1b in the appendix)
Gaskets (PTFE)	0.3 mm at both sides	0.3 mm at the cathode; 0.2 mm at the anode
Water flow rate	50 $ml\cdot min^{-1}$	25 $ml\cdot min^{-1}$
Operating temperature	80 °C	80 °C
Operating pressure	1 bar (absolute)	1 bar (absolute)

3.2.2 Electrochemical measurements set up

In chapters 4 and 5, the single tests were performed using an E60 test station from Greenlight (Figure 3.2). Deionized water (18.2 MΩ·cm) was circulated through both the cathode and anode compartments (50 $ml\cdot min^{-1}$) in separate water circuits for each cell. The temperature of the cell during the operation was controlled by the flow of heated water supplied to the cell. Water and water/gas temperatures were sensed at the cell inlet and outlet. The temperature setpoint was defined as the cell inlet temperature. In addition, the cell was also heated by two heating cartridges which are inserted directly into the flow fields. The single cell was heated up to 80 °C by applying temperature set points to the water flowing through both the anode and cathode. A current density of 0.2 $A\cdot cm^{-2}$ was applied to the cell for 30 min once the temperatures had been established. Later, the current density was increased to 1.0 $A\cdot cm^{-2}$ for another 30 min. Thereafter, the cell was continually operated at a voltage of 1.7 V until the current variation became less than 1% per hour. Performance curves were subsequently measured in 5 minute steps; starting from the open circuit, the current was increased in 0.02 $A\cdot cm^{-2}$ steps to 0.1 $A\cdot cm^{-2}$ and followed by 0.2 $A\cdot cm^{-2}$ until a maximum cell voltage of 2.0 V was reached [16].

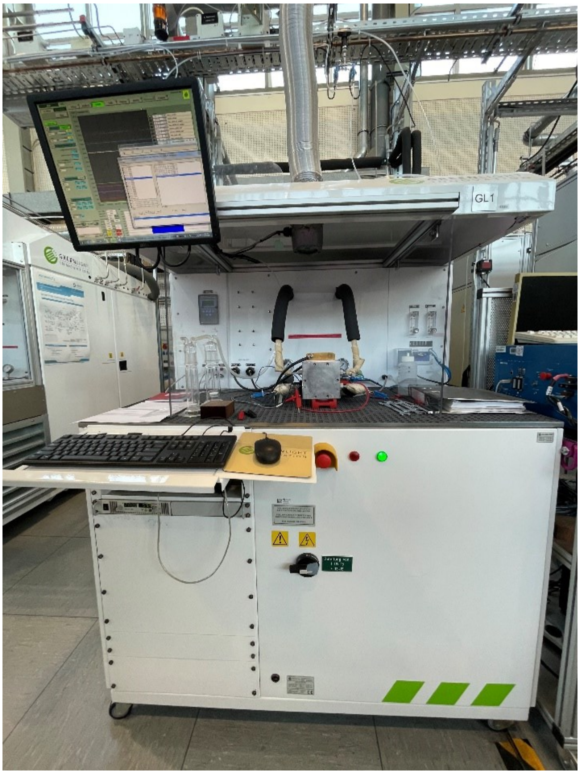

Figure 3.2 *Diagram* of E60 test rig from Greenlight.

In chapters 6, 7, and 8, all the single cell experiments were operated using test benches that were developed in-house (Figure 3.3). High purity feed water (18.2 MΩ·cm) was circulated through both the anode and cathode compartments (25 ml·min^{-1}) in separate water circuits for each cell compartment. The 'break-in' procedure is the same as described above. Polarization curves were recorded before and after the durability test using the DC power supply. The measurement commenced from the open circuit, and then the current was increased in 0.025 A·cm^{-2} steps to 0.1 A·cm^{-2} and followed by 0.2 A·cm^{-2} until a limiting cell voltage of 2V was reached, with a 5 minute hold per step. Specific cell characteristics and test conditions are displayed in Table 3.2.

Figure 3.3 *Diagram of long-term test rig.*

3.2.3 Electrochemical impedance spectroscopy (EIS)

The cell current was interrupted and the cell connected to a potentiostat (HCP 1005 Biologic) to carry out electrochemical impedance spectroscopy (EIS). EIS was run at a DC-bias of 0.5 A·cm^{-2} in Chapter 4, 0.15 A·cm^{-2} in Chapter 5, and 1.9 A·cm^{-2} in Chapter 6, 7 under a current perturbation of ± 5%, with a maximum perturbation of 10 mV between 100 kHz and 100 mHz.

3.2.4 Durability test

After the polarization curve and EIS measurement, the long-term test was performed at a current density of 2 V and 80 °C for 4000 h. According to our previous work and the literature [9-11, 29], electrolysis durability tests are typically run galvanostatically (applying current). However, in this study, we ran these tests potentiostatically (applying potential) to avoid any additional degradation phenomena triggered by increases in cell voltage when the cell is run under a fixed current. At a constant voltage (2 V) in this case, degradation will be expressed by a decrease in current density. A DC power supply (TDK Lambda GEN-20-76) was used as the current source, while the cell voltages were read by a multimeter (Keithley Model 2701). A LabVIEW-based software was then used to control all devices and record the data. At the end of the long-term test, the polarization curves and EIS measurements were performed again.

3.3 Physical-chemical characterization

Post-mortem measurements were performed to characterize the physical and chemical properties of materials.

3.3.1 Scanning Electron Microscopy (SEM) and Energy Dispersive X-ray Spectroscopy (EDX)

The surface morphology of PTLs was examined by means of scanning electron microscopy (SEM) using a Zeiss Gemini Ultra Plus instrument in IEK-14. The Energy Dispersive X-ray Spectroscopy (EDX) was used to investigate the chemical composition and the mapping provides the elemental distributions of the PTLs.

3.3.2 X-ray computed tomography (CT)

X-ray computed tomography (CT) is a non-destructive technique used to obtain the 3D structure of the porous materials from high quality 2D images on the micro- and nano-scales [109]. It is particularly useful for characterizing the fine structure of porous components of PEM fuel cell and electrolyzer, such as micro-porous layer (MPL) [109], catalyst layer (CL) [110], and porous transport layer (PTL) [16].

In this study, the 3D microstructures of the PTLs were characterized by means of nano-computed tomography using a Zeiss Xradia 410 Versa X-ray in IEK-14.

3.3.3 Focused ion beam - Scanning Electron Microscopy (FIB-SEM)

Focused ion beam - Scanning Electron Microscopy (FIB-SEM) combines the imaging capabilities of SEM with the precise milling and cross-sectioning ability of a FIB, enabling serialsectioning of a sample of interest to produce high-resolution 3-D reconstructions. It has been widely used for characterizing the structure of porous components of PEM fuel cell and electrolyzer, for example, catalyst layer [111, 112] and MPL [113].

The FIB-SEM measurements for the cross-sectional observation of our samples were performed on a Zeiss Crossbeam 540 dual beam microscope in IEK-4 (Forschungszentrum Jülich). On the top of each PTLs, two Pt coatings were deposited using electron beam and ion beam, respectively. A double deposition process was performed to protect the samples' surface as well as the prepared cross-section from scattered ions, thus reducing the artifacts of FIB milling (the so-called "curtaining effect") [111].

3.3.4 Focused ion beam (FIB) cross-section for one Ti fiber

FIB (FEI Helios NanoLab 460F1) was used to cut one titanium fiber from PTL [114]. EDX composition maps were performed in an FEI (Thermo Fisher Scientific) Titan 80 - 300 electron microscope equipped with a probe corrector (CEOS) and a HAADF detector [115]. Z - contrast" conditions were achieved by using a probe semi-angle of 25 mrad and an inner collection angle of the detector of 75 mrad. This measurement was conducted in IEK-9 and Ernst Ruska-Centre (E-RC) in Forschungszentrum Jülich).

3.3.5 Atomic Force Microscope (AFM)

Atomic Force Microscope (AFM) is a scanning force microscopy characterized by the interaction between probe and sample [116]. It can be used to examine the surface morphology, topography, and locally resolved conductivity of samples as demonstrated by Solmaz et al. [117].

The AFM measurements in this thesis were achieved with a Multimode 8 AFM (Bruker, Karlsruhe) in Deutsches Zentrum fur Luft- und Raumfahrt (DLR), Stuttgart. The sample was glued with conductive adhesive tape onto an AFM 12 mm disc either with the BPP or the CCM side facing up. The sample was additionally connected with another conductive tape from the top close to the measurement spot to ensure electrical connection. Platinum/iridium coated AFM tips (NCHPt 42 N/m, Nanoworld) were used in tapping mode with additional recorded current that gets averaged by a lock-in amplifier (PF-TUNA, Bruker). The 25 μm² measurements were recorded with 512 x 512 pixels at a scan rate of 0.5 Hz. For the conductive area evaluation, the threshold was set to 0.1 nA, the applied voltage was 1 V.

3.3.6 X-ray photoelectron spectroscopy (XPS)

X-ray photoelectron spectroscopy (XPS) is widely used to identify and characterize materials, and to determine their chemical composition and state of oxidation on a selected region of the surface.

The XPS measurements were performed in Deutsches Zentrum fur Luft- und Raumfahrt (DLR) in Stuttgart. Photoemission data were recorded at a setup with a hemispherical photoelectron analyzer (Thermo Scientific ESCALAB250) in a chamber base pressure of $5x10^{-10}$ mbar, using a conventional Al Ka X-ray source, with an intrinsic linewidth of (NACHSCHAUEN). Depth profiles were carried by bombarding the samples with a focused Ar^+ ion beam with an acceleration voltage of 2 kV at a chamber pressure of $4x10^{-8}$ mbar.

3.3.7 Time-of-flight secondary-ion mass spectrometry (ToF-SIMS)

Time-of-Flight secondary-ion mass spectrometry (ToF-SIMS) is a surface-sensitive analytical method. It is widely used for characterization of structure and composition when combined with sputter depth profiling as demonstrated by Gulin et al. [118].

In our study, ToF-SIMS measurements were performed using a ToF-SIMS 5 (ION TOF) at 30keV with 5µm lateral resolution using a Bi^{3+} primary ion source in Colorado School of Mines. The operating pressure in the analysis chamber was ~3.1E-10 mbar. Depth profiles were obtained using a 250 eV Cs^+ secondary ion source. Data was acquired using SurfaceLab 7 software. Data is plotted as a function of sputtering time; sputtering time increases from left to right and thus the sample is probed at deeper depths from left to right, respectively. For certain species, the pure metallic ion (such as Ir^+) displayed a stronger signal, while for others the Cs-containing ion complex (such as $CsPtO^+$) was more intense. This depends on the electronegativity of the element and both species will reflect the same trends, with varying intensity.

3.3.8 Interfacial contact resistance (ICR)

Figure 3.4 shows the schematic of interfacial contact resistance (ICR) device used in this thesis [16]. To measure through-plane resistance, the PTL was sandwiched between two conducting and gold-coated plates under a defined compression. All the samples were then exposed to a four-wire resistance measurement with DC current. The applied contact pressure was varied from 500 to 6000 kPa by an electric press. The sample was then exposed to a four-wire resistance measurement with DC current at 4A. The plate-to-plate voltage drop was then measured to calculate the through-plane resistance of the PTLs [119], i.e., the sum of the PTL resistance and the two contact resistances that are present between the tested PTLs and gold-coated plates. In the through-plane direction, the contact resistance is the major factor affecting conductivity [120]. It should be noted that in chapters 6 and 7, contact resistance measurements were performed on all samples before and after the durability test. All the measurements were carried out at 25 °C.

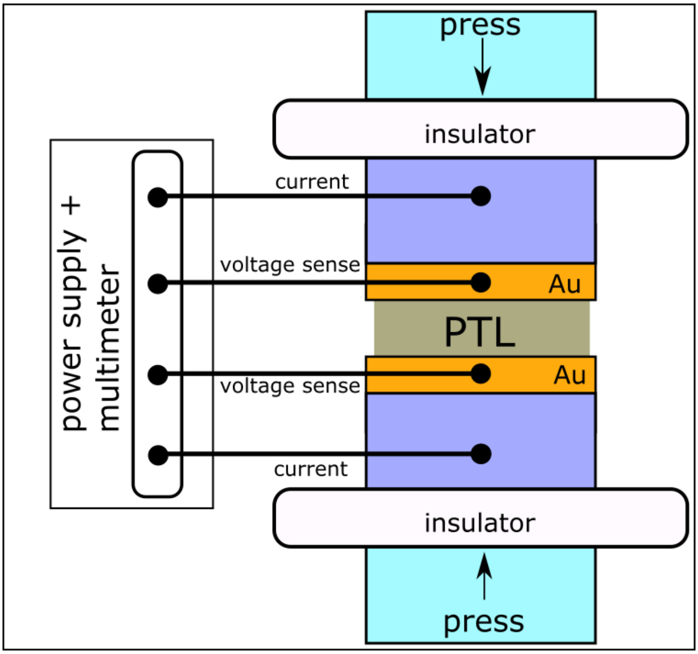

Figure 3.4 *Schematic diagram of the interfacial contact resistance (ICR) device [16].*

4. Noble metal coating

In PEM water electrolyzers, the harsh acidic conditions originate from the perfluorosulfonic acid (PFSA) membrane and ionomer in the catalyst layer, and high overpotential and an oxygen/ water mixture at the anode side demand the use of highly corrosion resistant materials such as titanium to construct bipolar plates and porous transport layers (PTLs). In consequence, the high cost of raw titanium and complex/expensive machining labor accounts for 50% of overall stack costs [14]. More importantly, titanium (Ti^0) changes its oxidation state over time in these harsh cell conditions, mostly depending on the levels of anode overpotential, pH, and cell temperature. These factors induce the formation of a thin but continuously growing layer of titanium passive layer (TiO_x). To circumvent this issue, titanium PTLs in PEM water electrolyzers are typically coated with platinum [10, 11] and gold [12]. Recently, we reported on a very simple and scalable method to protect titanium PTL from passivation by sputtering thin layers of iridium, which effectively decreased the contact resistance and significantly improved cell performance [16]. Carbon paper is usually used at the cathode side, however, it is also acceptably stable as a PTL for the anode of the PEM electrolyzer cell when the duration of the experiments is less than 20 h and can be used for initial electrochemical tests such as polarization curve and impedance [121].

In this chapter, we demonstrated a facile and economical approach to apply thin iridium, platinum, and gold layers to the top and bottom of titanium PTLs using a simple sputter process. Most of the results from this work have already been previously published [16]. The electrochemical cell performance of Ir-coated PTL is compared with Pt-coated and Au-coated titanium-based PTLs and carbon paper.

4.1 Schematic of noble metal coated PTL

Figure 4.1a shows the main components of PEM water electrolyzer cells. The anode porous transport layer (PTL) is a key component and works to transport water to the anode electrode, conduct electrons, and remove the produced oxygen. An X-ray computed tomography (CT) image of a titanium felt-type PTL is shown in Figure 4.1b. The image highlights the 3D structure of the PTL, which in this case, has a thickness of 350 µm, a porosity of 68%, and a fiber diameter of around 20 µm. Optimized cell compression is essential to provide excellent electrical contact between the electrode and PTL [15]. However, as illustrated in Figure 4.1c, a titanium PTL naturally forms a TiO_x surface-passivation layer after exposure to ambient air [79]. In this study, noble metals such as iridium, platinum, and gold are used as protective coatings on the porous transport layers (PTLs) to circumvent this issue. The loading of Ir, Pt, or Au on one side of the PTL is 0.05, 0.08, and 0.09 $mg \cdot cm^{-2}$, respectively (shown in Table 3.1).

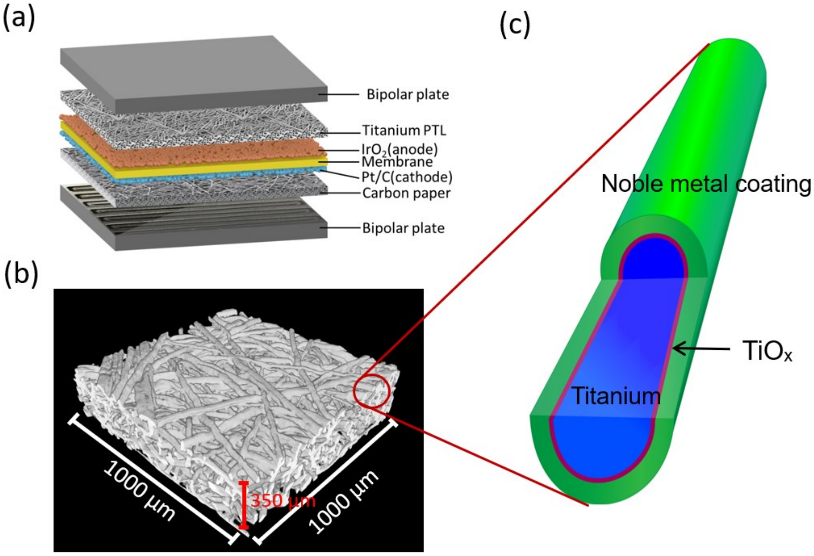

Figure 4.1 ***(a)*** *Schematic illustration of the key components inside a PEM electrolyzer [28];* ***(b)*** *X-ray computed tomography (CT) image of a noble metal-coated porous transport layer (PTL);* ***(c)*** *illustration of a single titanium top-fiber that is coated with iridium or other noble elements such as Pt or Au [28]. The naturally formed TiOx passivation layer was fully coated. The coating ultimately avoids further growth of the oxide layer on the titanium fiber, preventing the increase of the cell resistance over time.*

4.2 Deviation of the CCMs from the same batch

As this study is focused on PTLs with or without coatings, the deviation from the CCMs cannot be ignored. The deviation of CCMs from one batch could originate from the temperature of the lab when the MEAs are fabricated, the batch of the membrane, catalyst powders, and organic solvent, etc. In order to know how much deviation comes from CCMs, the measurements of polarization curves were performed for 13 CCMs from the same batch. Here, the same batch means the catalyst powders, solvent, membrane, and lab environment are identical. In order to exclude the deviation from the PTL, carbon paper (TGP-H 120, Toray®) from the same batch are used as PTLs at both anode and cathode. It can be seen from Figure 4.2 that the average deviation of 13 CCMs from the same batch is 4.84 mV at 2 A·cm^{-2}, indicating that the deviation from CCMs of all the polarization tests in this study is very low.

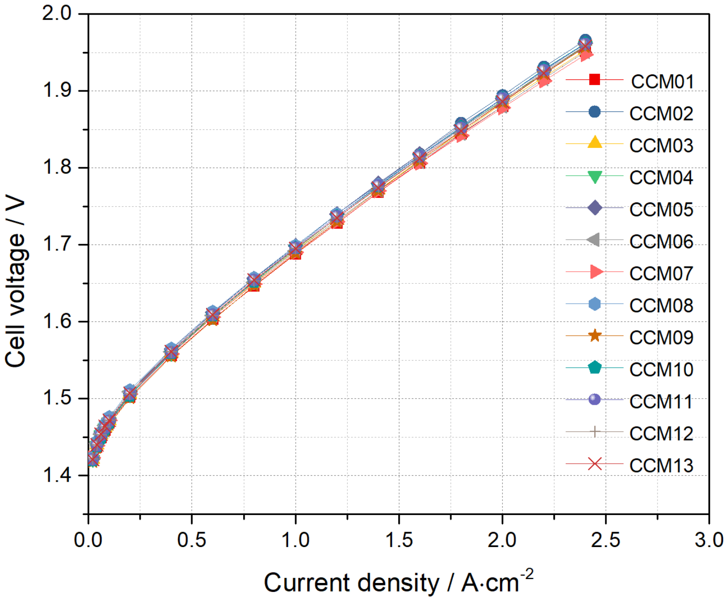

Figure 4.2 *Polarization curves of PEM water electrolyzer single cells assembled with carbon papers and CCMs from the same batch. The cell temperature was 80°C and under ambient pressure.*

4.3 Comparison between Uncoated, Ir-coated, Pt-coated, and Au-coated PTL and carbon paper

4.3.1 Electrochemical test

4.3.1.1 Polarization curve

Figure 4.3 compares the cell performance of carbon paper, uncoated PTL, and PTLs coated with iridium, platinum, and gold, respectively. The Ir-coated, Pt-coated PTL, and carbon paper samples delivered identical performance. The cell voltage is about 110 mV higher than with uncoated PTL sample at 1.0 A·cm^{-2}. Au-coated PTL also showed better performance than uncoated one. In the latter case, the voltage was 45 mV higher than uncoated one at 1.0 A·cm^{-2}. However, the cell voltage of Au-coated sample was still 64 mV higher than PTLs coated with iridium and platinum at 1 A·cm^{-2}. This indicates that Ir or Pt is more effective than Au when used as a coating on titanium-based PTLs in a PEM electrolyzer. Kang et al. reported a novel titanium PTL modified with Au thin film by sputtering and electroplating [12]. Though the modified PTLs achieved superior multifunctional performance and showed good short-term stability comparing to conventional titanium PTLs, the Au-coated PTLs only improved 40 mV cell performance at 1.0 A·cm^{-2} which is in agreement with our findings. Compared to an Ir or Pt-coated PTL, the performance enhancement is not very remarkable.

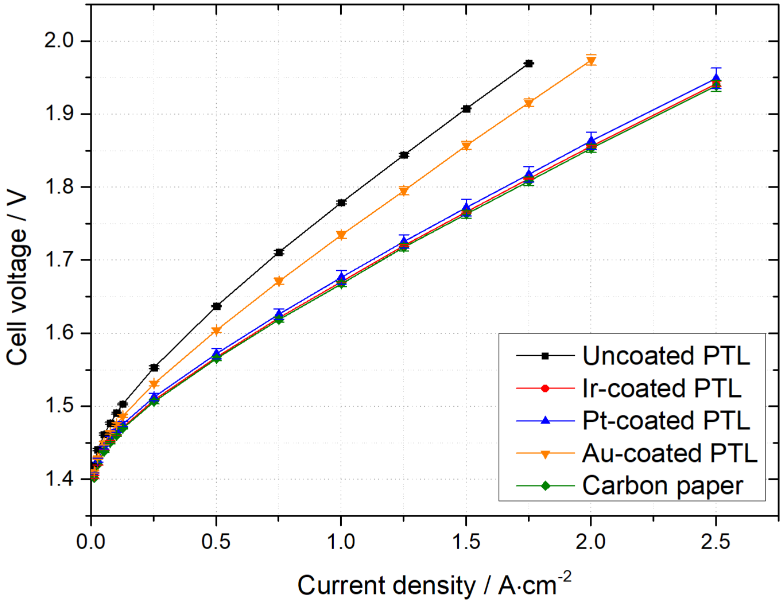

Figure 4.3 *Polarization curves of PEM water electrolyzer single cells assembled with uncoated, Ir-coated, Pt-coated, Au-coated PTL and carbon paper. The cell temperature was 80°C and under ambient pressure.*

4.3.1.2 Electrochemical Impedance Spectra (EIS)

In order to investigate the effect of different protective layers on the ohmic resistance and the electrochemical processes, electrochemical impedance spectra (EIS) were recorded as presented in Figure 4.4. In this chapter, EIS was conducted on PEM water electrolyzer single cells with different noble-metal coated PTLs after polarization curve measurements at 80 °C. EIS was run at a DC-bias of 0.5 A·cm^{-2} under a current perturbation of ±5%, with a maximum perturbation of 10mV between 100 kHz and 100 mHz. As shown in Fig. 4.4 (a), there are two x-intercepts: the left one (at the high frequency part) indicates the ohmic loss and the right one (at the low frequency part) is the sum of the resistance. The EIS results are consistent with polarization curve results. The high frequency resistances (HFR) are shown in Fig. 4.4b. Ir-coated and Pt-coated samples showed nearly the same HFR as carbon paper (0.17 Ω·cm^2 at 0.5 A·cm^{-2}). Compared to an uncoated PTL, HFRs at 0.5 A·cm^{-2} decreased by 0.11 Ω·cm^2 (extracted from EIS data) with an iridium or platinum coating. The iridium and platinum layers reduced the overall ohmic resistance of the interface between PTL and catalyst layer and improved the cell's performance to that achieved with carbon-based PTLs (carbon paper). The HFR of Au-coated sample decreased by 0.05 Ω·cm^2 comparing to an uncoated PTL, however, the decrease is not as remarkable as Ir or Pt PTLs.

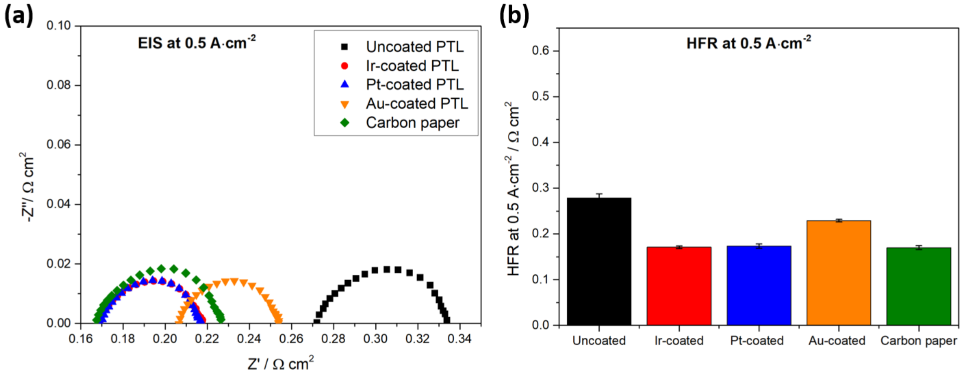

Figure 4.4 ***(a)*** *EIS results at 0.5 A·cm^{-2};* ***(b)*** *HFR at 0.5 A·cm^{-2}.*

Uncoated and Ir-coated PTLs after electrochemical measurements are shown in Figures 4.5 a and b, respectively. Discoloration can be observed for uncoated PTL, which might be an indication of either titanium passivation or corrosion. The flow field pattern can be seen on the uncoated sample after electrochemical tests, but cannot be observed on an Ir-coated PTL. It is not clear why the color of the channel is darker than the land/rib regions on the used uncoated PTL. This might be due to a higher contact pressure at the land vs. the channel region, but it is not yet confirmed. In contrast, no discoloration was observed before and after the electrochemical measurements on the Ir-coated PTL (polarization curve and EIS). This indicates that the iridium functions as a protective layer and effectively prevents titanium oxidation. Additional durability measurement results will be shown and discussed in chapter 6 and 7.

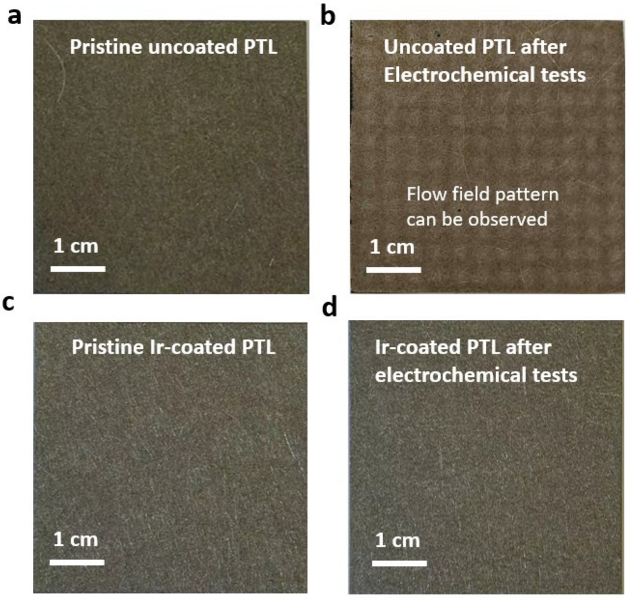

Figure 4.5 *Optical images of* ***(a)*** *pristine uncoated PTL;* ***(b)*** *Uncoated PTL after electrochemical tests;* ***(c)*** *pristine Ir-coated PTL;* ***(d)*** *Uncoated PTL after electrochemical tests.*

4.4 Characterization of uncoated, Ir-coated, Pt-coated, Au-coated PTLs

4.4.1 SEM and FIB of uncoated, Ir-coated, Pt-coated, Au-coated PTLs

Figure 4.6 shows the SEM images of uncoated, Ir-coated, Pt-coated, and Au-coated PTLs, respectively. As can be seen in Figure 4.6b, the surface of a pristine uncoated sample is smooth without any significant structures. Iridium, platinum, and gold are uniformly distributed on the surface of titanium-based PTLs (Figure 4.6d-h). Compared to the Ir-coated sample, the platinum and gold nanoparticles are more clearly observable, which is consistent with the results in the literature [12, 68].

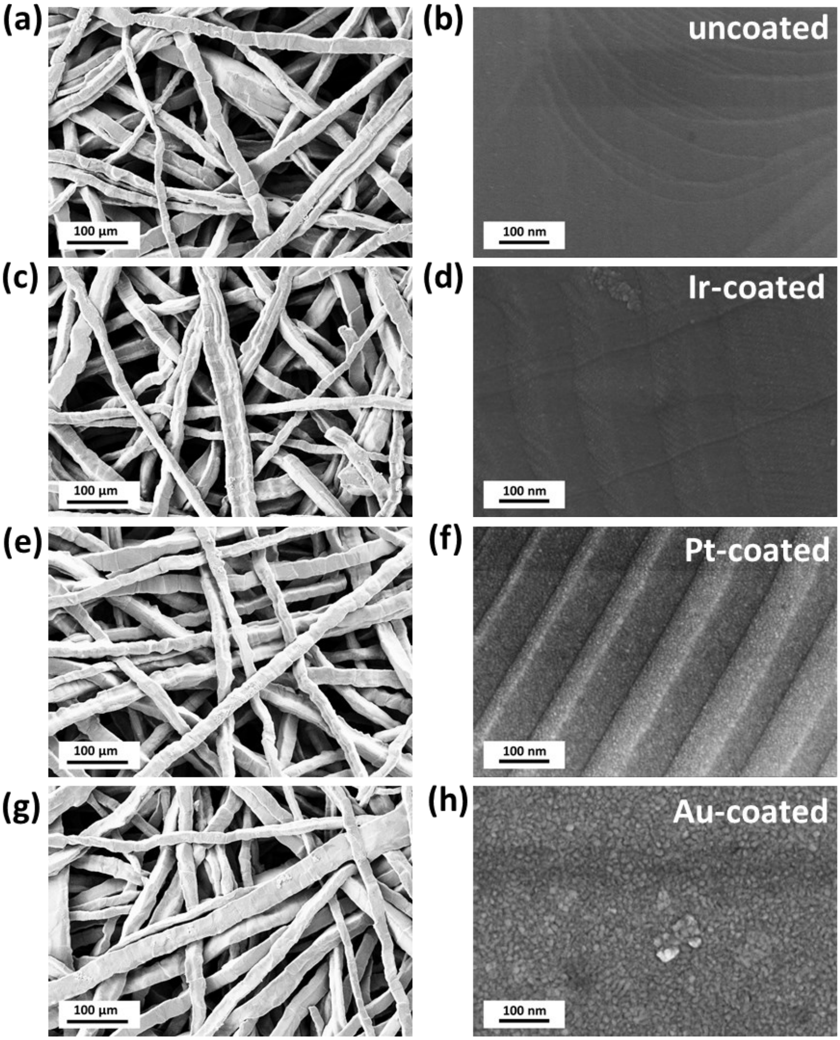

Figure 4.6 *Scanning electron microscopy (SEM) images of* ***(a, b)*** *uncoated PTL;* ***(c, d)*** *Ir-coated PTL;* ***(e, f)*** *Pt-coated PTL;* ***(g, h)*** *Au-coated PTL prior to operation [28].*

The thickness of the thin film Ir, Pt, Au layer was examined under FIB-SEM cross-sections (Figure 4.7). Ir, Pt, and Au layers were coated on titanium-based PTLs under the same sputtering time (Table 3.1). It should be noted that due to the limitation of the sputtering equipment, the loadings and thickness of the coatings cannot be controlled precisely when applying the same sputtering time. Therefore, the loadings and thickness of different metallic coatings are not the same. As can be seen in Figure 4.7 d-f, all three noble metals formed continuous films on the titanium-based PTLs and they are homogeneously distributed over the entire fiber. The thickness of Ir, Pt, and Au layers are around 25, 37, and 45 nm, respectively. Gravimetric analysis indicates that the Ir, Pt, and Au loadings on one side of the PTL are around 0.05, 0.08, and 0.09 $mg_{metal}·cm^{-2}$, respectively (Table 3.1). Titanium-based PTLs used in commercial electrolyzers are typically coated with platinum or gold and the loadings of their protective coatings are estimated to be around 1 $mg_{metal}·cm^{-2}$ [17]. The total amount of iridium on both sides of the PTL was 0.1 $mg_{Ir}·cm^{-2}$, which is 20 times less iridium compared to what is usually present in an anode catalyst layer [6], and a 10-times reduction of the Au or Pt protective layers typically used in contemporary commercial electrolyzers [17].

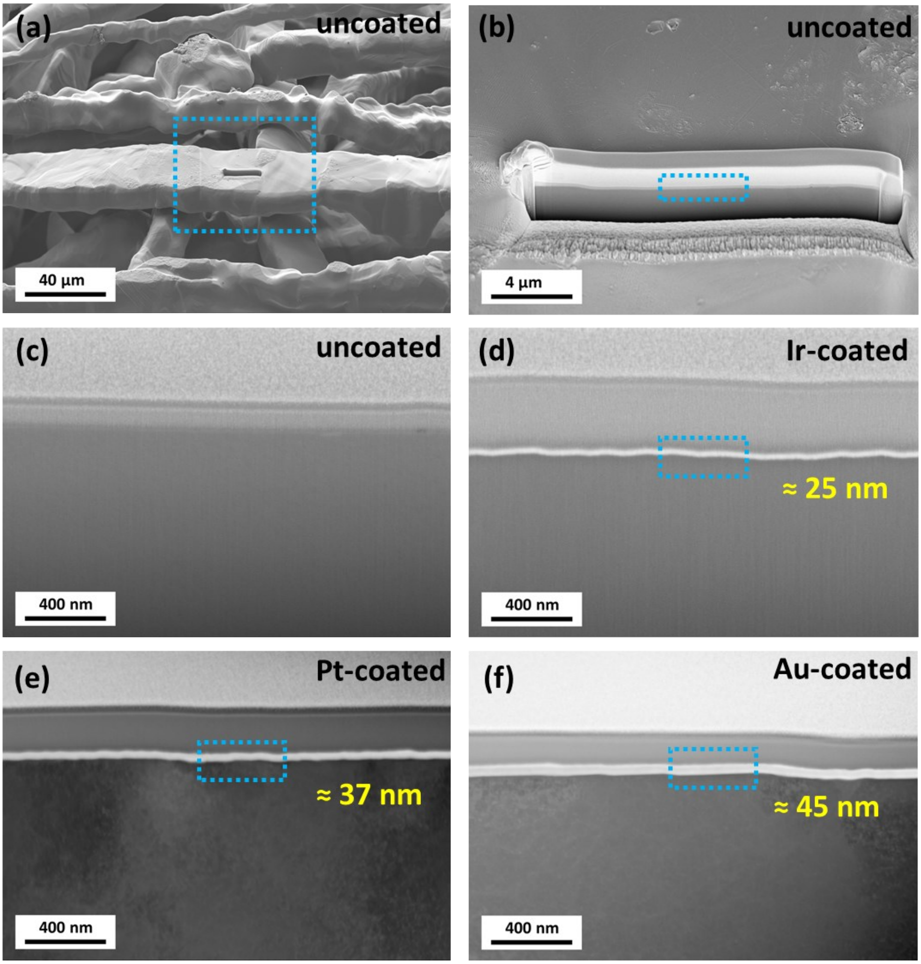

Figure 4.7 *FIB-SEM cross-sections images of* ***(a, b, c)*** *uncoated PTL;* ***(d)*** *Ir-coated PTL;* ***(e)*** *Pt-coated PTL;* ***(f)*** *Au-coated PTL.*

4.5 Interfacial contact resistance of Ir-coated PTL

As Ir-coated PTL showed similar electrochemical results as the Pt-coated sample, and significantly better performance than Au, here we just focus on the through-plane resistance results of iridium coating. It should be noted that all the PTLs used in the measurement of contact resistance are pristine samples. Figure 4.8 shows the through-plane resistance results of carbon paper, uncoated PTL, and Ir-coated PTL. Three different samples for each different types of PTLs were individually mounted between two gold-coated plates with increasing compression ranging from 500 to 4000 kPa. The measurement was carried out at 25 °C. The through plane resistance was determined using a four-wire DC resistance measurement for each compression. The plate-to-plate voltage drop was measured to calculate the through-plane resistance of the PTLs [119]. The sum of the PTL resistance and the two contact resistances that are present between the tested PTLs and gold-coated plates. In the through-plane direction, contact resistance is the major factor affecting the conductivity [120].

Ir-coated PTL and carbon paper presented identical through-plane resistances. However, the uncoated titanium PTL had a significantly higher resistance over the entire compression range. Compared to uncoated PTL, the contact resistance decreases by 70 $m\Omega \cdot cm^2$ at 500 kpa with an iridium coating. The contact resistance results corroborate well with the results obtained from the polarization curves (Figure 4.3). It should be noted that for all the PTLs, especially for the uncoated titanium PTL, the standard deviation decreased with increasing compression. This indicates that the contact resistance between gold plates and PTL sample is not only higher, but also less reproducible at lower pressures. The deviation of contact resistance may impact the variation of results when performing in-situ experiments (eg. polarization curves).

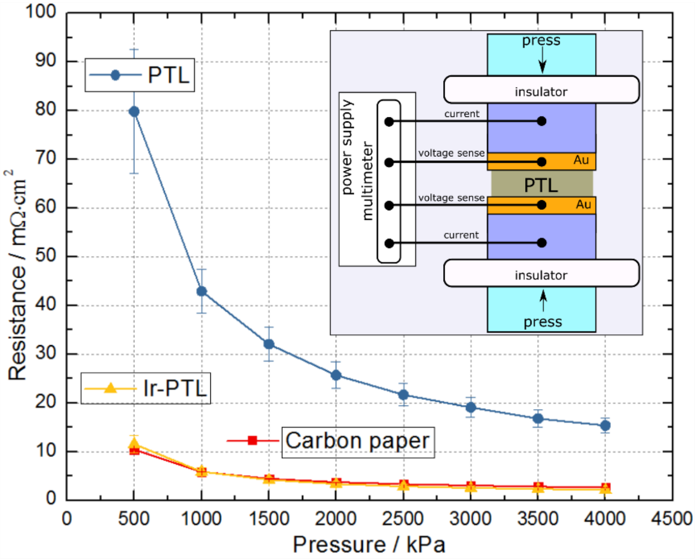

Figure 4.8 *Through-plane resistance of carbon paper (Toray), coated and uncoated PTLs using a conventional press setup where the PTLs are pressed between two gold-coated copper plates. The standard deviation is presented, with results coming from three different samples for all the experiments. The PTLs were mounted and tested dry, with tests run at 25 °C [16].*

4.6 Summary

In this chapter, a thin layer of iridium, platinum, or gold was sputter coated on the titanium-based PTLs as protective layers. The noble metal layers on the titanium fibers effectively decreased the interfacial contact resistance between the PTL and catalyst layer and significantly improved cell performance. The iridium and platinum layers reduced the ohmic resistance by 110 mΩ·cm^2 at 0.5 A·cm^2 and delivered nearly the same cell performance as carbon paper, which was 110 mV higher than with the uncoated titanium PTL at 1.0 A·cm^{-2}.

Developing a PTL that features minimal contact resistance values and enhanced long-term durability may enable operation at elevated anodic potentials while maintaining or even increasing the lifetime of PEM water electrolysis cells. The reduction of the coating loadings will be investigated and discussed in chapter 5. To better improve the understanding of corrosion/passivation processes of the noble metal, noble metal coated titanium layers, and titanium bulk, the long-term stability results of noble metal-coated PTLs will be comprehensively investigated and discussed in chapters 6 and 7.

5. Loading mitigation of iridium coating

The cell performance and durability of PEM water electrolyzers are restricted by the surface passivation of titanium-based porous transport layer (PTL). As mentioned in Chapter 4, titanium-based PTLs are typically coated with considerable amounts (≥ 1 mg·cm^{-2}) of noble metals (Pt and Au). The high cost of noble metals used as catalysts and coatings restricts the further development of PEM water electrolyzers. Chapter 4 compared the cell performance of using Au, Pt, or Ir as a protective layer on the titanium-based PTLs. Ir, Pt, and Au layer reduced the overall ohmic resistance of the PTL/catalyst layer interface and improves the cell performance to that achieved with carbon-based PTLs. As Ir-coated PTL showed similar electrochemical results as Pt-coated sample, and significantly better performance than Au, here in this chapter, different loadings of iridium ranging from 0.005 to 0.05 mg·cm^{-2} (Ir loading for one side of PTL) on titanium PTLs for enhancing the cell performance were investigated [108].

5.1 Characterization of iridium coating with different loadings

5.1.1 SEM and EDX

Figure 5.1a displays SEM images of the bare titanium felt PTL, which has an average thickness of 350 μm, with fiber diameters ranging from 15 to 50 μm [16]. Figure 5.1b shows the image of EDX mapping of Ti and Y of an uncoated PTL. Minor Y impurities were found, which most likely originate from the Ti felt production process [82]. From the EDX mappings of all the Ir-coated PTLs shown in Figure 5.1c-f, the surface of Ti fibers was all homogeneously covered with iridium. The brighter spots on the Ir mapping figures indicate an increase of the Ir concentration. Table 5.1 displays the elemental composition (wt %) of all the samples measured using SEM-EDX. The concentration of Ir is nearly proportional to sputtering time.

The Ir mapping showed spots for Ir is as follows: EDX shows the elemental concentration in the form of a map with different intensities. The image processing software shows the color bar in the best form. The highest intensity is amplified for better visibility. When titanium fiber is under sputtering, different regions are covered with different amounts of Ir. The regions especially on the top of the PTL are covered with more Ir, thus showing brighter dots.

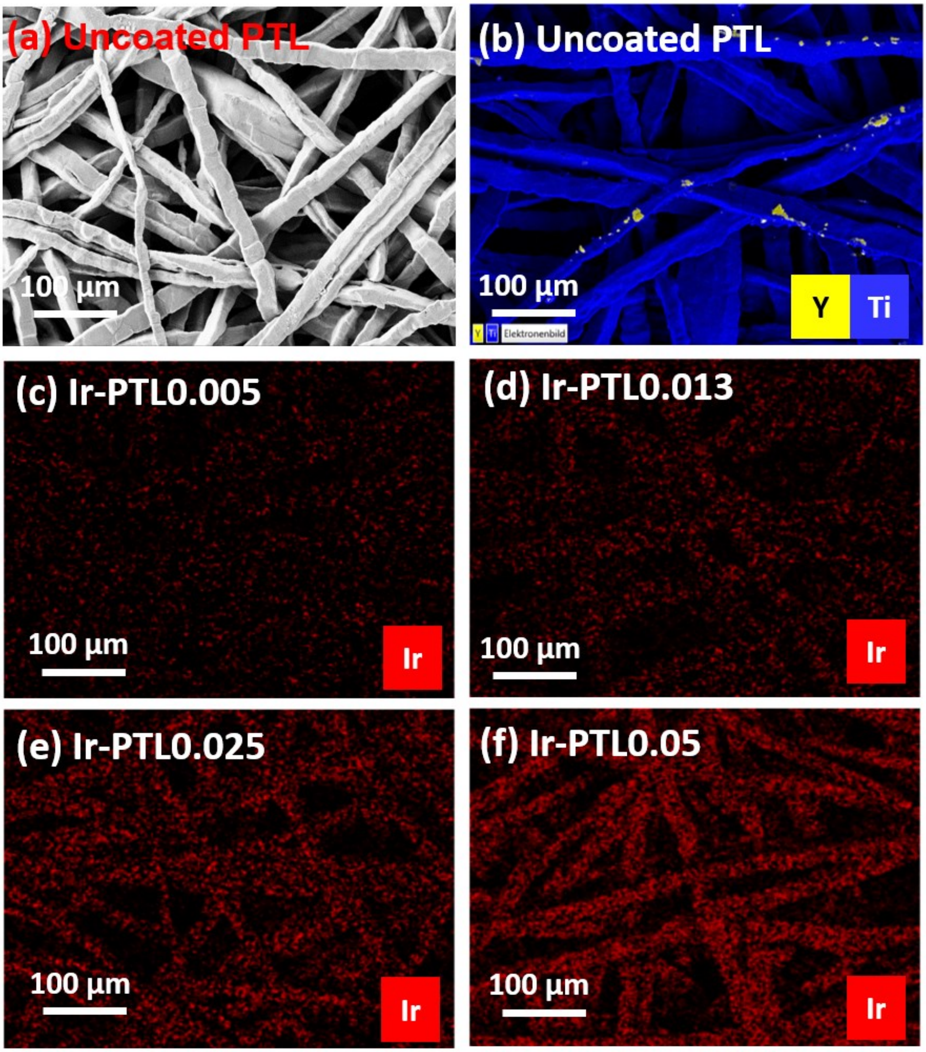

Figure 5.1 ***(a)*** *SEM image of uncoated PTL;* ***(b)*** *EDX mapping of Ti and Y of uncoated PTL;* ***(c)*** *EDX mapping of Ir of Ir-PTL0.005;* ***(d)*** *Ir-PTL0.013;* ***(e)*** *Ir-PTL0.025;* ***(f)*** *Ir-PTL0.05 using SEM [108].*

Table 5.1 Elemental concentration (wt %) of uncoated PTL, Ir-PTL0.005, Ir-PTL0.013, Ir-PTL0.025 and Ir-PTL0.05 using SEM-EDX [108].

Element (weight %)	**Ti**	**Ir**	**O**	**C**	**Y**
Uncoated PTL	83.8	0	9.1	6.8	0.4
Ir-PTL0.005	86.0	0.4	7.9	5.2	0.5
Ir-PTL0.013	85.4	2.0	7.0	5.3	0.3
Ir-PTL0.025	86.3	4.7	4.8	3.9	0.3
Ir-PTL0.05	81.9	9.6	4.1	4.0	0.4

5.1.2 FIB

Figure 5.2 shows the SEM images of FIB prepared cross-sections of all the samples. On the top of each PTLs, the Pt coating was deposited using electron beam and ion beam, respectively. A double deposition process was performed to protect the samples' surface as well as the prepared cross-section from scattered ions, thus reducing the artifacts of FIB milling (the so-called "curtaining effect") [111]. Compared to the uncoated sample, continuous and homogeneous films can be observed for all iridium-coated samples, even for the sample with the lowest Ir loading (Ir-PTL0.005 in Figure 5.2f). The thickness of iridium layers of Ir-PTL0.005, Ir-PTL0.013, Ir-PTL0.025, Ir-PTL0.05 are around 7 nm, 10 nm, 13 nm, and 27 nm, respectively. All the coated PTLs were homogeneously covered with Ir completely, which corroborated with the EDX data in Fig. 5.1.

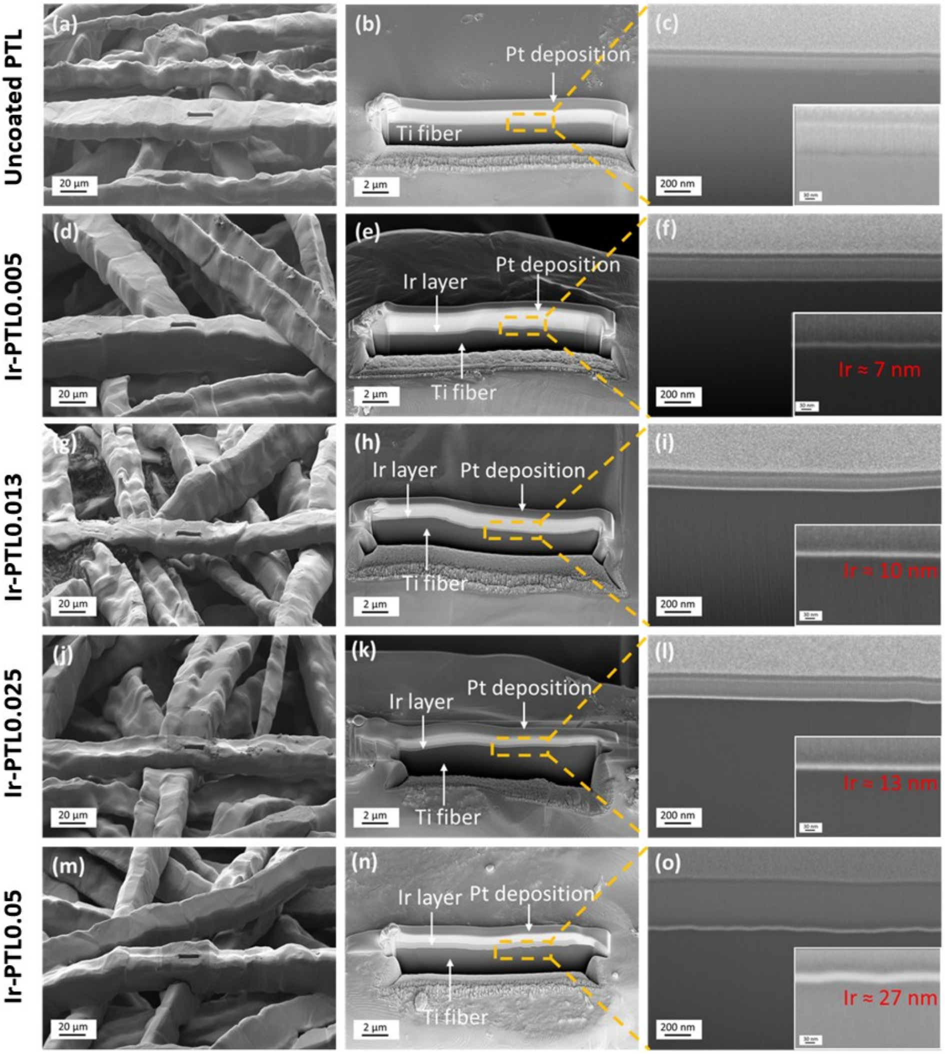

Figure 5.2 *FIB-SEM cross-sections image of* ***(a, b, c)*** *uncoated PTL;* ***(d, e. f)*** *Ir-PTL0.005;* ***(g, h, i)*** *Ir-PTL0.013;* ***(j, k, l)*** *Ir-PTL0.025;* ***(m, n, o)*** *Ir-PTL0.05 [108].*

5.2 Interfacial contact resistance (ICR)

Figure 5.3 shows the interfacial contact resistance (ICR) measurements performed under different pressures to characterize the electrical conductivity properties of the PTLs. The pressure used for clamping the test cells for polarization curves and EIS measurements is indicated as a shaded interval of the X-axis in Figure 5.3, which are the common pressure range for assembling a PEM water electrolyzer of the 25 cm^2 cell [121].

The ICR of uncoated PTL is higher throughout the entire compression range than all iridium-coated PTLs. As suggested from our previous publication and chapter 4, the higher contact resistance of uncoated PTL is caused by a naturally formed TiO_x surface passivation layer when exposed to ambient air [43]. For iridium-coated samples, the ICR gradually decreased with the increase of the sputtering time, indicating that the loadings of the iridium coating have a significant impact on the interfacial contact resistance. Ir-PTL0.025 and Ir-PTL0.05 had very similar results. Though there are overlaps of the standard deviation at lower compression at lower compaction forces (800 kpa - 2000 kpa), the contact resistance of these two samples is nearly identical over the whole compression pressure. The ICR results are in accordance with the polarization curves and impedance spectra presented in Figure 5.4 and 5.5.

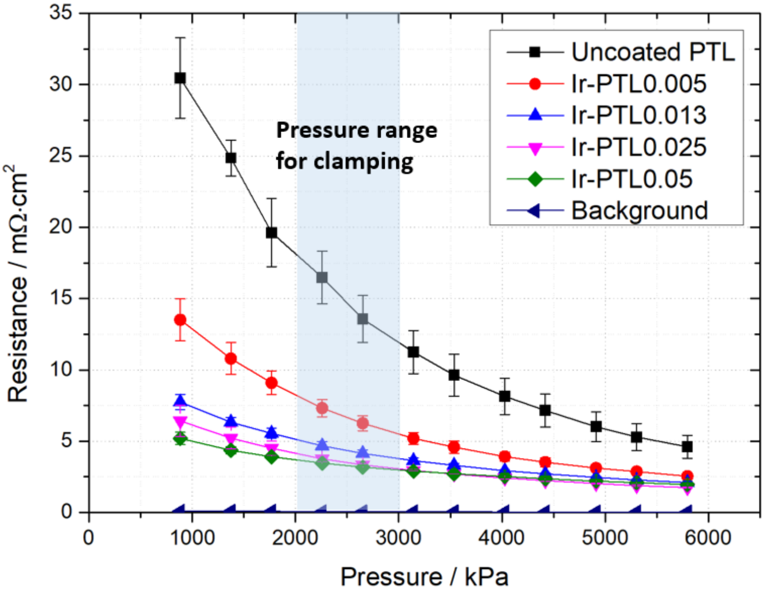

Figure 5.3 *Contact resistance of uncoated PTL, Ir-PTL0.005, Ir-PTL0.013, Ir-PTL0.025, and Ir-PTL0.05 using a conventional press setup where the PTLs are pressed between two gold-coated copper plates. The PTLs were mounted and tested dry, with tests run at 25 °C. Background: There is no sample between the two gold-coated plates [108].*

5.3 Electrochemical tests

5.3.1 Polarization curves

Figure 5.4 compares the cell performance of PTLs with different iridium loadings. Compared to the cell assembled with an uncoated PTL, the cell performances with Ir-PTL0.005 and Ir-PTL0.013 were improved by 50 mV and 70 mV at 1 A·cm^{-2}, respectively. The Ir-PTL0.025 and Ir-PTL0.05 showed identical performances, with both presenting an improved cell performance by 80mV at 1 A·cm^{-2}. However, the loading of Ir-PTL0.025 is only half of the loading of Ir-PTL0.05, which guarantees superior cell performance simultaneously with lower usage of iridium. The cell performance no longer depends on the loading of iridium coating above 0.025 mg·cm^{-2}. This value corresponds to the minimum amount of iridium coating required to obtain a good contact and electronic conduction between PTL and electrode. It should be noted that the performance difference between Ir-PTL0.013 and Ir-PTL0.025 is only around 10 mV, which might be due to the deviation from the MEAs. As previously mentioned, the deviation between the MEAs with the highest and lowest overvoltage from the same batch could be 11 mV. We speculated that the lowest loading of the Ir-coated PTL which can show the identical or close cell performance with Ir-PTL0.05 is around 0.013 to 0.025 mg·cm^{-2}.

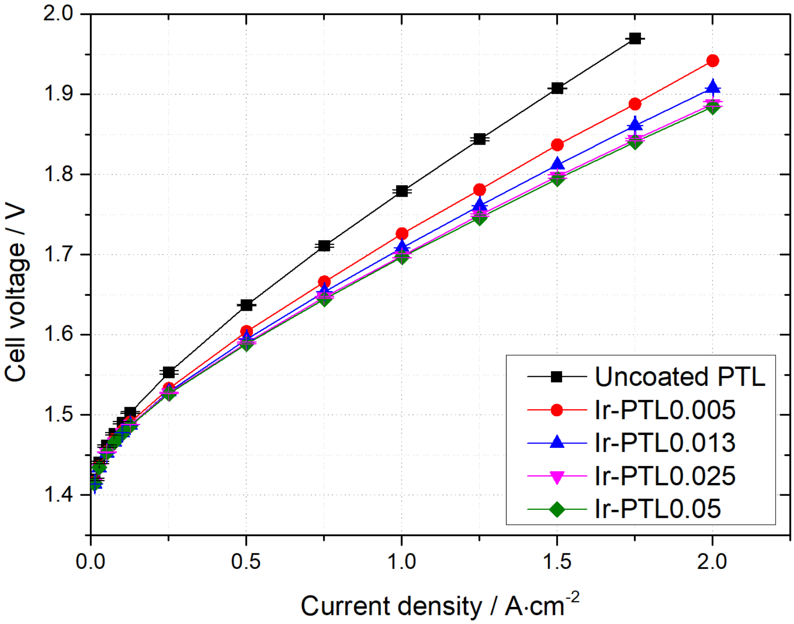

Figure 5.4 *Polarization curves of PEM water electrolyzer single cells assembled with uncoated PTL and iridium coated PTLs having different iridium loadings. The cell temperature was 80°C and under ambient pressure [108].*

Table 5.2 All different parameters, specifications, and results obtained for the PTLs tested in this study [108].

Sample	Sputter time/s	Ir Loading / mg·cm^{-2}	ICR@ 3000kpa/mΩ cm^2	E@ 1.0 A·cm^{-2}/V
Uncoated PTL	0	0	11.92	1.779
Ir-PTL0.005	30	0.005	5.50	1.726
Ir-PTL0.013	90	0.013	3.78	1.709
Ir-PTL0.025	180	0.025	3.06	1.699
Ir-PTL0.05	360	0.05	2.98	1.697

Note: The final Ir loading of the Ir-coated PTLs was calculated only for one side of them.

5.3.2 Electrochemical impedance spectra (EIS)

Electrochemical impedance spectra (EIS) of samples with different Ir loadings at the anodic PTL were recorded to investigate the effect of the Ir loading on the electrochemical processes. After measuring the polarization curve of each sample, the EIS was performed at 0.15 A·cm^{-2} and 80 °C. The Nyquist plots in Figure 5.5 show strongly distorted semi-arcs, which suggest the presence of two badly resolved processes with similar time constants, i.e. a smaller semi-arc at high frequencies and a larger semi-arc at low frequencies. Both semi-arcs are associated with the charge transfer in the rate determining step(s) of OER and double-layer charging in the anode catalyst layer. However, the reason for the appearance of two semi-arcs is still not clear. The EIS spectra were modeled by the equivalent electrical circuit shown in Figure 5.5. The low fitting error is less than 1%, which indicates that the fitting curves were in agreement with fitting the experimental data. The equivalent circuit consists of the ohmic resistance R_{Ω}, and two resistances R_{hf} and R_{lf} connected in parallel with constant phase elements, CPE_{hf} and CPE_{lf}, which result in two semi-arcs. The fitting parameters of EIS of different PTLs at 0.15 A·cm^{-2} are shown in Table 5.2 and Figure 5.5b.

The approximate values of double layer capacitances, $C_{dl,hf}$ and $C_{dl,lf,}$ can be determined from CPE values, their exponents n and the corresponding resistances by using Brug equation [122, 123]. The C_{dl} values shown in Table 5.3 are normalized to the geometric area. C_{dl} is not only proportional to the active surface but also depends on the coverage and the properties of the adsorbed intermediates in the potential range where Faradaic reactions like oxygen evolution reaction (OER) take place. Considering a roughness factor of several hundred up to thousand per mg of catalyst, the C_{dl} values correspond to pseudo double layer capacitances in the range of some tens of $\mu F/cm^2$ up to more than 100 $\mu F/cm^2$. The relatively high values are comparable with the results in the literature. In the case of OER on Pt in acid solutions, Conway observed a potential-dependent decrease of the pseudo-capacitance from values of more than 300 $\mu F/cm^2$ at $U/RHE < 1.5$ V down to values of less than 100 $\mu F/cm^2$ at potentials higher than 1.6 V[124]. The pseudo-capacitances are much higher than the capacity values in the range of some tens of $\mu F/cm^2$ obtained under non-Faradaic conditions, which means the pseudo-capacitance of the OER active area is higher than the double-layer capacitance of those parts of the catalyst/ionomer interface, which are less active or even inactive with respect to the OER. The outer parts of the catalyst layer close to the PTL are less active, and the reduced OER activity is caused by the resistance of proton transport in the catalyst layer. Inactive parts of the catalyst/ionomer interface have no contact with continuous paths of electron and/or proton conduction [125].

In any case, even the Ir-coated PTL with the lowest Ir loading (Ir-PTL0.005) causes a significant increase in C_{dl}. If an increase in active surface of the PTL would be the only reason for the higher C_{dl} values, a smaller effect would have been expected because the active area of the catalyst layer should be much larger than the sputtered coated Ir layer on the PTL. It can be assumed that the contact resistance plays an important role because the largest decrease of the ICR is obtained when the PTL was coated with only 0.005 $mg_{Ir}\cdot cm^{-2}$. If a poor contact between the catalyst layer and PTL would impede the electron supply to Ir particles in the catalyst layer, the catalyst utilization, and thus the active area and C_{dl} values would decrease. Correspondingly, the catalyst utilization and the C_{dl} values increase when applying the Ir coating.

The relatively small effect of higher Ir loadings on the ICR would also explain why a further increase in Ir loading does not have a great impact on C_{dl}. It should be noted that the fitting error (see error bars in Figure. 5.5b) and the approximate values derived from the Brug equation should be taken into account as well. When the PTL was coated with 0.005 $mg_{Ir}\cdot cm^{-2}$, the relative decrease of CPE and C_{dl} is larger for the high frequency capacitance. This suggests that the high frequency semi-arc may be associated with processes on Ir catalyst sites in the outer part of the catalyst layer respectively the PTL. However, the main impact of the ICR is on the ohmic resistance. Therefore the largest part of the gain in performance when sputtering a protective layer of Ir on the PTL is due to a considerable decrease in R_Ω (compare the high frequencies intercepts). In contrast, the sum of the resistances R_{hf} and R_{lf} decreases to a much smaller extent (compare the differences of low frequency and high frequency intercepts in Figure 5.5a).

Generally, the ohmic loss of a PEM water electrolyzer cell is the sum of the ohmic resistances originating from the bulk resistances of each component including membrane, catalyst layers, PTLs, bipolar plate, etc., as well as the interfacial resistances between the components [58]. The main part of the ohmic loss stems from the membrane and interface between each component [12]. The bulk components that were used for the MEAs are the same, and the only difference is whether the surface is modified by Ir coating or not. Therefore, it is the decrease of the interfacial resistance of the PTL that resulted in the decrease in ohmic resistance. Although the R_Ω decreases almost linearly with the decrease of interfacial resistance, the effect of Ir loading on R_Ω is nearly one order of magnitude higher than compared to the effect of Ir loading on the ICR (compare the change of the R_Ω and ICR values in Table 5.2). According to the previous publication in our group, this result can be explained by the considerable difference of the ex-situ conditions of the ICR tests and electrolyzer cell operating conditions regarding pressing force, temperature, materials, etc [10].

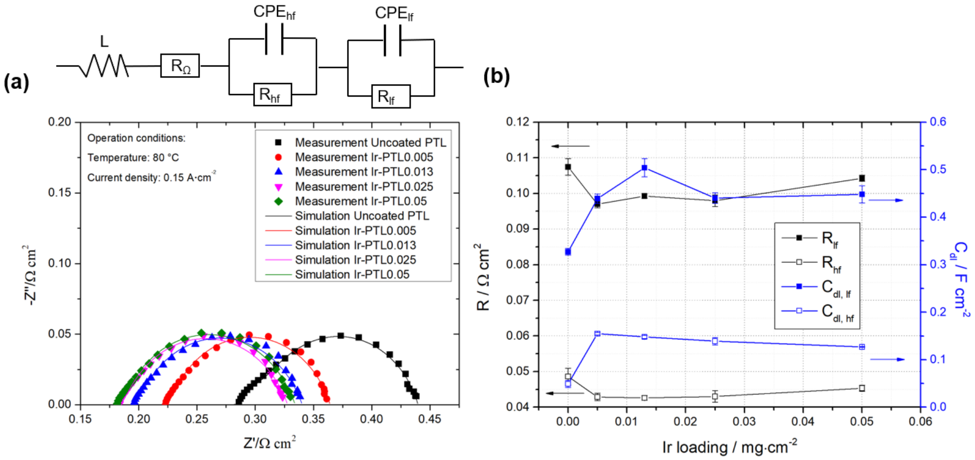

Figure 5.5 (a) *EIS results at 0.15 A·cm*$^{-2}$ *and equivalent circuit fitting;* ***(b)*** *Kinetic resistances,* R_{hf}/R_{lf}*, and double layer capacitances,* $C_{dl,hf}/C_{dl,lf}$*, obtained from the fits of the impedance spectra shown in Fig. 5.5****a****. The error bars show the individual fitting errors of each value [108].*

Table 5.3 The fitting parameters of EIS of different PTLs at 0.15 A·cm^{-2} [108].

Sample	R_Ω/Ω cm^2	R_{lf}/Ω cm^2	R_{hf}/Ω cm^2	CPE$_{lf}$/ Ω^{-1}s^{n}cm^{-2}	CPE$_{hf}$/ Ω^{-1}s^{n}cm^{-2}	n_{lf}/-	n_{hf}/-	$C_{dl,lf}$/ F cm^{-2}	$C_{dl,hf}$/ F cm^{-2}
Uncoated PTL	0.283	0.107	0.049	0.545	0.516	0.848	0.611	0.327	0.049
Ir-PTL0.005	0.222	0.097	0.043	0.648	0.672	0.877	0.707	0.439	0.155
Ir-PTL0.013	0.195	0.099	0.043	0.719	0.664	0.882	0.704	0.504	0.148
Ir-PTL0.025	0.183	0.098	0.043	0.642	0.659	0.88	0.696	0.440	0.139
Ir-PTL0.05	0.181	0.104	0.045	0.636	0.651	0.886	0.683	0.448	0.127

As shown in Figure 5.6 and Table 5.2, the ohmic loss, the interfacial contact resistance (ICR) at 3000 kPa, and the cell voltage at 1.0 A·cm^{-2} decrease exponentially with increasing Ir loading. R_Ω, ICR and cell voltage remain virtually constant when the Ir loading on PTL is of 0.013 mg·cm^{-}

^{2} or more. Hence, concerning a reduction of the precious metal costs, an Ir loading of 0.013 - 0.025 mg·cm^{-2} would be sufficient to achieve the identical cell performance as Ir-PTL with higher Ir loading. From the overall decrease of the cell voltage, a decrease of the overall resistance ΔR_{sum} for each current density can be calculated. Because cell voltage and R_Ω were both measured under electrolyzer operating conditions, the decrease in the overall resistance should be similar to the decrease in the ohmic resistance, ΔR_Ω. This is indeed the case: when comparing uncoated PTL and Ir-PTL0.05, values of ≈ 0.08 Ω·cm^2 (ΔR_{sum}) and ≈ 0.09 Ω·cm^2 (ΔR_Ω) are obtained at a current density of 1.5 A·cm^{-2}. This result also confirms that the considerable gain in performance is predominantly due to the significant reduction of the interfacial resistance of the PTL and the adjacent layers based on the suppression of Ti oxide formation in the presence of the Ir coating.

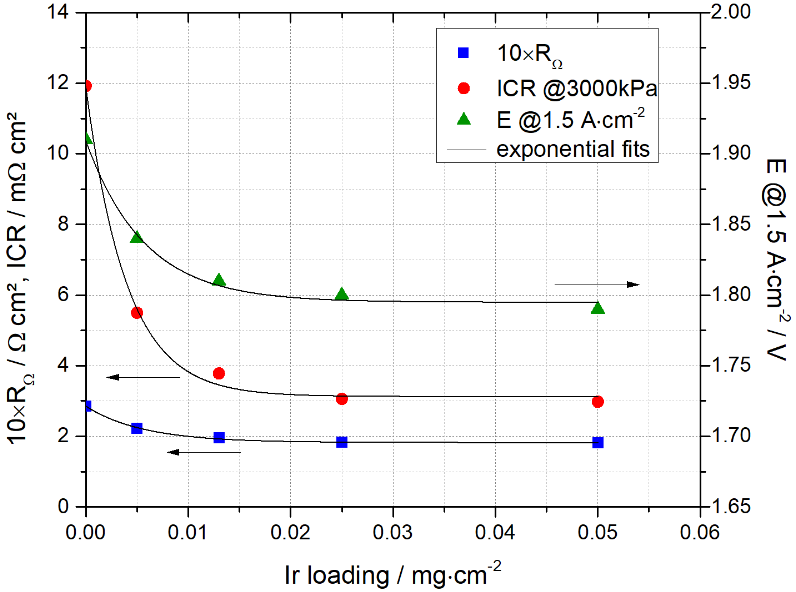

Figure 5.6 *Cell voltage versus Ir loading at 1.5 A·cm^{-2} (compare Figure 5.4); Contact resistance versus Ir loading at 3000 kPa (compare Figure 5.3); Ohmic resistance measure by impedance spectroscopy at 0.15 A·cm^{-2} multiplied by a factor of 10 to extrapolate to 1.5 A·cm^{-2} where the cell voltage was measured (compare Table 5.3) [108].*

However, as shown in Figure 5.5b, the small decrease of R_{hf} and R_{lf} cannot be neglected. Both resistances decrease by about 10% when increasing the Ir loading from 0 to 0.025 mg·cm^{-2}. Totally,

R_{hf} and R_{lf} contribute about 13% of the overall decrease of the total resistance, and 87% is due to the decrease of R_{Ω}. This additional gain in performance can be explained by the electrochemical activity of the Ir coating layer towards the OER, which is demonstrated in Figure 5.7: here, both MEAs include an Ir-coated PTL on the anode side, but one of them were assembled with a “half-side CCM”.

The half-sided CCM assembled with Ir-coated PTL were manufactured without IrO_2 catalyst layer at the anode side but with 0.8 $mg_{Pt}\cdot cm^{-2}$ Pt at the cathode side. Figure 5.7 shows that electrochemical activity is observed for the half-sided sample, although their cell performance was, as expected, lower than that of the reference CCM with the same Ir loading. When the Ir-coated PTL is pressed on the soft Nafion membrane, the latter will to some extent penetrate into the porous Ir-coated PTL to some extent (and *vice versa*), supposedly forming a three-phase boundary of the Ir, Nafion membrane, and gas phase, which represents the active area. However, despite the same Ir loading, the anode catalyst layer in the CCM0.1 showed significantly higher performance than the sputtered Ir layer. Compared to an Ir-coated PTL, the reference CCM0.1 shows a higher active area. The electrochemically-active area of the Ir-coated PTL shall be significantly smaller than that of a normal catalyst layer because the pore structure is much coarser and there is no additional ionomer to extend the catalyst/ionomer contact area (compare this with the top view of the Ir-coated PTL and CCM samples in Figure 5.8).

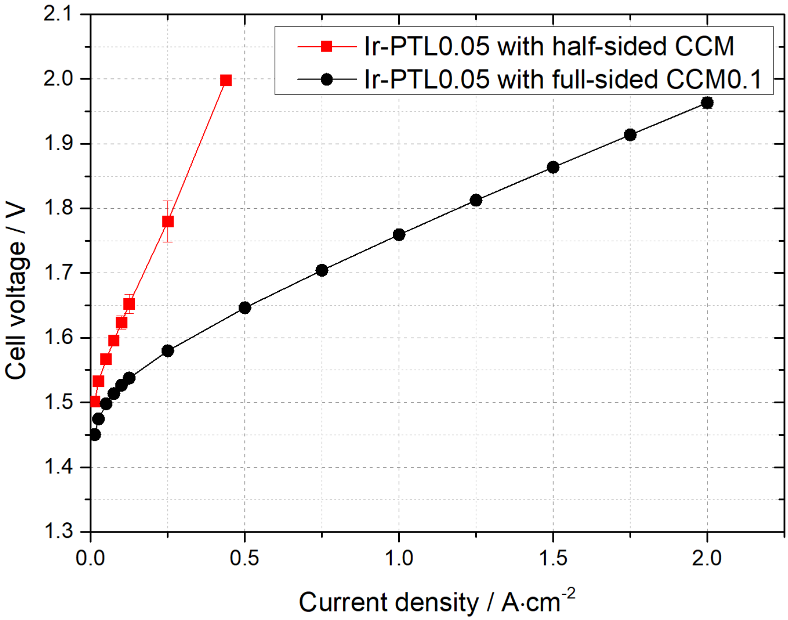

Figure 5.7 *Polarization curves of PEM water electrolyzer single cells assembled with Ir-PTL0.05; one is with normal(full-sided) CCM containing 0.1 mg·cm*$^{-2}$ *IrO*$_2$ *at anode and 0.8 mg·cm*$^{-2}$ *Pt/C at cathode (black), the other one (referred to as half-sided CCM) is without IrO*$_2$ *at anode but just 0.8 mg·cm*$^{-2}$ *Pt/C at the cathode (red).*

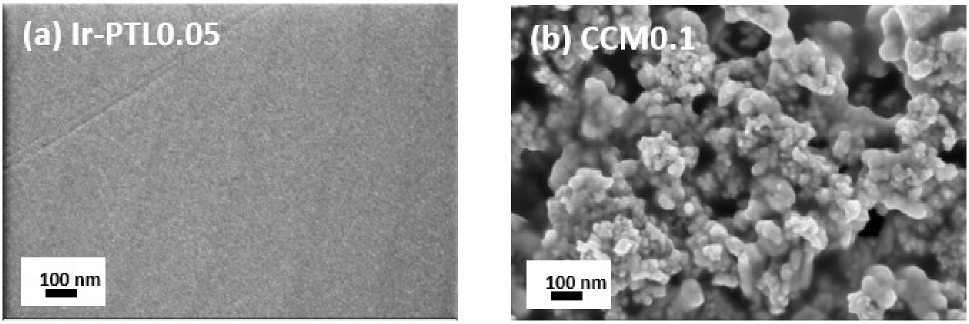

Figure 5.8 *High-resolution SEM images of:* ***(a)*** *Ir-PTL0.05;* ***(b)*** *CCM0.1 [108].*

5.4 Summary

In this chapter, the effects of different loadings of iridium as a protective layer on titanium-based PTLs were comprehensively investigated. The Ir loadings of Ir-coated PTLs were modified by changing the sputtering time, and the specific thickness of the loading was confirmed by using cross-sectional FIB-SEM. The results showed that all different loadings of iridium layers on titanium-based PTLs, even the lowest loading of 0.005 $mg_{Ir}\cdot cm^{-2}$, reduced contact resistance between PTLs and catalyst layers and increased the cell performance. The Ir layer not only decreases the ohmic resistance, which is the biggest part of the performance gain but also decreases the resistances associated with charge transfer towards OER. The amount of iridium was reduced to 0.025 $mg\cdot cm^{-2}$ and showed identical cell performance as PTLs with higher iridium loading. Compared to uncoated PTL, the overpotential of the cell with this loading decreased by 80 mV operated at 1.0 $A\cdot cm^{-2}$. Moreover, electrochemical activity is observed on the Ir-coated PTL. The Ir protective layer on the PTL not only decreases the ohmic resistance significantly, which is the largest part of the gain in performance, but moreover, the oxygen evolution reaction (OER) activity of the iridium layer makes it promising as a cost-effective catalyst layer. The results in this chapter not only demonstrate a scalable and easy approach to reduce interface resistivity between PTL and electrode, but also provide a promising way to reduce the overall costs of PEM water electrolyzers.

6. Durability of Ir-coated PTL

Titanium is typically used to construct cell and stack components including porous transport layers (PTLs) and bipolar plates. Due to the harsh acidic conditions, high cell overpotentials, and oxygen gas evolution at the anode, titanium (Ti^0) changes its oxidation state over time, leading to the drastic degradation of the components on the anode side. The critical passivation of titanium-based PTL is one significant factor that restricts the development of PEM water electrolyzers [15, 16]. Chapter 5 investigates the effects of the loading of Ir on the PTLs. In chapter 6, the durability of Ir-coated and uncoated titanium-based PTLs is investigated via a 4000 hours durability test at 2V and 80 °C and a series of post-mortem analysis. This chapter investigates how the interface of well-protected titanium fiber behaves against passivation after 4000 hours under real electrolysis conditions. This work was published [126].

6.1 Electrochemical characterization

6.1.1 Durability measurement

Figure 6.1 shows the relative current density over the 4000 hours for cells assembled with uncoated and Ir-coated PTL(total Ir loading is 0.1 $mg\cdot cm^{-2}$). Both cells were operated at a constant voltage of 2V and 80 °C. The average value of current density in 200 ~ 250 h (conditioning) was determined to be 100%. The cell assembled with Ir-coated PTL did not show any significant decay (less than 1%) in performance over 4000 hours. However, the cell assembled with an uncoated PTL showed a 55% current density decrease after 4000 hours of operation.

In order to distinguish the degradation at different period more clearly, the operating durability time can be divided into three timescales (Figure 6.2): I) up to 250 h (conditioning), II) 288-2490 h, and III) 2859-4000 h. The first zone from beginning to 250 h is regarded as conditioning or 'break-in' mode (Figure 6.2a). In this period, both cells were unstable. It should be noted that to get the degradation rate after the cells ran constantly, the first points of the second and third periods (at 288 h and 2859 h) were removed when calculating the degradation rate. The interruption of the measurements between 250 h ~ 288 h and 2490 h ~ 2859 h caused reversible parts of degradation to recover and resulted in a substantially reduced degradation [9], which showed an increase of current density at these two initial points at 288 h and 2859 h. During these two interruptive periods, the cells just ran with water flow but without warm-up and potential. In the second period from

288~2490 h regarded as the constant mode (Figure 6.2b), the cell with Ir-coated PTL showed degradation of 2.3 mA·h^{-1}, while the degradation rates for the cell with uncoated PTL was 5.7 mA·h^{-1}. During the period from 2859 to 4000 h (Figure 6.2c), some interruptions in performance with subsequent recovery, such as the point that can be seen at 3434, 3559, and 3758 hours are related to variation in cell operating conditions, variation in power, and water supply, and other typical issues arise when running electrochemical devices for a long period time [9-11]. Uncoated PTL showed a significantly higher degradation rate than Ir-coated PTL during this period, which indicates that uncoated PTL was not able to survive with intermittent power supply in a real PEM water electrolyzer application. The degradation rates in different periods are shown in Table 6.1.

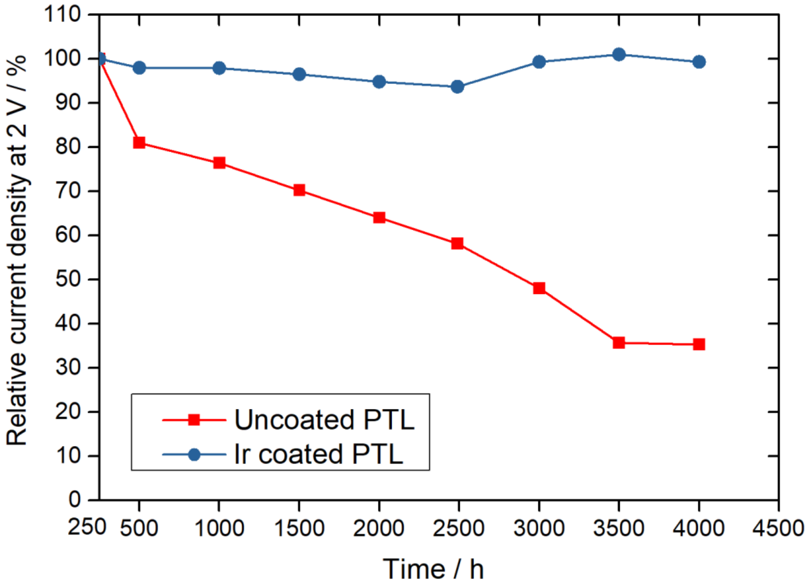

Figure 6.1 *Relative current density at 2 V (the average value of current density in 200-250 h (conditioning) was determined to be 100%); The current density at the starting point for Ir-coated PTL is 2.87 A·cm^{-2}, uncoated PTL is 2.58 A·cm^{-2}.*

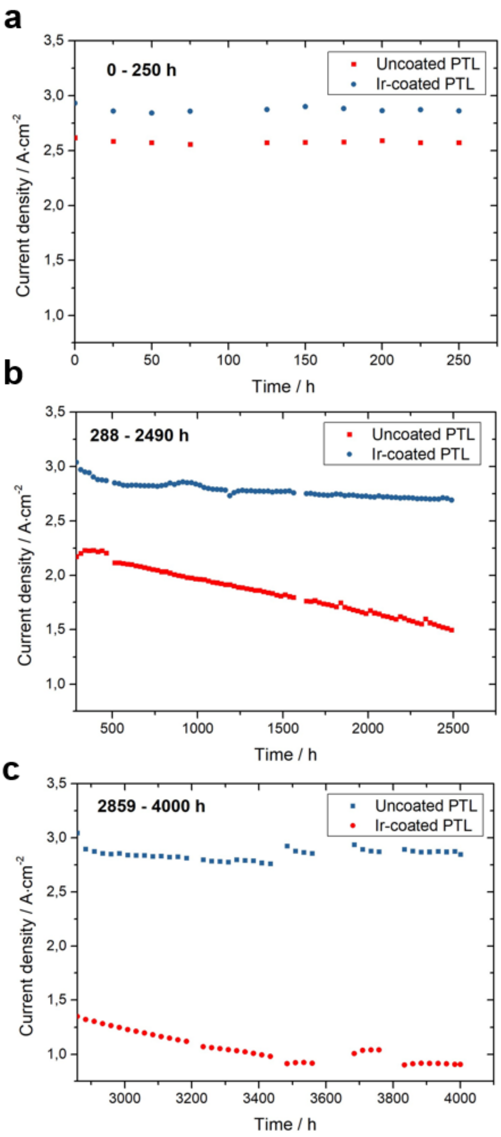

Figure 6.2 (a) *Current density at 80 °C during long-term operation at 2 V from beginning to 250h;* ***(b)*** *Current density at 80 °C during long-term operation at 2 V from 288h to 2490h;* ***(c)*** *Current density at 80 °C during long-term operation at 2 V from 2859h to 4000h.*

Table 6.1 Degradation rate of Ir-coated, and uncoated-PTL at different periods.

Zone	Ir-PTL	Uncoated-PTL
0-250h	Conditioning	Conditioning
288-2490h	2.3	5.7
2859-4000h	0.8	6.3

Degradation rate: mA·h^{-1}

6.1.2 Polarization curve

Figure 6.3 compares the polarization curves of cells assembled with Ir-coated and uncoated PTLs taken at the beginning and end of the test, which are in agreement with the long-term profiles. At the beginning of the test, the cell voltage of Ir-coated PTL was 40 mV lower at 2 A·cm^{-2} than the uncoated sample, which was due to the use of Ir coating on PTL at the anode side. In Chapter 4, the results showed that the iridium layer reduces the overall ohmic resistance of the PTL/catalyst layer interface and improves cell performance. After 4000 hours of operation, cells with Ir-coated PTL showed identical cell performance as the performance at the beginning of the test. However, decreased cell performance can be observed for uncoated PTL. This indicates that the cell with Ir-coated PTL is very stable over the 4000 hours operation, and the iridium protective coating effectively mitigated the degradation of the cell.

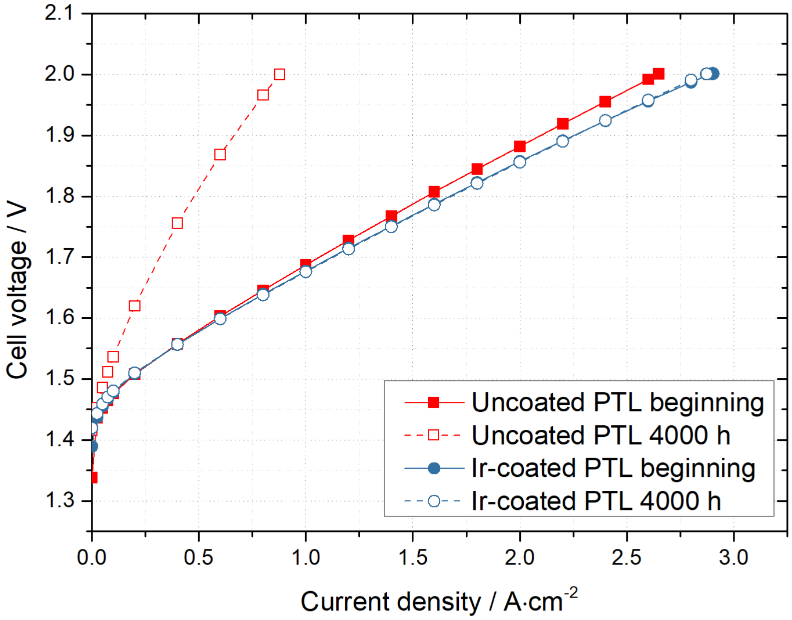

***Figure 6.3** Polarization curves of PEM water electrolyzer single cells assembled with uncoated and Ir-coated PTL before and after 4000 hours.*

6.1.3 EIS

Figure 6.4 compares the electrochemical impedance spectroscopy (EIS) results of the cells assembled with Ir-coated and uncoated PTL, respectively. EIS was run at a DC-bias of 1.9 A·cm^{-2} under a current perturbation of ±5%, with a maximum perturbation of 10mV between 100 kHz and 100 mHz, at 80°C. Prior to the durability test (2V, 80°C), the high frequency resistance (HFR) of Ir-coated sample was 0.161 Ω cm^2, while the HFR of uncoated sample was 0.179 Ω cm^2. After 4000 hours of operation, the HFRs of Ir-coated PTL were not significantly changed. However, the HFR of uncoated sample increased from 0.179 Ω·cm^2 to 0.347 Ω·cm^2. This indicates that the ohmic loss can be decreased dramatically by using iridium as a protective coating. It should be noted that the way to show EIS spectra here is unusual, as the Nyquist plots should have the same scale size on both axes.

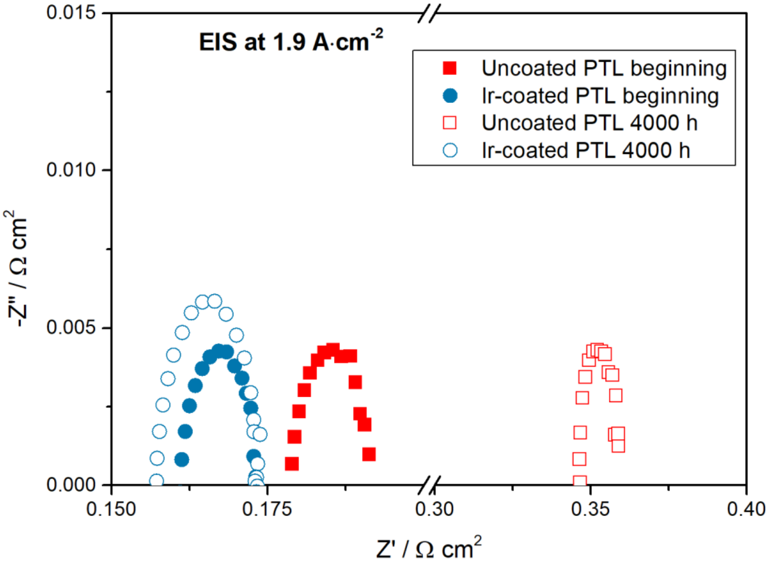

***Figure 6.4** EIS results at 1.9 A·cm^{-2}.*

6.2 Post-mortem characterization

6.2.1 Interfacial contact resistance (ICR)

Interfacial contact resistance (ICR) was performed under different compressions to investigate the improved electrical and interfacial contact behavior of the coatings, and aid the interpretation of the degradation rates presented. To calculate the through-plane resistance, which is the sum of the PTL resistance, along with the two contact resistances presenting between the samples and gold-coated plates, the plate-to-plate voltage drop was measured. In the through-plane direction, contact resistance is the major factor affecting the conductivity of PTL [119]. Figure 6.5 compares the interfacial contact resistance of uncoated and Ir-coated PTLs before and after the durability test. The pristine Ir-coated PTL showed higher contact resistance throughout the entire compression range, while the pristine uncoated PTL showed a significantly higher resistance over all compression ranges. This was due to the use of Ir coating on the Ir-coated PTL. After 4000 hours, the Ir-coated PTL did not show any significant increase in contact resistance. The pressure used for clamping the test cells for polarization curves and EIS measurements is indicated as a shaded interval of the X-axis in Figure 6.5, which is the common pressure range for assembling a

PEM water electrolyzer of the 25 cm^2 cell [121]. Compared to an Ir-coated PTL, an uncoated PTL showed a dramatic increase in contact resistance of 79.6 mΩ·cm^2 at 3000 kpa. However, there is only a minor increase of interfacial contact resistance in an Ir-coated PTL, indicating that Ir-coated PTL is quite stable over the 4000 h durability test. These contact resistance results corroborate well with the results obtained from the polarization curves and durability profiles.

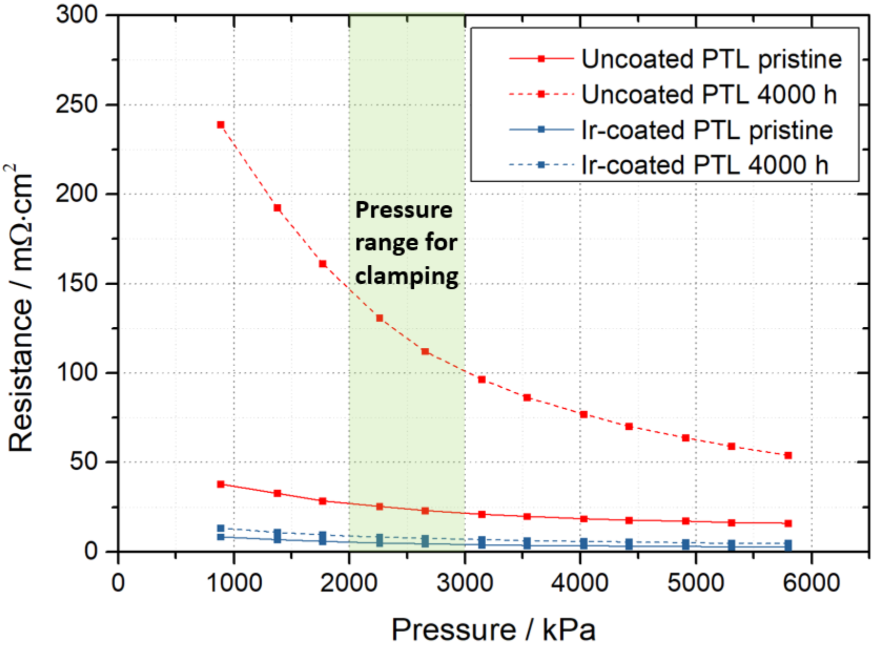

Figure 6.5 *Contact resistance of uncoated and Ir-coated PTL before and after 4000 hours using a conventional press setup where the PTLs are pressed between two gold-coated copper plates. The PTLs were mounted and tested dry, with tests run at 25 °C.*

6.2.2 Optical and SEM images

To explain the drop in performance exhibited by the uncoated PTL, it is necessary to look into the results obtained using optical and SEM images. Figure 6.6 display the surface images of the uncoated PTL before and after 4000 hours of operation. The image highlights the detrimental impact of operating an uncoated PTL for ≈ 4000 hours under real electrolysis operating conditions. On the side that faces the CCM (electrode), the catalyst residuals can be observed due to the delamination from the catalyst layer (Figure 6.6d-f). The other region without catalyst residuals is titanium, which showed corrosion-yielding structures of 30 nm scale. A similar morphology change of titanium was observed on the other side that faces to bipolar plate (Figure 6.6 i). However, no catalyst delamination was observed in the Ir-coated PTL before and after 4000 hours of operation (Figure 6.7d-f). With regard to the Ir-coated sample, only minor catalyst layer peeling off from the membrane was observed on the side that faces CCM. Figure 6.7 e, f, h, i showed almost no morphology changes, which indicates that the iridium protective layer is fully stable over 4000 hours at 2V.

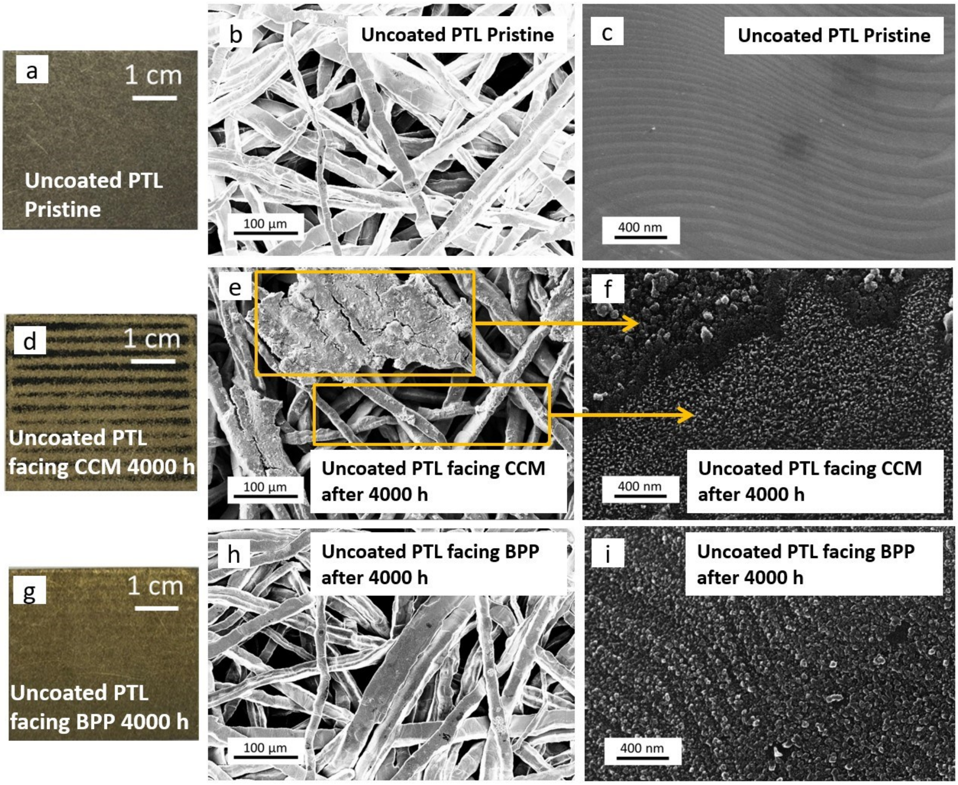

Figure 6.6 (a, b, c) *Optical and scanning electron microscopy (SEM) images of pristine uncoated PTL;* ***(d, e, f)*** *Optical and scanning electron microscopy (SEM) images of uncoated PTL facing CCM side after 4000 hours of operation;* ***(g, h, i,)*** *Optical and scanning electron microscopy (SEM) images of uncoated PTL facing CCM side after 4000 hours of operation [28].*

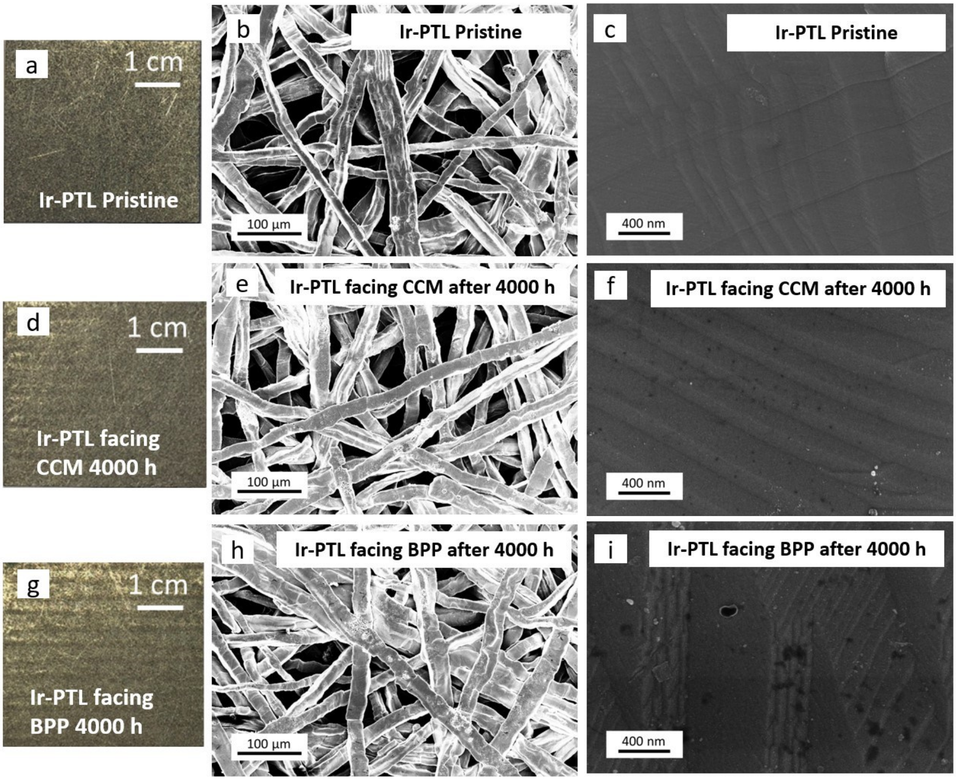

Figure 6.7 ***(a, b, c)*** *Optical and scanning electron microscopy (SEM) images of pristine Ir-coated PTL;* ***(d, e, f)*** *Optical and scanning electron microscopy (SEM) images of Ir-coated PTL facing CCM side after 4000 hours;* ***(g, h, i)*** *Optical and scanning electron microscopy (SEM) images of Ir-coated PTL facing CCM side after 4000 hours [28].*

6.2.3 AFM

Atomic force microscopy (AFM) measurements were taken to obtain additional information on the conductivity of all the PTLs before and after the durability test. The AFM results are in agreement with the SEM results. Compared to pristine Ir-coated PTL (Figure 6.9 d), the pristine uncoated sample showed a much lower conductivity (Figure 6.8 d). After 4000 hours of operation, on the side facing the bipolar plate, numerous spots that had a much higher deformation than the surrounding titanium were observed (Figure 6.8b). On the side facing the CCM, the conductivity of the uncoated PTL was significantly higher than the pristine uncoated sample due to the good conductivity of the catalyst residuals, which were transferred from the CCM to the PTL (Figure 6.8 f). However, as shown in Figures 6.9 d-f, a comparable amount of conductive area on the Ir-coated PTL was observed before and after the durability test, which indicates that the iridium coating remains stable throughout the 4000 hours of operation.

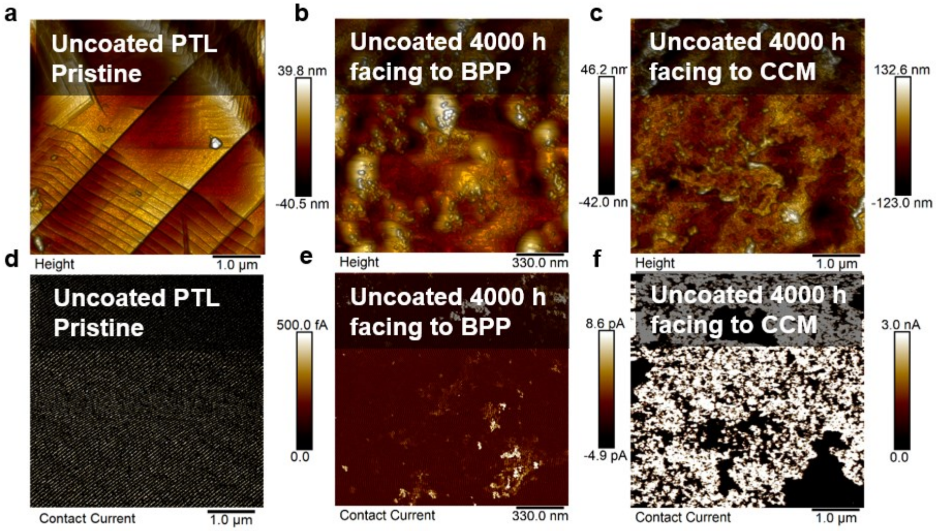

Figure 6.8 ***(a)*** *AFM height measurement of pristine uncoated PTL;* ***(b)*** *AFM height measurement of aged uncoated PTL facing to BPP side;* ***(c)*** *AFM height measurement of aged uncoated PTL facing to CCM side;* ***(d)*** *AFM conductivity measurement of pristine uncoated PTL;* ***(e)*** *AFM conductivity measurement of aged uncoated PTL facing to BPP side;* ***(f)*** *AFM conductivity measurement of aged uncoated PTL facing to CCM side [28].*

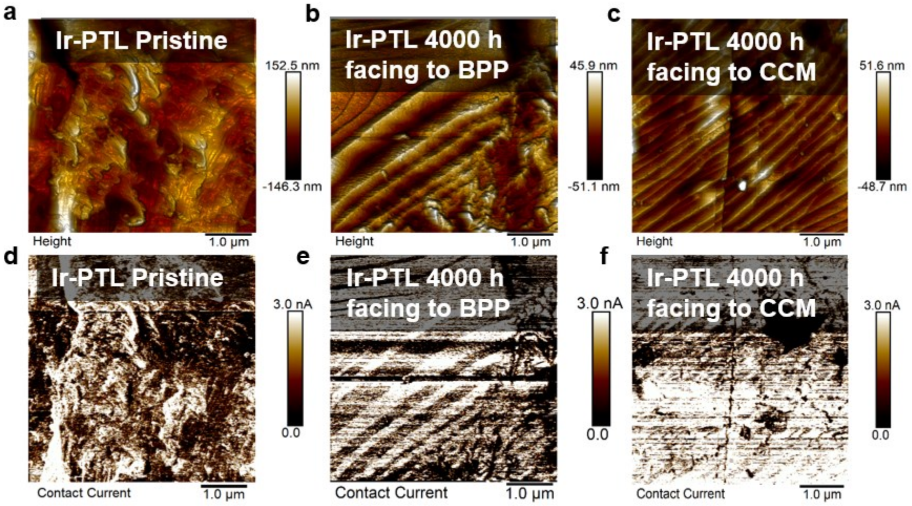

Figure 6.9 (a) *AFM height measurement of pristine Ir-coated PTL;* ***(b)*** *AFM height measurement of aged Ir-coated PTL facing to BPP side;* ***(c)*** *AFM height measurement of aged Ir-coated PTL facing to CCM side;* ***(d)*** *AFM conductivity measurement of pristine Ir-coated PTL;* ***(e)*** *AFM conductivity measurement of aged Ir-coated PTL facing to BPP side;* ***(f)*** *AFM conductivity measurement of aged Ir-coated PTL facing to CCM side [28].*

6.2.4 EDX after FIB cross-section

Figure 6.10 shows the EDX composition mapping images after the FIB cross-section. The natural titanium oxide layer (pink) of pristine PTL is around 7 nm, which corresponds to the range reported in the literature for titanium films after oxidation when exposed to air [79]. After 4000 hours durability test, TiO_x layer was deteriorated and became thicker in the absence of a protective layer. In addition, the TiO_x layer increased to 40 at% oxygen in terms of its composition after 4000 h.

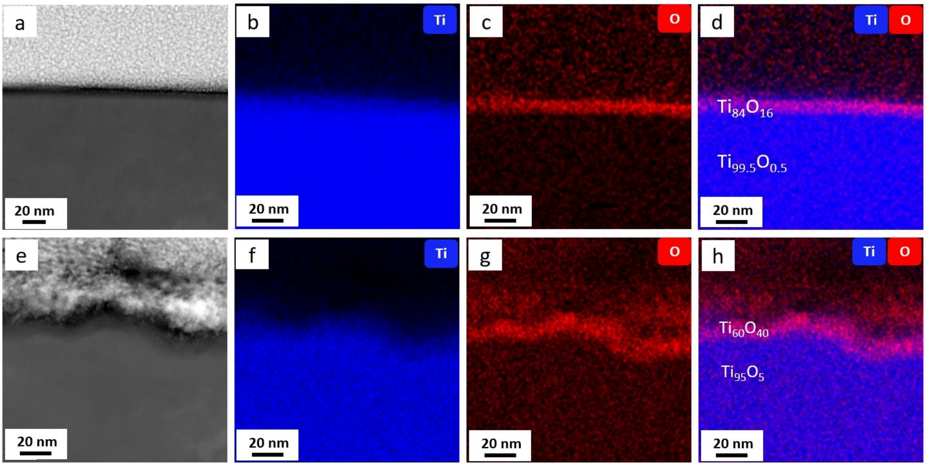

Figure 6.10 *High-angle annular dark-field scanning transmission electron microscopy (HAADF-STEM) images* ***(a)*** *pristine uncoated PTL;* ***(e)*** *aged uncoated PTL; Elemental distribution of Ti (blue) and Ir (red) in EDX composition maps after FIB cross-section of* ***(b, c, d)*** *pristine PTL;* ***(f, g, h)*** *aged uncoated PTL [28].*

Figure 6.11 shows the real morphology of the interface of an Ir-coated PTL before and after 4000 hours of operation under PEM water electrolysis anodic conditions. Figure 6.10a and b display the EDX composition maps after the focused ion beam (FIB) cross-section, which indicate that the protective metallic iridium layer contains 2 at% oxygen (green) and has a thickness of only 20 nm before the operation. The naturally formed titanium oxide layer (pink) is around 5 nm and lies beneath the added Ir layer. The bulk titanium of the fiber has a ratio of 90:10 Ti:TiO$_x$ prior to operation. After 4000 hours of operation, the iridium layer (green) on the fiber maintains its 20 nm thickness and remains intact and does not show any decrease in thickness. Additionally, the results show that the iridium layer is mostly in its metallic state, which increases to only 8 at% oxygen in terms of its composition. The results in Figure 6.11f-h indicate that the oxygen present in the iridium layer is localized, more specifically at the surface (red). This suggests that the iridium layer was subjected to an initial oxidation process that most likely occurred in the first hours of operation, while further oxidation of metallic iridium did not propagate to the bulk during the entire test. Therefore, iridium oxidation and the subsequent dissolution that typically happens with iridium catalysts might not apply to iridium layers over PTLs. Here, the iridium layer is subjected to different conditions due to its different location, outside the acidic condition produced by the Nafion ionomer in the catalyst layer inside the cell. With metallic iridium remaining in bulk, the iridium layer provided optimal conditions to ensure both acceptable electrical conductivity and corrosion resistance. However, the most remarkable result is that the thin layer of iridium prevented the growth of the TiO_x (or passivation layer) underneath the iridium (Figure 6.11f-h, in pink), which would have led to a significant increase in cell resistance. Further improvements such as the elimination of the passivation layer, do not seem to promise any significant benefits, as the expected performance gain would not exceed a few mV.

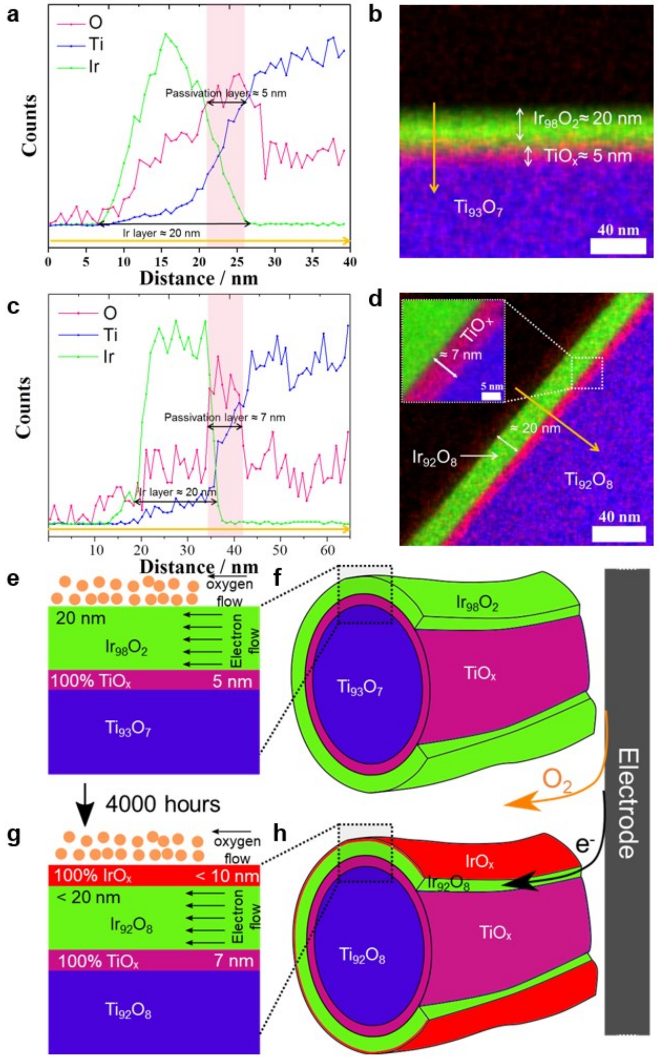

Figure 6.11 *EDX composition analysis of Ir-coated PTL.* ***a, c,*** *Line scanning profile after FIB cross-section of Ir-coated PTLs* ***(a)*** *Pristine Ir-coated PTL;* ***(c)*** *Ir-coated PTL after 4000 h operation.* ***b, d,*** *Elemental distribution of Ir (green), O (red) and Ti (blue) in EDX composition maps* ***(b)*** *Pristine Ir-coated PTL;* ***(d)*** *Ir-coated PTL after 4000 hours of operation.* ***e, g,*** *Corresponding schematics of elemental distribution of Ir, O, Ti in EDX composition maps* ***(e)***

Pristine; ***(g)*** *After 4000 h operation.* ***f, h,*** *Schematics of one Ir-coated Ti fiber* ***(f)*** *Pristine;* ***(h)*** *After 4000 h operation [28].*

6.2.5 XPS

X-ray photoelectron spectroscopy (XPS) depth profile analysis for the PTLs before and after the durability test is shown in Figure 6.12, which was used to determine material changes before and after the durability test. More XPS depth profiles can be found in Figure 12.4 in the appendix. The results strongly correlate with the cross-section data presented in Figure 6.11. Both Ir-coated and uncoated PTLs were etched under the argon ion beam to remove atomic layers and thus access deeper areas during continuous analysis. In order to quantify the oxide and metal species, the Ti 2p and Ir 4f signals were deconvoluted (Figure 6.12b and d). Figure 6.12a shows the corresponding oxide-metal ratios versus the etching time. The metal ratio of TiO_x of the pristine uncoated PTL decreased with Ar^+ etching time, which indicates that the titanium oxide passive layer was formed naturally before long-term operation. At the surface ($t_{etching}$= 0s) of the uncoated sample, the TiO_x:Ti atomic ratio equals 20:1. After an etching time of 110 s, the TiO_x:Ti atomic ratio drops to almost zero, i.e., the Ti-metallic peaks (Ti $2p_{1/2}$ at 460.4 eV and Ti $2p_{3/2}$ at 454.5 eV) become prominent species, while oxide peaks (Ti $2p_{1/2}$ at 464 eV and Ti $2p_{3/2}$ at 458 eV [43]) vanish, which corresponds to the transition from the surface oxide layer to the metallic Ti bulk. The surface TiO_x:Ti ratios of aged uncoated PTL equal 40-60:1 in the range <100 s, which demonstrate the increase in TiO_x concentration at the surface of uncoated PTL after 4000 hours of operation. In contrast, the IrO_x:Ir (Ir^{4+} $4f_{5/2}$ / $4f_{7/2}$: 65.4 eV / 62.3 eV; Ir^0 $4f_{5/2}$ / $4f_{7/2}$: 63.8 eV /60.7 eV;) atomic ratio of Ir-coated PTL is close to zero, with exemption of a topmost IrO_x layer, significantly smaller than that of the uncoated PTL.. After 4000 hours of operation, the ratios remain almost identical. This is also in accordance with the EDX composition maps and line scan results, which show that the ratio of iridium to oxygen is around 92:8 after 4000 hours of operation (Figure 6.11). The results clearly indicate the iridium layer was stable during the 4000 hours of operation.

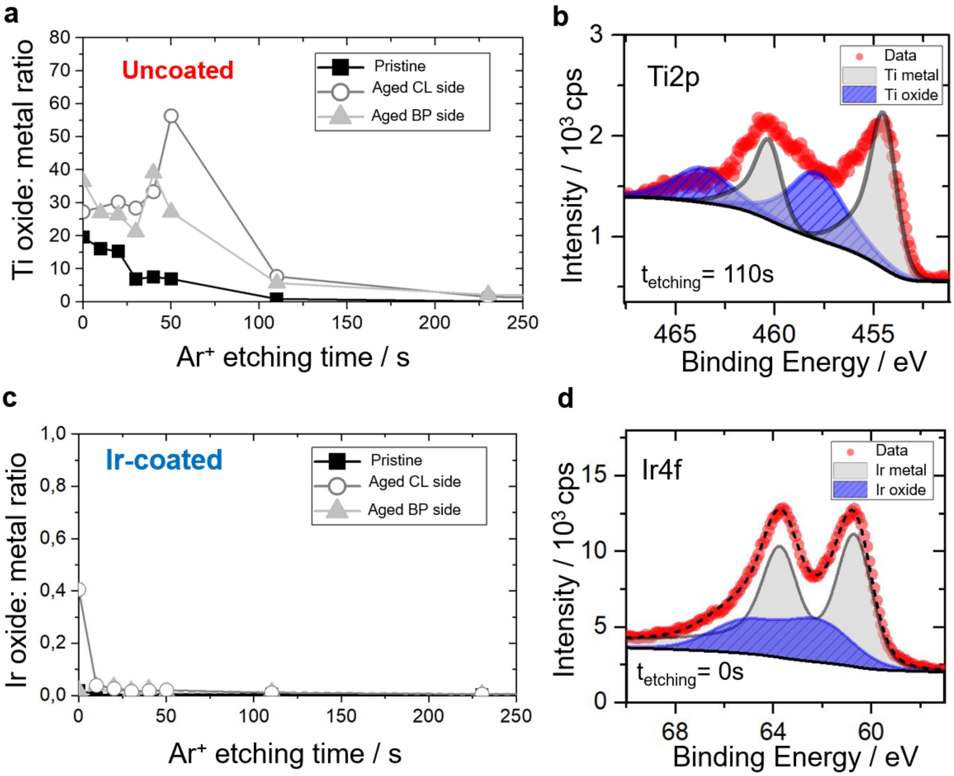

Figure 6.12 *XPS analysis of the PTLs. Oxide-to-metal ratios of the pristine and aged (side-facing to CCM (CL side) and side-facing to the bipolar plate (BP side)) surfaces after the indicated ion etching time ($t_{etching}$) of **(a)** uncoated; **(c)** Ir-coated PTLs (depth profile). (**b**), (**d**) provide the signal deconvolutions used to determine the oxide and metal species [28].*

6.2.6 ToF-SIMs

Figure 6.13 shows the ToF-SIMS depth profiles of uncoated and Ir-coated samples before and after 4000 hours of operation. There are five major species of interest presented here for the four samples. The counts corresponding to Ti-containing ions from the Ti fibers (Ti^+ and TiO^+), Ir-containing ions from the Ir-coating (Ir^+ and $CsIrO^{2+}$), and Cs_2O^+ are plotted versus etching time in Figure 6.13. The Cs_2O^+ species is representative of all oxide species present, regardless of which metal is oxidized, while the other species represent the specific features listed above. Both metallic and oxidized species were observed for pristine and aged samples, indicating that TiO_x was present in the pristine sample. After 4000 hours of operation, the longer, less well-defined tail with the less steep slope demonstrated a thicker and rougher TiO_x layer. The gray shadow in Figure 6.13 b and d highlighted the interfacial oxide region, which shows the presence of Ir oxide between the interface of Ir and TiO_x. The sharp signals of ablated $CsIrO^{2+}$ (dark green) indicated the presence of both TiO_2 and Ir at the interface between the fiber and surface coating. There is a minor increase of oxide layer after 4000 hours, but the growth of oxide is significantly less pronounced than the uncoated sample, indicating the Ir protective layers are capable of mitigating oxidation of the PTL.

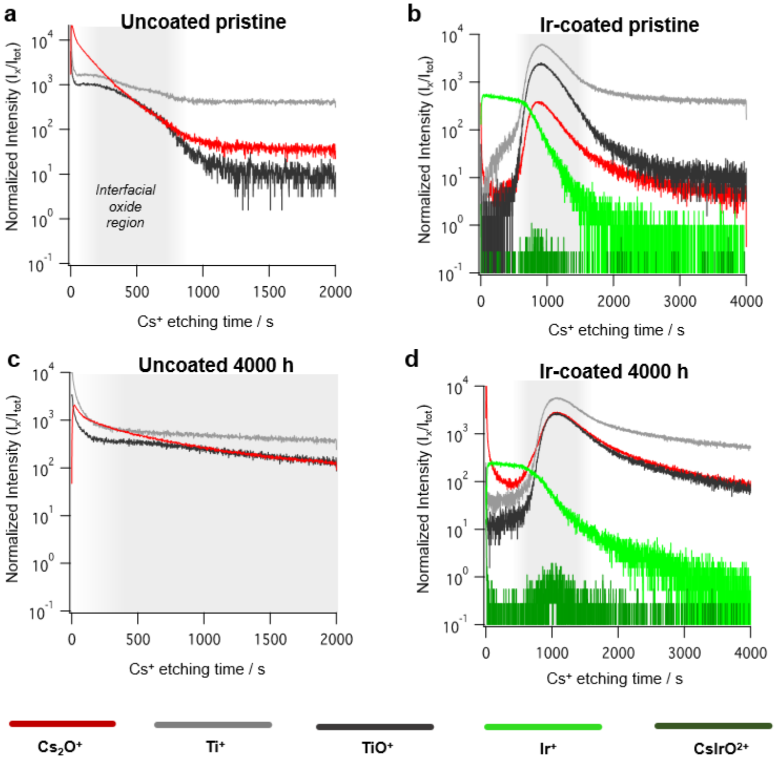

Figure 6.13 *ToF-SIMS profiles of **(a, c)** Pristine and aged uncoated PTLs, **(b, d)** Pristine and aged Ir-coated PTLs. All relevant species are listed in the table. Sputtering time provides profile on relevant metallic and oxide species present from surface to bulk of the Ti PTL fibers. Note the different x-axis range on the uncoated samples compared to the coated samples [28].*

6.3 Summary

In this chapter, the durability of Ir-coated and uncoated titanium-based PTLs were compared and investigated via a 4000 hours long-term test at 2 V and 80 °C. The main conclusion is that 4000 hours of stable durability profiles are achieved when PTL is coated with only 0.1 mg·cm^{-2} of Ir. The following results were observed:

i. The cell assembled with uncoated PTL showed a 55% current density decrease after 4000 hours of operation. However, the cell assembled with Ir-coated PTL did not show any significant decay (less than 1%) in performance over 4000 hours. The polarization curves and contact resistance results performed before and after long-term operation corroborate well with the results obtained from the durability profiles.

ii. For uncoated PTL after 4000 hours of operation, the catalyst residuals can be observed due to the migration or delamination from the catalyst layer on the side that faces the CCM (electrode). The titanium on this side and the other side that faces to bipolar plate showed corrosion-yielding structures of around 30 nm scale. However, no catalyst migration or delamination was observed in the Ir-coated PTL after 4000 hours of operation.

iii. After the formation of a very thin iridium oxide layer on the surface of the iridium coating of the Ir-coated PTL, bulk iridium was preserved to its elemental oxidation state, remaining remarkably stable throughout the entire test. The TiO_x layer underneath the iridium did not undergo further passivation, in contrast to the unprotected PTL, preventing the cell from undergoing further degradation.

Chapter 6 shows that the use of iridium as a protective layer on the titanium-based PTL is significantly effective in mitigating the corrosion of titanium-based PTL and degradation of PEM water electrolyzer in a long-term operation. The comparison with other noble metal coatings such as Pt and Au will be discussed in Chapter 7.

7. Comparison of durability of Pt-coated and Au-coated PTL

Typically, titanium-based PTLs used in commercial electrolyzers are coated with noble metal elements, most commonly platinum or gold with loadings around 1 mg·cm^{-2} [10-12]. The results in Chapter 6 showed that the corrosion/passivation of titanium-based PTL can be effectively mitigated by using Ir as a protective layer on the surface of PTL. The total amount of iridium on both sides of the PTLs was only 0.1 mg$_{Ir}$·cm^{-2}, which is 20 times less iridium compared to what is usually present in an anode catalyst layer, and a 10-time reduction of typically applied Au or Pt protective layers currently used in commercial electrolyzers and other publications [17]. In this chapter, the same 4000 hours durability test at 2 V and 80°C as chapter 6 was performed on the Pt-coated and Au-coated PTLs in the same period, to compare the durability of Ir with Pt and Au coatings on titanium-based PTLs. Post-mortem tests including SEM, AFM, XPS, ToF-SIMs, and X-ray CT were done to characterize the noble metal coated PTLs, and investigate the morphology change, chemical composition, and state of oxidation before and after the long-term operation. This work was published [126].

7.1 Electrochemical characterization

7.1.1 Durability measurement

The relative drop in current density over 4000 hours of operation for all cells assembled with different PTLs is shown in Figure 7.1. The measurements were operated at a constant voltage of 2 V and 80 °C. It should be noted that the average value of current density during the conditioning period (200 ~ 250 h) was determined as 100%. As discussed in Chapter 6, the cell assembled with Ir-coated PTL did not show any significant decay (less than 1%) in performance over 4000 hours. Here, Pt-coated PTL showed very similar results as Ir-coated PTL, which indicates that Pt coating is very stable over 4000 hours of operation as well. However, the cell assembled with Au-coated PTL showed a 35 % current density decrease after 4000 hours of operation.

As is shown in Chapter 6, the current density vs. time curve was divided into 3 zones (Figure 7.2). Each point of current was the average value every 25 h. In the first period from beginning to 250 h (conditioning), all the cells were unstable. The first points of the second and third periods (at 288 h and 2859 h) were removed to ensure all the cells run constantly when calculating the degradation rate. The comparison of the degradation rate of each sample is shown in Table 7.1. In the second period from 288~2490 h regarded as the constant mode, the cell with Pt-coated PTL and Au-coated PTL showed the degradation of 1.1 and 2.1 mA·h^{-1}, respectively. However, the degradation rate of Au-coated PTL was 15.3 mA·h^{-1} during the third period (2859 ~ 4000 h), which was much higher than the Pt-coated sample (just 0.6). It should be noted that the interruptions at 3434, 3559 and 3758 hours are due to the variation in power and water supply or some other arising issues during a long-term test. For Ir-coated and Pt-coated samples, the interruption led to reversible degradation, thus an increase of current density was observed at these points [9-11]. Nevertheless, the current density of Au-coated PTL decreased dramatically which indicates that Au-coated PTL was not able to survive with intermittent power supply in a real PEM water electrolyzer application.

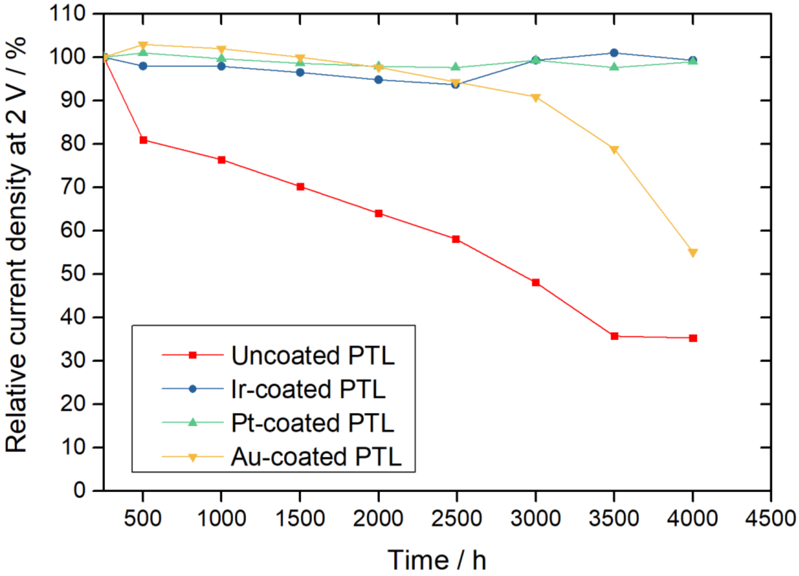

Figure 7.1 *Relative current density at 2 V (the average value of current density in 200-250 h (conditioning) was determined to be 100%) [28].*

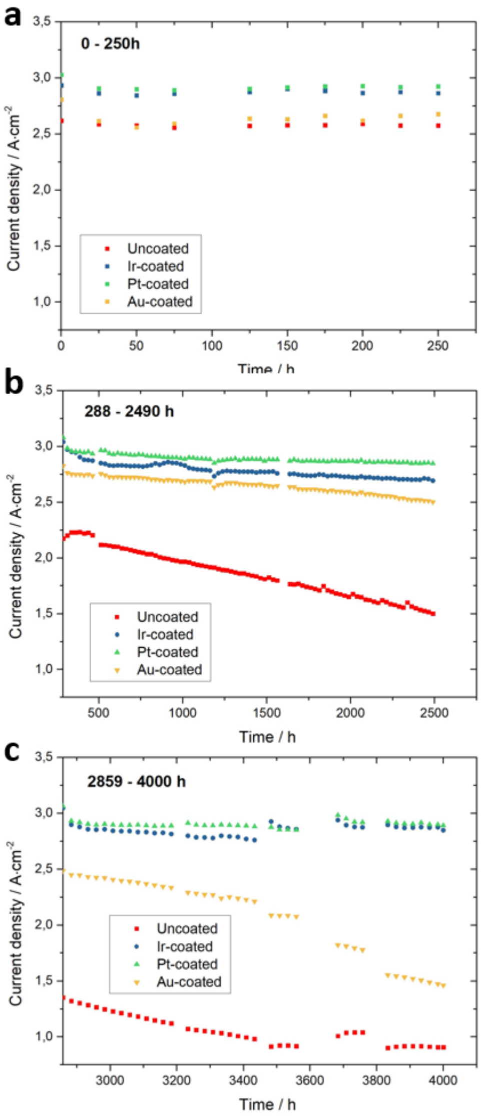

***Figure 7.2 (a)** Current density at 80 °C during long-term operation at 2 V from beginning to 250h; **(b)** Current density at 80 °C during long-term operation at 2 V from 288h to 2490h; **(c)** Current density at 80 °C during long-term operation at 2 V from 2859h to 4000h [28].*

Table 7.1 Degradation rate of Ir-coated, Pt-coated, Au-coated and uncoated-PTL at different period [28].

Zone	**Uncoated-PTL**	**Ir-PTL**	**Pt-PTL**	**Au-PTL**
0-250h	Conditioning	Conditioning	Conditioning	Conditioning
288-2490h	5.7	2.3	1.1	2.1
2859-4000h	6.3	0.8	0.6	15.3

Degradation rate: mA·h^{-1}

7.1.2 Polarization curve

Figure 7.3 compares the polarization curves of all samples at the beginning and end of the 4000 h long-term test. Au-coated and uncoated PTLs showed dramatically decreased performance after 4000 h. The cell voltage of Au-coated and uncoated PTLs increased by 156 mV and 306 mV at 0.75 A·cm^{-2}, respectively. However, Ir-coated and Pt-coated PTLs showed identical cell performance which corroborated the results from long-term profiles (Figure 7.1) and contact resistance results (Figure 7.5, It will be discussed later) before and after 4000 hours of operation. The results indicate that the degradation can be mitigated by using Ir and Pt coatings on the surface of PTLs.

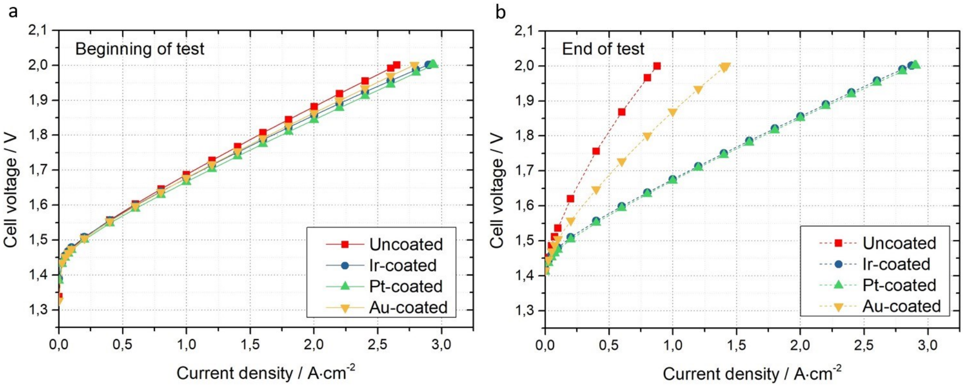

Figure 7.3 (a) *polarization curves of all PEM electrolyzer single cells assembled with Ir-coated, Pt-coated, Au-coated and uncoated PTLs before 4000 hours operation;* ***(b)*** *polarization curves of all PEM water electrolyzer single cells after 4000 hours operation [28].*

7.1.3 EIS

EIS results of uncoated and Ir-coated PTL have been discussed in a previous chapter. Prior to 4000 hours of operation, the EIS results show that all the samples have nearly identical EIS spectra (Figure 7.4a, c). The high frequency resistances (HFR) for the samples at 1.9 A·cm^{-2} are very close at the beginning of the test. The HFR of Au-coated and uncoated samples are only 0.01 and 0.02 Ω·cm^{2} higher than Ir-coated and Pt-coated samples. After 4000 hours durability test at 2 V was performed, the HFRs of Ir-coated and Pt-coated PTL were not significantly changed. However, the HFR of Au coated sample increased by 0.124 Ω·cm^{2}, and uncoated PTL increased by 0.168 Ω·cm^{2} (Figure 7.4b, c). This indicates that the ohmic loss can be decreased dramatically by using iridium and platinum as protective coatings.

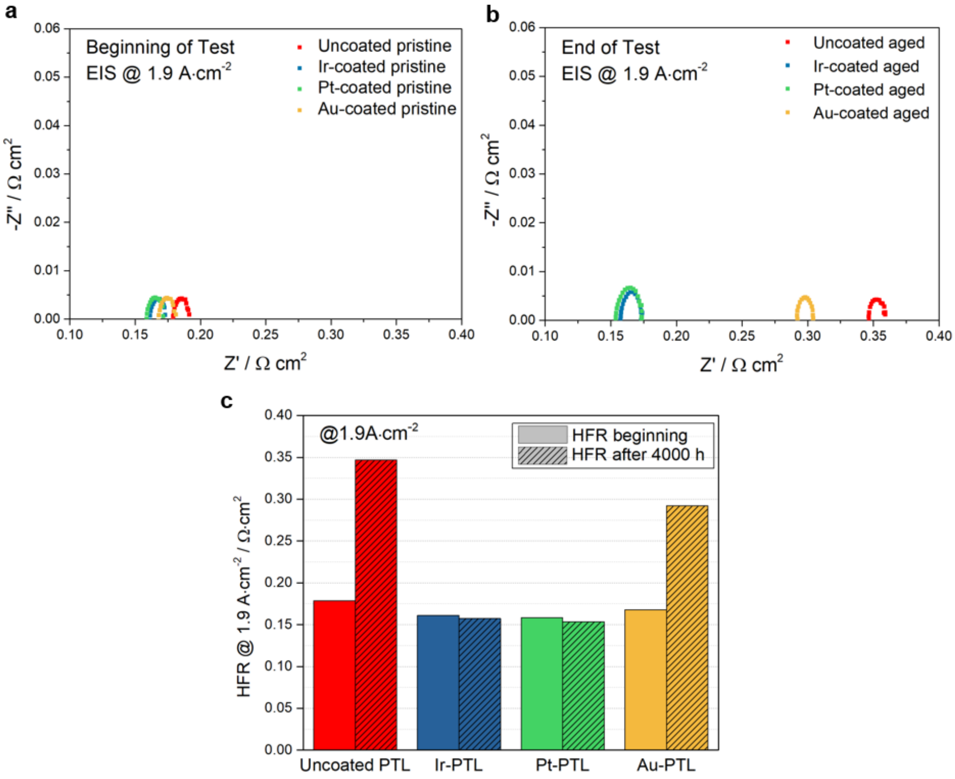

Figure 7.4 (a, b) *EIS results at 1.9 A·cm^{-2} of Ir-coated, Pt-coated, Au-coated and uncoated PTLs;* ***(c)*** *HFR at 1.9 A·cm^{-2} of Ir-coated, Pt-coated, Au-coated and uncoated PTLs before and after 4000 hours of operation [28].*

7.2 Interfacial contact resistance (ICR)

Interfacial contact resistance (ICR) analysis was performed under different cell compressions to investigate the improved electrical and interfacial contact behavior of the coatings before and after 4000 hours of operation. Pristine iridium, platinum, and gold-coated PTLs had identical resistances throughout the entire compression range, while the pristine uncoated PTL showed a significantly higher resistance over all compression ranges (Figure 7.5a) [16]. All the noble metal coatings (Ir, Pt, Au) in this study reduced the interfacial contact resistance between PTL and catalyst layer. After a 4000 hours durability test under 2 V, nearly no increase in contact resistance was observed for Ir- and Pt-coated PTL. However, Au-coated and uncoated PTL showed significantly higher resistance throughout all the compression.

To compare the change in contact resistance in specific pressure, Figure 7.5b compares the interfacial contact resistance of all PTLs before and after the durability test at 3000 kPa, which is the optimal pressure value used for assembling PEM water electrolysis cells [121]. Prior to the long-term operation, Ir-coated, Pt-coated, and Au-coated samples had nearly the same contact resistance, while the uncoated PTL had a higher resistance of 17 mΩ·cm^2 than other samples at 3000 kPa. After 4000 hours of operation, no significant increase in contact resistance was observed for Ir-coated and Pt-coated PTLs. However, the Au-coated and uncoated PTL showed a dramatic increase in contact resistance of 59.6 and 79.6 mΩ·cm^2, respectively. These results corroborate well with the results obtained from the polarization curves and durability profiles and further indicate that Ir and Pt effectively protected the surface of titanium-based PTLs in PEM water electrolyzer.

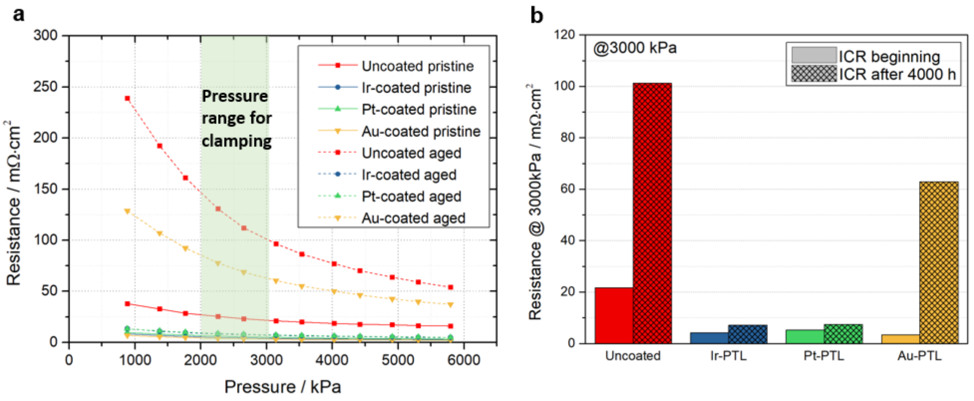

***Figure 7.5 (a)** Interfacial contact resistance of Ir-coated PTL, Pt-coated PTL, Au-coated PTL and uncoated PTL before and after 4000 hours using a conventional press setup where the PTLs are pressed between two gold coated copper plates; **(b)** Interfacial contact resistance at 3000 kPa. The PTLs were mounted and tested dry, with tests run at 25 °C [28].*

7.3 Post-mortem characterization

7.3.1 Optical and SEM image of Pt and Au coated PTLs

Figure 7.6 and 7.7 show the optical and SEM images of Pt-coated and Au-coated PTLs before and after 4000 hours of operation. Pt-coated PTL shows very similar results as the Ir-coated sample. No discoloration and obvious morphology change were observed after the durability test (Figure 7.6). It should be noted that for pristine Pt-coated PTL, the diagonals in Figure 7.6c were originated from titanium felt fabrication, which was observed for other pristine samples as well.

However, Au-coated PTL shows totally different results from Ir-coated and Pt-coated PTL. Strong Au delamination from the titanium fibers was observed on both sides facing the bipolar plate and electrode. At the side that faces the CCM (electrode), catalyst delamination/migration phenomenon from CCM to the Au-coated PTL (black imprints on Figure 7.7d) was observed, which was similar to uncoated PTL. On the other side faces the bipolar plate, and the titanium fibers became exposed after the detachment of the Au layer (Figure 7.7i). Compared to the pristine sample, the remaining gold on this side showed a more porous morphology. This strongly indicates that when the protective layer over the PTL is damaged or in the absence of an effective coating, higher contact resistances given by the passivated or corroded PTL trigger degradation mechanisms over the catalyst layer attached to the membrane. More analysis and discussion about Au delamination will be shown in the next section.

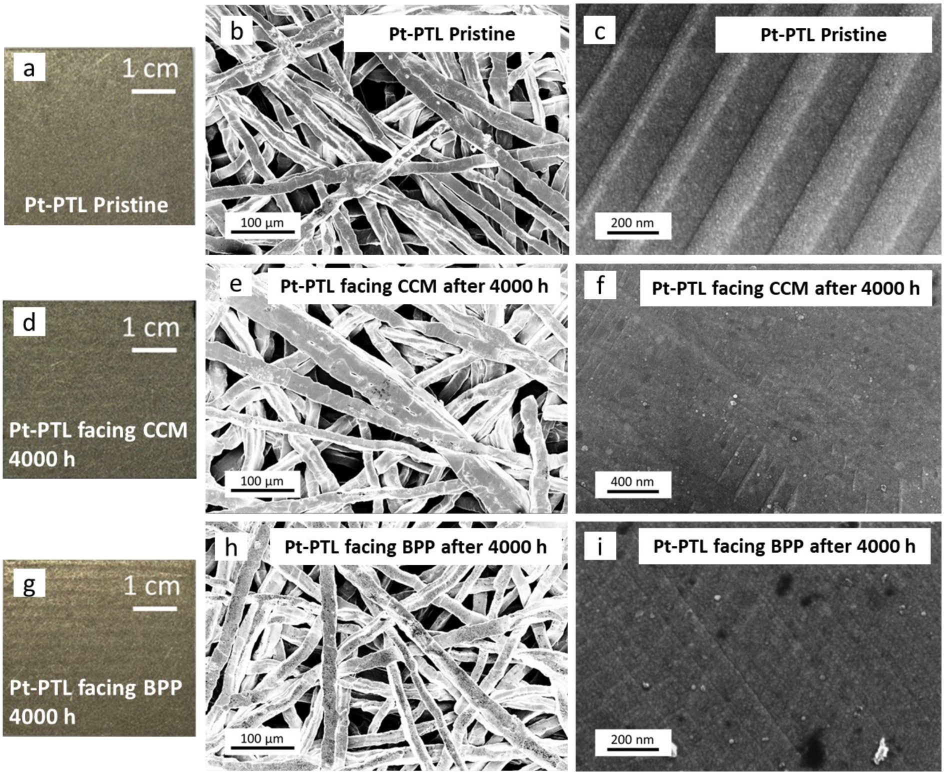

Figure 7.6 (a, b, c) *Optical and scanning electron microscopy (SEM) images of pristine Pt-coated PTL;* ***(d, e, f)*** *Optical and scanning electron microscopy (SEM) images of Pt-coated PTL facing CCM side after 4000 hours;* ***(g, h, i)*** *Optical and scanning electron microscopy (SEM) images of Pt-coated PTL facing bipolar plate side after 4000 hours [28].*

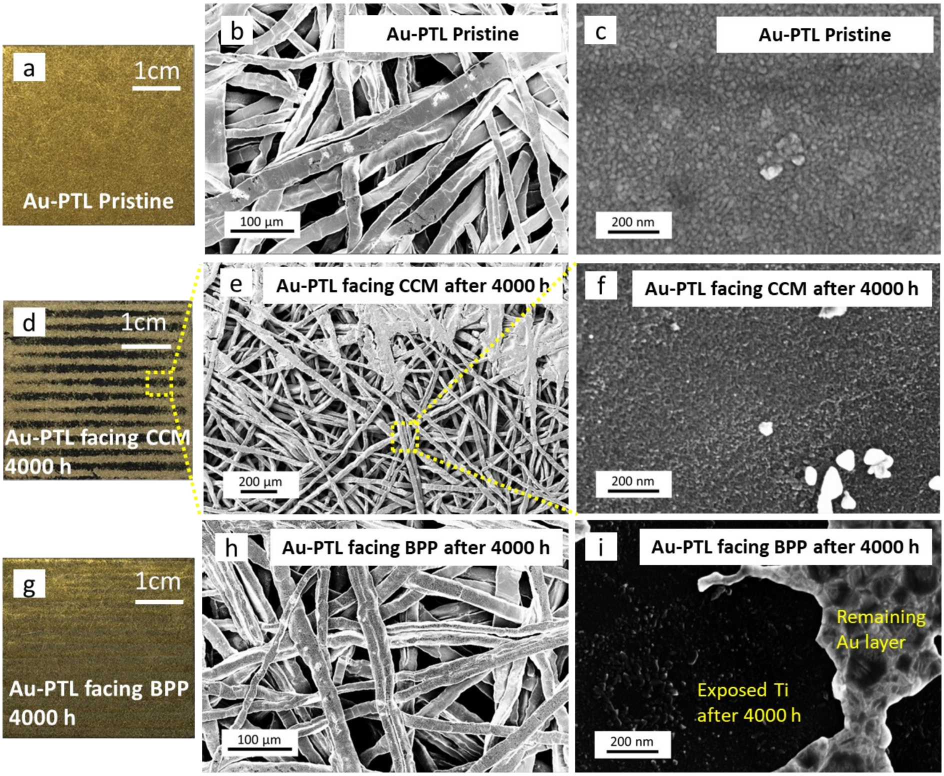

***Figure** 7.7 **(a, b, c)** Optical and scanning electron microscopy (SEM) images of pristine Au-coated PTL; **(d, e, f)** Optical and scanning electron microscopy (SEM) images of Au-coated PTL facing CCM side after 4000 hours; **(g, h, i)** Optical and scanning electron microscopy (SEM) images of Au-coated PTL facing bipolar plate side after 4000 hours [28].*

7.3.2 Detachment of Au layer

7.3.2.1 EDX of Au-coated PTL

Compared to a pristine Au-PTL (Figure 7.8a, b), strong Au delamination was observed on both sides after 4000 h, i.e. the one facing the bipolar plate (BP) and that facing the catalyst layer (CL). On the side facing the bipolar plate, the titanium fibers became exposed after detachment of the Au layer (Figure. 7.8d). The remaining gold on this side showed a porous structure compared to the pristine sample (Figure. 7.8b). Au was only detected in the points with the remaining gold layer, however, on the points of the exposure of Ti, Au was not observed (Table 7.3). On the other side that faces the catalyst layer, no Au was detected (Table 7.4), which indicates that all Au on this side totally dissolved (Figure 7.8f).

The mechanism of the detachment of the Au layer has been reported by Gago et al., who used Au coating on the surface of the bipolar plate. They found strong Au detachment in water electrolyzers after 6 h at 2 V vs. RHE in a half cell [41]. The growth of amorphous $Au(OH)_3$ is hindered by a monolayer oxide film that passivates the surface related to the $Au_2O_3 \cdot 3H_2O$. At 2 V, the oxygen evolution reaction (OER) occurs as some of the monolayer oxide material is converted into AuO_2 species, which in turn decomposes, yielding to oxygen gas. Both the oxygen gas evolution and hydrous oxide growth may involve the formation of unstable AuO_2 species [127]. This phenomenon, along with the increasing passivation and/or corrosion of titanium, leads to the detachment of the Au nanoparticles [41].

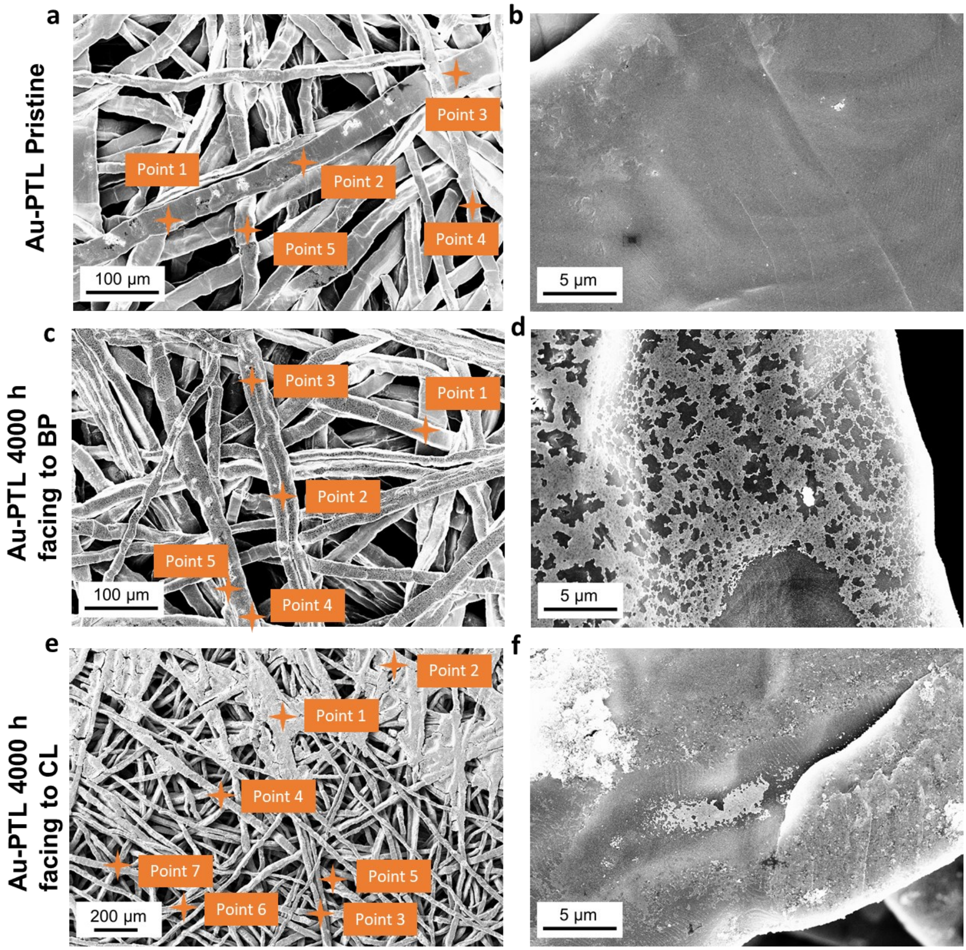

***Figure** 7.8 SEM images of **(a, b)** Pristine Au-coated PTL; **(c, d)** Au-coated PTL that faces the bipolar plate (BP) side after 4000 h; **(e, f)** Au-coated PTL that faces the catalyst layer (CL) side after 4000 h. The points in Figure 7.8a, c, e indicate the elemental concentration (weight %) of the samples (see Table 7.2 – 7.4) [28].*

Table 7.2 Elemental concentration (weight %) of pristine Au-coated PTL using SEM-EDX (Fig. 7.8a) [28].

Element (wt %)	C	Ti	Au
Point 1	3.95	76.81	19.24
Point 2	3.39	75.88	20.73
Point 3	4.14	75.7	20.15
Point 4	3.17	74.69	22.14
Point 5	4.62	74.26	21.13

Table 7.3 Elemental concentration (weight %) of aged Au-coated PTL that faces BP side after 4000 h using SEM-EDX (Fig. 7.8c) [28].

Element (wt %)	C	O	Ti	Au
Point 1	2.8	2.84	71.03	23.33
Point 2	1.71	7.42	90.88	0
Point 3	1.46	9.37	89.17	0
Point 4	3.08	4.53	72.76	19.63
Point 5	1.73	2.34	95.93	0

Table 7.4 Elemental concentration (weight %) of aged Au-coated PTL that faces CL side after 4000 h using SEM-EDX (Fig 7.8e) [28].

Element (wt %)	C	O	F	S	Ti	Ir
Point 1	8.98	11.77	11.5	1.48	0	66.26
Point 2	10.13	7.78	16.49	1.13	0.74	63.73
Point 3	1.12	4.22	0	0	94.65	0
Point 4	2.87	3.58	0	0	93.55	0
Point 5	2.25	8.82	8.16	0	62.53	18.24
Point 6	2.28	6.41	0	0	90.54	0.77
Point 7	2.16	9.85	2.33	0	84.53	1.13

7.3.2.2 EDX after FIB cross-section of Au-coated PTL

Figure 7.9 showed the optical and HAADF-STEM images and EDX composition mapping after the FIB cross-section of Au-coated PTL before and after 4000 h of operation. The protective Au layer has a thickness of 50 nm (Figure 7.9c). No Au was detected on the Au-coated Ti fibers of the side that faces the catalyst layer after 4000 hours of operation (Figure 7.9f, h). It should be noted that Au was not found in both the regions with or without catalyst residuals (black imprints on Figure 7.9d). This collaborated well with the EDX results in Figure 7.8e and Table 7.4, indicating Au totally dissolved at the interface between the catalyst layer and PTL. It should be noted that catalyst migration from the catalyst layer to the PTL fibers only happened on the side that faces to catalyst layer. The IrO_x residuals migrated from catalyst layer showed a ratio of 32:68 Ir:O (Figure 7.9h).

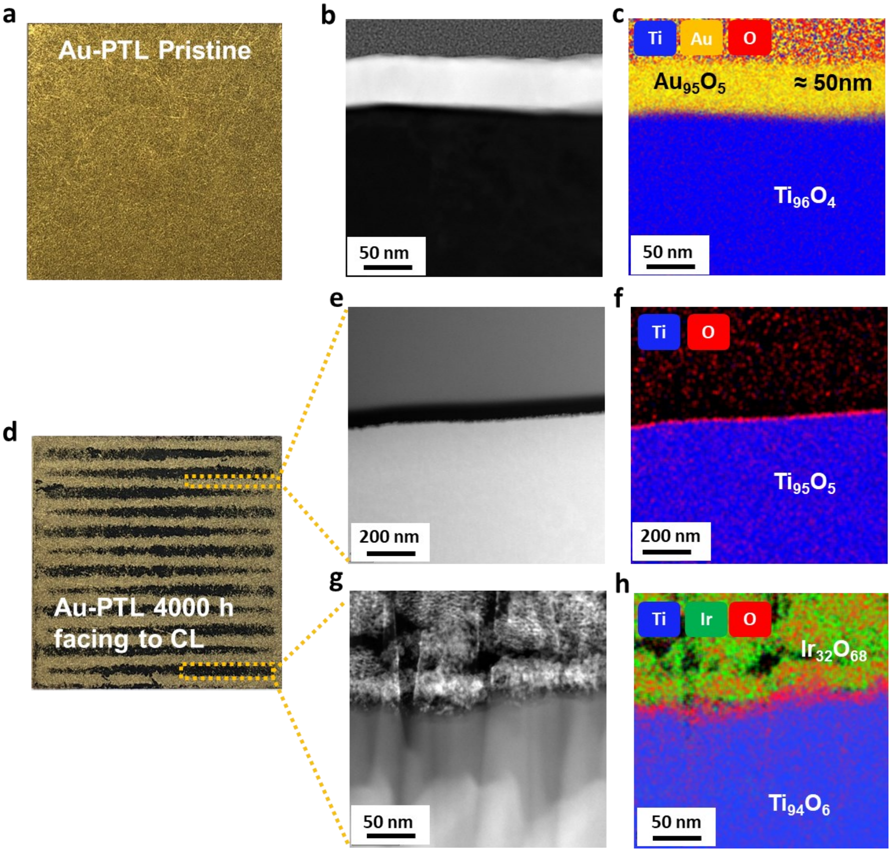

Figure 7.9 ***(a)*** *Optical image of Au-coated PTL;* ***(b, c)*** *HAADF-STEM image and elemental distribution of Ti (blue), Au (yellow), and O (red) in EDX composition maps after FIB cross-section of Au-coated PTL;* ***(d)*** *Optical image of Au-coated PTL that faces the CL side after 4000 h;* ***(e, f)*** *HAADF-STEM image and elemental distribution of Ti (blue) and O (red) in EDX composition maps after FIB cross-section of Au-coated PTL that faces CL without catalyst residuals;* ***(g, h)*** *HAADF-STEM image and elemental distribution of Ti (blue), Ir (green), and O (red) in EDX composition maps after FIB cross-section of Au-coated PTL that faces the CL with catalyst residuals [28].*

7.3.3 AFM of Pt-coated and Au-coated PTLs

7.3.3.1 AFM of Au-coated PTL

Atomic force microscopy (AFM) measurements were performed to obtain additional information on the conductivity of all the PTLs before and after the durability test. Au-PTL is not as stable as Ir-coated and Pt-coated PTL. The pristine Au-coated PTL showed a very homogenous conductivity which indicates a complete covering layer of gold on the top of the titanium fiber. After 4000 hours of operation, the conductivity is nearly gone at the side that faces bipolar plate (Figure 7.10e), which is due to the delamination of the gold layer and the formation of low conductive gold oxide. At the side that faces CCM (electrode), the bright area indicates the IrO_x residuals migrated from catalyst layer (Figure 7.10f). Additionally, the detachment of Au layer was detected at the nonconductive spots. The nonconductive area showed a depth of around 35 nm, which is in the range of the coating.

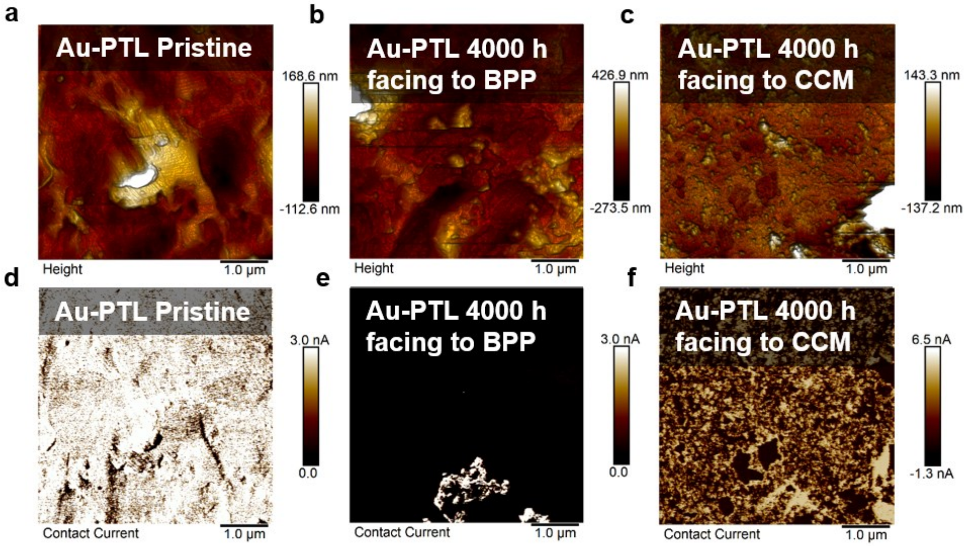

Figure 7.10 ***(a)*** *AFM height measurement of pristine Au-coated PTL;* ***(b)*** *AFM height measurement of operated Au-coated PTL (BPP side);* ***(c)*** *AFM height measurement of operated Au-coated PTL (CCM side);* ***(d)*** *AFM conductivity measurement of pristine Au-coated PTL;* ***(e)***

AFM conductivity measurement of operated Au-coated PTL (BPP side); ***(f)*** *AFM conductivity measurement of operated Au-coated PTL (CCM side) [28].*

7.3.3.2 AFM for Pt-coated PTL

The Pt-coated PTLs showed a comparable amount of conductive area before and after the long-term operation (Figure 7.11d-f), which are similar to the Ir-coated PTL in chapter 6. This indicates that the platinum coating was stable over the 4000 hours of operation as well. On the other side that faces the bipolar plate, only minor areas are less conductive, which might be due to the formation of less conductive platinum oxide.

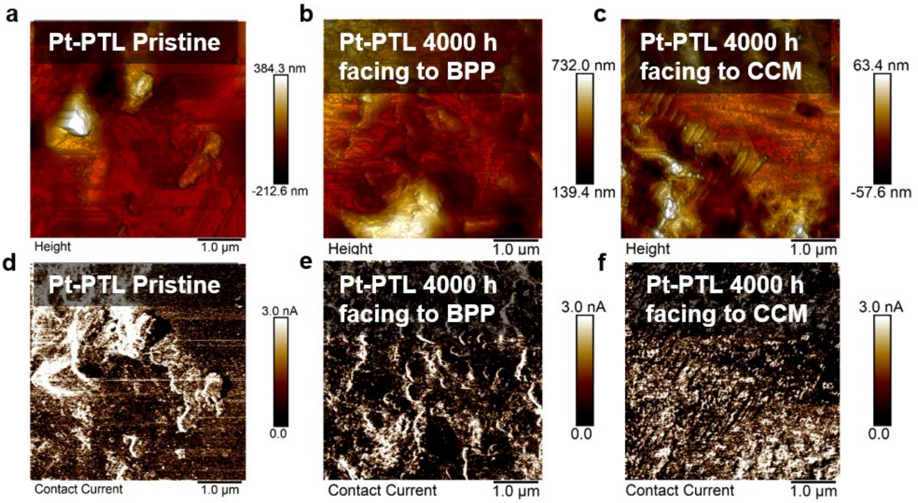

Figure 7.11 (a) *AFM height measurement of pristine Pt-coated PTL;* ***(b)*** *AFM height measurement of operated Pt-coated PTL (BPP side);* ***(c)*** *AFM height measurement of operated Pt-coated PTL (CCM side);* ***(d)*** *AFM conductivity measurement of pristine Pt-coated PTL;* ***(e)*** *AFM conductivity measurement of operated Pt-coated PTL (BPP side);* ***(f)*** *AFM conductivity measurement of operated Pt-coated PTL (CCM side) [28].*

7.3.4 XPS of Pt-coated PTL

Figure 7.12 shows X-ray photoelectron spectroscopy (XPS) depth profile analysis for Pt-coated PTL before and after 4000 hours of operation. As the Au dissolution has been confirmed from EDX results in the section above, XPS was just performed on the Pt-coated PTL. The Pt-coated sample was etched under the argon ion beam to remove atomic layers and access deeper areas during continuous analysis. Briefly, it shows the oxide-metal ratios versus the sputtering time of the sample. In order to quantify the oxide and metal species, Pt4f signals have been deconvoluted (Figure 7.12b). The PtO_x:Pt (Pt^{4+} $4f_{5/2}$ / $4f_{7/2}$: 77.6 eV / 74.4 eV; Pt^0 $4f_{5/2}$ / $4f_{7/2}$: 74.0 eV / 70.8 eV) atomic ratio is close to zero for pristine Pt-coated PTL with exemption of a topmost PtO_x layer, significantly smaller than that of the uncoated PTL. After 4000 hours of operation, a slightly increased oxide metal ratio to 0.1 was observed for the Pt-coated sample, however, it is significantly lower than for uncoated sample (Figure 6.12).

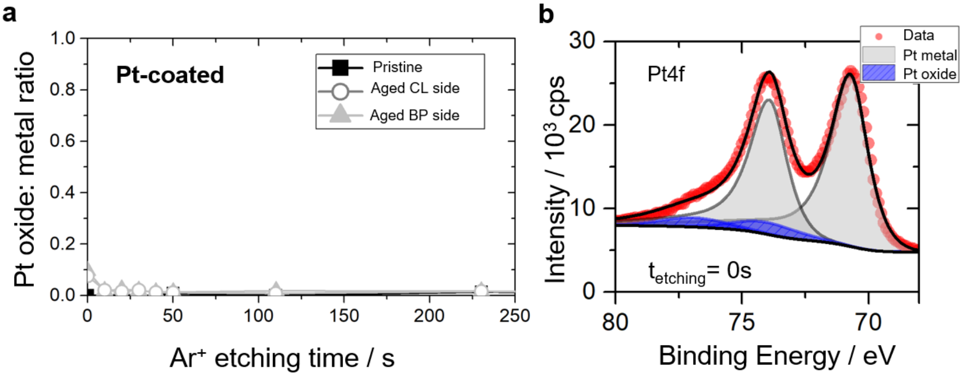

***Figure 7.12** XPS analysis of the PTLs. **(a)** Oxide-to-metal ratios of the pristine and aged (side-facing to CCM (CL side) and side-facing to the bipolar plate (BP side)) surfaces of Pt-coated PTL versus ion etching time (depth profile); **(b)** provide the signal deconvolutions used to determine the oxide and metal species [28].*

7.3.5 ToF-SIMs of Pt-coated PTL

To complement the XPS data and further elucidate the difference in the interfacial region present in the Ir-coated and Pt-coated samples, Time-of-flight secondary ion mass spectrometry (ToF-SIMS) depth profiles were taken for uncoated, Ir-coated and Pt-coated samples before and after 4000 hours of operation. Figure 7.13 shows ToF-SIMs depth profiles of Pt-coated PTL before and after 4000 hours of operation. The counts corresponding to Pt-containing ions from the Pt-coating (Cs_2Pt^{2+} and $CsPtO^+$). The Cs_2O^+ species is representative of all oxide species present, regardless of which metal is oxidized. Pt-coated PTL shows a very similar general trend as Ir-coated PTL: both pristine samples show metallic Pt or Ir species on the surface of the titanium fibers, and both samples have an interfacial oxide region, as highlighted by the gray boxes in Figure 7.13a. The sharp signals of $CsPtO^+$ (dark blue) indicated the presence of both TiO_x and Pt at the interface between the fiber and surface coating. After 4000 hours of operation, minor increase of Pt oxide was observed, while it is significantly less than uncoated sample. This indicates that the Pt thin layer is effective for mitigating the oxidation of titanium PTL.

Interestingly, different trends were shown in the interfacial oxide regions of Ir-coated PTL and Pt-coated PTL after 4000 hours of operation. For Ir-coated PTL (Figure 6.13), the oxide layer appears to increase after 4000 hours which indicates the growth of oxide in the interfacial region. However, for the Pt-coated PTL, after 4000 hours the oxide interface appears slightly sharper and shows a steeper slope compared to the pristine sample (Figure 7.13b).

In summary, although there is a minor change in the interfacial oxide layer of Ir-coated and Pt-coated PTLs after 4000 hours of operation, the growth of the oxide is significantly less pronounced than in the uncoated sample. ToF-SIMS and XPS results indicate that the use of protective coatings can prevent more enhanced oxide growth on PTL fibers in PEM water electrolyzer.

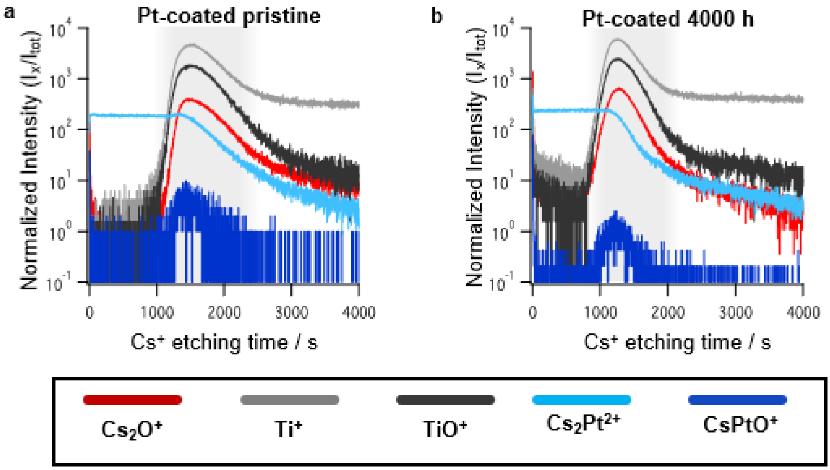

Figure 7.13 *ToF-SIMS profiles of pristine and aged Pt-coated PTLs. All relevant species are listed in the table. Sputtering time provides profile on relevant metallic and oxide species present from*

surface to bulk of the Ti PTL fibers. Note the different x-axis range on the uncoated samples compared to the coated samples [28].

7.4 Summary

This chapter investigates the durability of Pt and Au as a protective layer on titanium-based PTLs in a PEM water electrolyzer. The durability and post-mortem characterization results of Pt-coated and Au-coated PTLs are compared with Ir-coated and uncoated PTLs in chapter 6.

i. Pt-coated PTL showed very similar results as the Ir-coated sample in Chapter 6. The cell assembled with Pt-coated PTL showed nearly no current density decrease, indicating the Pt-coated sample is very stable over the 4000 hours of operation at 2 V and 80 °C as well. However, the cell assembled with Au-coated PTL showed a 35 % current density decrease after 4000 hours of operation.

ii. No obvious morphology change was found on Pt-coated PTL after 4000 hours of durability test. However, strong Au delamination was observed on both sides (the side that faces bipolar plate and CCM) of Au-coated PTL after the long-term operation. Catalyst residuals migrated from CCM were observed only on the side that faces CCM, which is similar to the uncoated PTL after long-term operation.

iii. After 4000 hours of operation, the Pt layer is mostly in its metallic state. Only minor Pt oxide layer was found on the surface of the sample. The growth of the oxide is significantly less pronounced than in the uncoated sample, which indicates that the Pt protective coating is capable of mitigating TiO_x layer growth in the PTL.

8. Partially coated PTL

In order to: 1) exclude the possibility of using a non-functional catalyst coated membrane (CCM); 2) to avoid any possible error when assembling the cells; and 3) to guarantee that all the coated and uncoated PTLs are subjected to the same cell conditions, a special PTL with 4 different sections was fabricated (Figure 8.1a). The special PTL was coated with Ir, Pt, and Au on three different sections of the same PTL, while the final section remained uncoated. The cell with this special PTL was operated for 4000 hours under the same conditions (at 2 V and 80 °C) as the other PTLs mentioned in Chapter 6 and 7. This work was published [126].

8.1 4-sections coated PTL

The results of the 4-sections coated PTL corroborate well with the PTLs with one single or no coating showed in Chapter 6 and 7 (Figure 8.1). Catalyst delamination was observed on the sections that are unstable (Au-coated) or absent (uncoated), while no obvious change was found in Ir-coated and Pt-coated sections. Figure 8.1b shows the X-ray computed tomography (CT) image of an Au-coated section of the PTL after 4000 hours of operation. The grey color represents titanium fibers, the blue color represents catalyst particles, yellow color represents catalyst with higher concentration or agglomeration. This image clearly demonstrates how the catalyst layer (in blue), which was previously coated on the membrane, is transferred to the PTL. The catalyst particles lay on the surface of the PTL but did not deposit into the inner structures. Yellow dots on the top of the CT image are large agglomerated areas or the highly concentrated spots of catalysts. These results indicate that a lack of PGM coating is decisive for triggering delamination over to the catalyst layer. The increase in interface contact resistance of a PTL not only increases the overall cell resistance but also further triggers the degradation of the electrodes. It is apparent that the Pt and Ir coatings prevented the transfer of catalyst layer material onto the PTL surface, which only took place when the protective layer was not stable enough (Au-coated) or not present (uncoated).

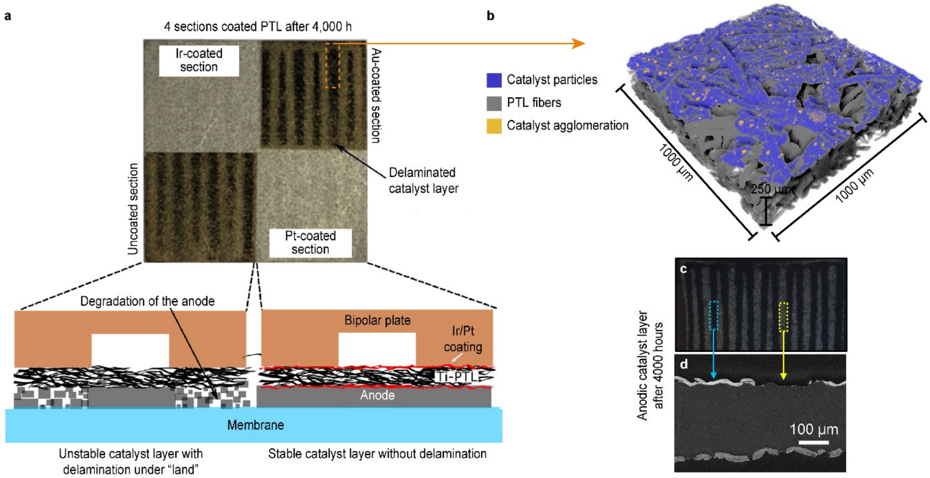

Figure 8.1 (a)*, Optical image of four sections of coated PTL after 4000 hours;* ***(b)****, X-ray CT image of Au-coated section after 4000 hours (catalyst residuals are shown in blue, larger particles/ catalyst agglomeration in yellow);* ***(c)****, optical image of aged CCM assembled with uncoated PTL;* ***(d)****, cross-section SEM images of aged CCM assembled with uncoated PTL [28].*

8.2 Migration of catalyst layer

The entire catalyst layer locally migrated to the uncoated PTL (Figure 8.1 c. d). One plausible explanation is the following. Titanium oxide has a lower thermal conductivity (4.8-11.8 $\mathrm{W\cdot m^{-1}\cdot k^{-1}}$) than titanium (15.6-22.5 $\mathrm{W\cdot m^{-1}\cdot k^{-1}}$), which again has a lower thermal conductivity than Pt (Pt = 71.5 $\mathrm{W\cdot m^{-1}\cdot k^{-1}}$) or Ir coated titanium (Ir = 147 $\mathrm{W\cdot m^{-1}\cdot k^{-1}}$)[128]. Heat is generated at the active sites where the oxygen evolution takes place during the OER. Here, the active sites are regarded as heat sources. Moreover, the results also indicate that this effect is more pronounced at the point of contact (land vs. channel) from flow fields/PTLs/catalysts layer; in other words, where there is a higher flux of electrons. The TiO_x layer of the uncoated titanium PTL grows and becomes highly passivated due to operation. This reduces the heat flux away from the reaction sites and may cause an increase of local temperature when the heat generation is larger than the heat conduction flux. As a result, hot spots are formed, which may decrease the binding characteristics of the catalyst layer, compromising its mechanical stability. This process is indicated by the delamination of the catalyst layer and its transfer from the electrode to PTL. It is apparent that the process is suppressed when using materials with a much higher thermal conductivity such as Ir-coated titanium PTLs.

However, it should be noted that the current of the cell with the uncoated PTL decreased overtime but still the generated heat might not be as well dissipated by the TiO_x compared to the Pt and Ir protective layers.

Another plausible explanation is due to the strong tendency of both Ir and Ti forming bonds with oxygen [126]. The uncoated titanium PTL oxidizes at high potentials, taking the oxygen not only from the evolved gas but also from IrO_2 catalysts. It is reported that it continuously forms unstable species during OER that will eventually recombine again with oxygen [129, 130]. This oxygen can be found at the interface between the uncoated titanium PTL and the catalyst layer. After the long-term operation, more and more of this unstable Ir bonds strongly with the oxygen at the interface with the uncoated titanium PTL from the passivation. Lastly, the polymers (Nafion in the catalyst layer) may adhere stronger to oxidized surfaces than metal ones [131]. Future investigation should be done, for example: inserting micro-temperature sensors in the PTLs or perform adhesion measurements on the catalyst layers directly deposited on the PTLs.

8.3 Summary

The results from 4-section PTL indicate that unprotected or malfunctioning PTLs fatally trigger drastic delamination of the anodic catalyst layer, which indicate that the degradation mechanisms at electrode are attributed to another component present in common cell configurations of PEM water electrolyzers.

9. Discussion

In a PEM water electrolyzer, titanium porous transport layers (PTLs) situated on the anode side are subjected to harsh oxidizing conditions such as high anode overpotential, low pH, and oxygen evolution [6, 15]. Titanium (Ti^0) changes its oxidation state over time under these harsh conditions, which induces the formation of a thin but continuously growing layer of passivated titanium (TiO_x). Consequently, the electrical conductivity of titanium fibers is adversely affected, critically decreasing cell performance and durability [10, 16]. To circumvent this issue, the titanium PTLs in PEM water electrolyzers are typically coated with noble metals such as platinum [10, 11] and gold [12], and loadings of the noble metal coatings are estimated to be around 1 $mg_{metal}\cdot cm^{-2}$ [17].

In this thesis, we demonstrated a facile approach to applying 20 to 50 nm-thick noble metal coatings (Ir, Pt, Au) to titanium-based PTLs using a simple sputtering process. The amount of iridium, platinum, or gold on each side of the PTL was 0.05 ~ 0.09 $mg_{metal}\cdot cm^{-2}$, which is around 40 times less compared to what is currently used in an anodic catalyst layer, and a 20 times reduction in noble metal coating typically used as a protective layer on the PTL in contemporary commercial electrolyzers. It has been reported that the bipolar plates in a PEM water electrolyzer stack account for 48% of the stack cost, and MEAs owns 24% of its cost [19]. Therefore, compared to the high cost in bipolar plates and MEAs of a stack, the total amount of only 0.1 $mg_{Ir}\cdot cm^{-2}$ Ir or 0.16 $mg_{Pt}\cdot cm^{-2}$ Pt coating on the PTL with a close to zero degradation performance over a long-term operation is very ignorable.

The critical passivation of titanium-based PTLs affects the electrical resistivity of the surface and fatally decreases cell performance and durability. Apparent discoloration can be observed on the surface of an uncoated PTL just after a few hours' initial electrochemical measurements, which is an indication of either titanium passivation or corrosion. In contrast, no discoloration was found before and after the electrochemical measurements on the surface of an Ir-coated, Pt-coated or Au-coated PTL, indicating that the noble metal coatings function as a protective layer and prevent oxidation of titanium (at least for initial performance measurement). The noble metal coatings (Ir, Pt, and Au) on the titanium fibers decreased the interface resistance between the PTL and catalyst layer and significantly improved the cell performance. For example, the iridium and platinum layers reduced the ohmic resistance by 110 $m\Omega\cdot cm^2$ at 0.5 $A\cdot cm^2$ and delivered nearly the same cell performance as carbon paper, which was 80 mV higher than with the uncoated titanium PTL at 1.0 A·cm^{-2}.

As Ir-coated PTL showed better cell performance than Au-coated PTL and nearly identical electrochemical results as Pt-coated sample, more post-mortem investigation was done on iridium-coated PTL in this thesis. Though the iridium coating on the PTL only accounts for a very minor part of the entire cost of the cell components of a PEM water electrolyzer stack, the iridium is a noble metal and very rare on the earth. The Ir loading of the coated PTLs can be further reduced by decreasing sputtering time. All different loadings of iridium layers on titanium fibers, even the lowest loading of 0.005 mg$_{Ir}$·cm^{-2}, reduced contact resistance between PTLs and catalyst layers, and the coated PTL showed a better cell performance than uncoated PTL. The iridium-coated PTL containing 0.025 mg$_{Ir}$·cm^{-2} Ir showed identical cell performance as PTLs with higher iridium loading. Additionally, the iridium layer on the PTL showed OER activity as well. The iridium thin film on the titanium-based PTL is not only proposed to be a protective layer that protects titanium from passivation with a very low Ir loading but also the OER activity of the iridium layer makes it promising to act as a cost-effective catalyst layer.

To date, PEM water electrolyzers can achieve lifetimes on the order of 50000 h [30]. Unfortunately, the scientific community has devoted very little attention to understanding the degradation mechanisms of cell and stack components. It is of significant importance to understand the interplay between components and materials that affect efficiency and durability and elucidate how these coatings behave under realistic cell operating conditions, especially after long-term operation. After 4000 hours under 2V and 80 °C, the cells assembled with Ir-coated and Pt-coated PTLs did not show any significant decay in performance. In contrast, the cells assembled with Au-coated and uncoated PTL showed a 35% and 55% current density decreased after the same period of long-term operation, respectively. Beyond the classical observation of the morphology changes on the surface of the titanium-based PTL fibers, it is much more relevant yet highly complex to monitor the interface between the PTL fiber and the protective layer. Investigating this interface will shed light on the interrelated mechanisms exerted on multiple materials and components inside the cell. Traditional lab-scale durability analysis, using liquid electrolyte and three electrode cell setups, for instance, might not provide such a picture, as it does not include crucial parameters relating to real cell operating conditions or contributions to the PTL by other key cell components such as the membrane, catalyst layer, ionomer, bipolar plates, etc. It is therefore crucial to bridge the information gained from lab-scale testing to real-world, long-term device performance by using advanced characterization methods, enabling the use of new information that can drive the development of future materials [126]. For the first time, the interfacial region of an Ir-coated PTL before and after ≈ 4000 hours operation under real PEM water electrolysis conditions was observed and investigated by energy-dispersive X-ray (EDX) elemental composition maps and line-scanning profile after the focused ion beam (FIB) cross-section. The bulk iridium was preserved in its metallic state and remained remarkably stable throughout the long-term test after the formation of a < 10 nm IrO_x layer on the iridium-coated PTL. In contrast to the uncoated PTL, the TiO_x layer underneath the iridium did not further passivate, thus preventing the cell from undergoing critical degradation. Moreover, the catalyst layer on the membrane was transferred to the uncoated and Au-coated PTLs during the 4000 h experiment. However, the Ir and Pt coatings prevented the transfer of catalyst layer material onto the PTL surface, which only took place when the protective layer was not stable enough (Au-coated) or not present. The results indicate that uncoated or poorly-coated PTLs trigger severe degradation of the catalyst layer, which suggests that catalyst layer degradation can be caused by secondary components used in the cell.

In this work, a very simple and scalable method is used to protect the titanium PTL from passivation by sputtering very thin layers of noble metal coatings onto porous transport layers. The results will aid researchers in identifying other degradation mechanisms and developing superior accelerated stress tests for these electrochemical devices. More importantly, active and stable noble metal coated PTLs are not only relevant to reducing the costs associated with the titanium components but also provide a pathway to extended device lifetime, offsetting the high cost of PGM-based catalysts. This study also opens new possibilities for transforming other materials, electrodes, and components where critical interface resistances using PGM or non-PGM materials play a crucial role in the long-term service life typically observed in complex devices beyond water electrolyzers, such as batteries, solar cells, and sensors [126].

10. Conclusions

This thesis comprehensively investigates the noble metal coating (iridium, platinum and gold) as a protective layer on the surface of titanium-based PTLs. The cell performance and durability of Ir-coated PTL were compared with Pt-coated and Au-coated PTLs. The effect of the loading of iridium as a protective layer was investigated.

The main conclusions of this thesis are as follows:

- The 20 to 50 nm thick noble metal coatings (Ir, Pt, Au) on the titanium fibers effectively decreased the interfacial contact resistance between PTL and catalyst layer and significantly improved the cell performance. The iridium and platinum layers reduced the ohmic resistance by 110 $m\Omega \cdot cm^2$ at 0.5 $A \cdot cm^2$ and delivered nearly the same cell performance as carbon paper, which was 110 mV higher than with the uncoated titanium PTL at 1.0 $A \cdot cm^{-2}$. Au-coated PTL also showed better performance than uncoated one, but the increase is not as high as Ir-coated and Pt-coated ones, which was 45 mV higher than the uncoated sample at 1.0 $A \cdot cm^{-2}$.
- The loadings of Ir as a protective layer on the PTL have an impact on the cell performance. All different loadings (from 0.005 to 0.05 $mg \cdot cm^{-2}$) of iridium layers, even the lowest loading of 0.005 $mg \cdot cm^{-2}$, reduced contact resistance between PTLs and catalyst layers. The amount of iridium was reduced to 0.025 $mg \cdot cm^{-2}$ and showed identical cell performance as PTLs with higher iridium loading, which effectively reduced the cost of the Ir.
- 4000 hours stable durability profiles are achieved when PTL is skinned with only ≈20 nm thick Ir. The cell assembled with Ir-coated and Pt-coated PTLs did not show any significant decay (less than 1%) in performance over 4000 hours operation at 2 V, 80°C. In contrast, the cells assembled with Au-coated and uncoated PTL showed a 35% and 55% current density decrease after the same period, respectively. After the formation of a < 10 nm IrO_x layer on the iridium-coated PTL, bulk iridium was preserved in its metallic state, remaining remarkably stable throughout the entire test. In contrast to the unprotected PTL, the TiO_x layer underneath the iridium did not further passivate, thus preventing the cell from undergoing critical degradation.

- Ir and Pt coatings prevented the transfer/migration of catalyst layer material onto the titanium-based PTL surface, which only took place when the protective layer was not stable enough (Au-coated) or not present (uncoated). Unprotected PTLs induce critical damage across the anodic catalyst layer, with a drastic deactivation observed when the uncoated PTLs were used. For the first time, we were able to identify and translate degradation effects occurring at the electrode that are caused by a secondary component present in the common cell configurations of water electrolyzers.

11. Bibliography

[1] M.G. Schultz, T. Diehl, G.P. Brasseur, and W. Zittel, *Air pollution and climate-forcing impacts of a global hydrogen economy.* Science, 2003. **302**(5645): p. 624-627.

[2] J.A. Turner, *Sustainable hydrogen production.* Science, 2004. **305**(5686): p. 972-974.

[3] C. Niether, S. Faure, A. Bordet, J. Deseure, M. Chatenet, J. Carrey, B. Chaudret, and A. Rouet, *Improved water electrolysis using magnetic heating of FeC–Ni core–shell nanoparticles.* Nature Energy, 2018. **3**(6): p. 476-483.

[4] A. Landman, H. Dotan, G.E. Shter, M. Wullenkord, A. Houaijia, A. Maljusch, G.S. Grader, and A. Rothschild, *Photoelectrochemical water splitting in separate oxygen and hydrogen cells.* Nature Materials, 2017. **16**: p. 646.

[5] J.N. Tiwari, S. Sultan, C.W. Myung, T. Yoon, N. Li, M. Ha, A.M. Harzandi, H.J. Park, D.Y. Kim, S.S. Chandrasekaran, W.G. Lee, V. Vij, H. Kang, T.J. Shin, H.S. Shin, G. Lee, Z. Lee, and K.S. Kim, *Multicomponent electrocatalyst with ultralow Pt loading and high hydrogen evolution activity.* Nature Energy, 2018. **3**(9): p. 773-782.

[6] M. Carmo, D.L. Fritz, J. Merge, and D. Stolten, *A comprehensive review on PEM water electrolysis.* International Journal of Hydrogen Energy, 2013. **38**(12): p. 4901-4934.

[7] L. Yu, Q. Zhu, S. Song, B. McElhenny, D. Wang, C. Wu, Z. Qin, J. Bao, Y. Yu, S. Chen, and Z. Ren, *Non-noble metal-nitride based electrocatalysts for high-performance alkaline seawater electrolysis.* Nature Communications, 2019. **10**(1): p. 5106.

[8] J.K. Mo, Z.Y. Kang, S.T. Retterer, D.A. Cullen, T.J. Toops, J.B. Green, M.M. Mench, and F.Y. Zhang, *Discovery of true electrochemical reactions for ultrahigh catalyst mass activity in water splitting.* Science Advances, 2016. **2**(11): p. 7.

[9] C. Rakousky, U. Reimer, K. Wippermann, S. Kuhri, M. Carmo, W. Lueke, and D. Stolten, *Polymer electrolyte membrane water electrolysis: Restraining degradation in the presence of fluctuating power.* Journal of Power Sources, 2017. **342**: p. 38-47.

[10] C. Rakousky, U. Reimer, K. Wippermann, M. Carmo, W. Lueke, and D. Stolten, *An analysis of degradation phenomena in polymer electrolyte membrane water electrolysis.* Journal of Power Sources, 2016. **326**: p. 120-128.

[11] C. Rakousky, G.P. Keeley, K. Wippermann, M. Carmo, and D. Stolten, *The stability challenge on the pathway to high-current-density polymer electrolyte membrane water electrolyzers.* Electrochimica Acta, 2018. **278**: p. 324-331.

[12] Z.Y. Kang, J.K. Mo, G.Q. Yang, Y.F. Li, D.A. Talley, S.T. Retterer, D.A. Cullen, T.J. Toops, M.P. Brady, G. Bender, B.S. Pivovar, J.B. Green, and F.Y. Zhang, *Thin film surface modifications of thin/tunable liquid/gas diffusion layers for high-efficiency proton exchange membrane electrolyzer cells.* Applied Energy, 2017. **206**: p. 983-990.

[13] H.Y. Jung, S.Y. Huang, and B.N. Popov, *High-durability titanium bipolar plate modified by electrochemical deposition of platinum for unitized regenerative fuel cell (URFC).* Journal of Power Sources, 2010. **195**(7): p. 1950-1956.

[14] K.E. Ayers, E.B. Anderson, C.B. Capuano, B.D. Carter, L.T. Dalton, G. Hanlon, J. Manco, and M. Niedzwiecki, *Research Advances Towards Low Cost, High Efficiency PEM Electrolysis*, in *Polymer Electrolyte Fuel Cells 10, Pts 1 and 2*, H.A. Gasteiger, et al., Editors. 2010, Electrochemical Soc Inc: Pennington. p. 3-15.

[15] K. Ayers, N. Danilovic, R. Ouimet, M. Carmo, B. Pivovar, and M. Bornstein, *Perspectives on Low-Temperature Electrolysis and Potential for Renewable Hydrogen at Scale*, in *Annual Review of Chemical and Biomolecular Engineering, Vol 10*, J.M. Prausnitz, Editor. 2019, Annual Reviews: Palo Alto. p. 219-239.

[16] C. Liu, M. Carmo, G. Bender, A. Everwand, T. Lickert, J.L. Young, T. Smolinka, D. Stolten, and W. Lehnert, *Performance enhancement of PEM electrolyzers through iridium-coated titanium porous transport layers.* Electrochemistry Communications, 2018. **97**: p. 96-99.

[17] P. Millet and S. Grigoriev, *Water electrolysis technologies.* Renewable Hydrogen Technologies: Production, Purification, Storage, Applications and Safety, 2013: p. 19-41.

[18] A. Buttler and H. Spliethoff, *Current status of water electrolysis for energy storage, grid balancing and sector coupling via power-to-gas and power-to-liquids: A review.* Renewable and Sustainable Energy Reviews, 2018. **82**: p. 2440-2454.

[19] Q. Feng, X.Z. Yuan, G.Y. Liu, B. Wei, Z. Zhang, H. Li, and H.J. Wang, *A review of proton exchange membrane water electrolysis on degradation mechanisms and mitigation strategies.* Journal of Power Sources, 2017. **366**: p. 33-55.

[20] I. Vincent and D. Bessarabov, *Low cost hydrogen production by anion exchange membrane electrolysis: A review.* Renewable and Sustainable Energy Reviews, 2018. **81**: p. 1690-1704.

[21] D. Li, E.J. Park, W. Zhu, Q. Shi, Y. Zhou, H. Tian, Y. Lin, A. Serov, B. Zulevi, and E.D. Baca, *Highly quaternized polystyrene ionomers for high performance anion exchange membrane water electrolysers.* Nature Energy, 2020: p. 1-8.

[22] J.R. Varcoe, P. Atanassov, D.R. Dekel, A.M. Herring, M.A. Hickner, P.A. Kohl, A.R. Kucernak, W.E. Mustain, K. Nijmeijer, and K. Scott, *Anion-exchange membranes in electrochemical energy systems.* Energy & environmental science, 2014. **7**(10): p. 3135-3191.

[23] A. Brisse, J. Schefold, and M. Zahid, *High temperature water electrolysis in solid oxide cells.* International journal of hydrogen energy, 2008. **33**(20): p. 5375-5382.

[24] W. Dönitz and E. Erdle, *High-temperature electrolysis of water vapor—status of development and perspectives for application.* International Journal of Hydrogen Energy, 1985. **10**(5): p. 291-295.

[25] Y. Wang, W. Li, L. Ma, W. Li, and X. Liu, *Degradation of solid oxide electrolysis cells: Phenomena, mechanisms, and emerging mitigation strategies—A review.* Journal of Materials Science & Technology, 2020. **55**: p. 35-55.

[26] M.P. Hoerlein, M. Riegraf, R. Costa, G. Schiller, and K.A. Friedrich, *A parameter study of solid oxide electrolysis cell degradation: Microstructural changes of the fuel electrode.* Electrochimica Acta, 2018. **276**: p. 162-175.

[27] M. Felgenhauer and T. Hamacher, *State-of-the-art of commercial electrolyzers and on-site hydrogen generation for logistic vehicles in South Carolina.* International Journal of Hydrogen Energy, 2015. **40**(5): p. 2084-2090.

[28] C. Liu, M. Shviro, A.S. Gago, S.F. Zaccarine, G. Bender, P. Gazdzicki, T. Morawietz, I. Biswas, M. Rasinski, and A. Everwand, *Exploring the Interface of Skin-Layered Titanium Fibers for Electrochemical Water Splitting.* Advanced Energy Materials, 2021. **11**(8): p. 2002926.

[29] S. Siracusano, V. Baglio, N. Van Dijk, L. Merlo, and A.S. Arico, *Enhanced performance and durability of low catalyst loading PEM water electrolyser based on a short-side chain perfluorosulfonic ionomer.* Applied Energy, 2017. **192**: p. 477-489.

[30] K.E. Ayers, J.N. Renner, N. Danilovic, J.X. Wang, Y. Zhang, R. Maric, and H. Yu, *Pathways to ultra-low platinum group metal catalyst loading in proton exchange membrane electrolyzers.* Catalysis Today, 2016. **262**: p. 121-132.

[31] J. Tymoczko, F. Calle-Vallejo, W. Schuhmann, and A.S. Bandarenka, *Making the hydrogen evolution reaction in polymer electrolyte membrane electrolysers even faster.* Nature communications, 2016. **7**(1): p. 1-6.

[32] S. Cherevko, S. Geiger, O. Kasian, N. Kulyk, J.P. Grote, A. Savan, B.R. Shrestha, S. Merzlikin, B. Breitbach, A. Ludwig, and K.J.J. Mayrhofer, *Oxygen and hydrogen evolution reactions on Ru, RuO2, Ir, and IrO2 thin film electrodes in acidic and alkaline electrolytes: A comparative study on activity and stability.* Catalysis Today, 2016. **262**: p. 170-180.

[33] P. Millet, R. Ngameni, S. Grigoriev, N. Mbemba, F. Brisset, A. Ranjbari, and C. Etiévant, *PEM water electrolyzers: From electrocatalysis to stack development.* International Journal of hydrogen energy, 2010. **35**(10): p. 5043-5052.

[34] Y. Murakami, S. Tsuchiya, K. Yahikozawa, and Y. Takasu, *Preparation of ultrafine IrO2□ Ta2O5 binary oxide particles by a sol-gel process.* Electrochimica acta, 1994. **39**(5): p. 651-654.

[35] A.J. Terezo, J. Bisquert, E.C. Pereira, and G. Garcia-Belmonte, *Separation of transport, charge storage and reaction processes of porous electrocatalytic IrO2 and IrO2/Nb2O5 electrodes.* Journal of Electroanalytical Chemistry, 2001. **508**(1-2): p. 59-69.

[36] A. Marshall, B. Børresen, G. Hagen, M. Tsypkin, and R. Tunold, *Electrochemical characterisation of IrxSn1− xO2 powders as oxygen evolution electrocatalysts.* Electrochimica Acta, 2006. **51**(15): p. 3161-3167.

[37] J. Polonsky, I.M. Petrushina, E. Christensen, K. Bouzek, C.B. Prag, J.E.T. Andersen, and N.J. Bjerrum, *Tantalum carbide as a novel support material for anode electrocatalysts in polymer electrolyte membrane water electrolysers.* International Journal of Hydrogen Energy, 2012. **37**(3): p. 2173-2181.

[38] C. Van Pham, M. Bühler, J. Knöppel, M. Bierling, D. Seeberger, D. Escalera-López, K.J. Mayrhofer, S. Cherevko, and S. Thiele, *IrO2 coated TiO2 core-shell microparticles advance performance of low loading proton exchange membrane water electrolyzers.* Applied Catalysis B: Environmental, 2020. **269**: p. 118762.

[39] G. Liu, J. Xu, Y. Wang, and X. Wang, *An oxygen evolution catalyst on an antimony doped tin oxide nanowire structured support for proton exchange membrane liquid water electrolysis.* Journal of Materials Chemistry A, 2015. **3**(41): p. 20791-20800.

[40] H.Y. Jung, S.Y. Huang, P. Ganesan, and B.N. Popov, *Performance of gold-coated titanium bipolar plates in unitized regenerative fuel cell operation.* Journal of Power Sources, 2009. **194**(2): p. 972-975.

[41] A.S. Gago, A.S. Ansar, P. Gazdzicki, N. Wagner, J. Arnold, and K.A. Friedrich, *Low Cost Bipolar Plates for Large Scale PEM Electrolyzers*, in *Polymer Electrolyte Fuel Cells 14*, H.A. Gasteiger, et al., Editors. 2014, Electrochemical Soc Inc: Pennington. p. 1039-1048.

[42] G.Q. Yang, S.L. Yu, J.K. Mo, Z.Y. Kang, Y. Dohrmann, F.A. List, J.B. Green, S.S. Babu, and F.Y. Zhang, *Bipolar plate development with additive manufacturing and protective coating for durable and high-efficiency hydrogen production.* Journal of Power Sources, 2018. **396**: p. 590-598.

[43] A.S. Gago, S.A. Ansar, B. Saruhan, U. Schulz, P. Lettenmeier, N.A. Canas, P. Gazdzicki, T. Morawietz, R. Hiesgen, J. Arnold, and K.A. Friedrich, *Protective coatings on stainless steel bipolar plates for proton exchange membrane (PEM) electrolysers.* Journal of Power Sources, 2016. **307**: p. 815-825.

[44] P. Lettenmeier, R. Wang, R. Abouatallah, B. Saruhan, O. Freitag, P. Gazdzicki, T. Morawietz, R. Hiesgen, A.S. Gago, and K.A. Friedrich, *Low-Cost and Durable Bipolar Plates for Proton Exchange Membrane Electrolyzers.* Scientific Reports, 2017. **7**: p. 12.

[45] P. Lettenmeier, R. Wang, R. Abouatallah, F. Burggraf, A.S. Gago, and K.A. Friedrich, *Coated Stainless Steel Bipolar Plates for Proton Exchange Membrane Electrolyzers.* Journal of the Electrochemical Society, 2016. **163**(11): p. F3119-F3124.

[46] G. Chisholm, P.J. Kitson, N.D. Kirkaldy, L.G. Bloor, and L. Cronin, *3D printed flow plates for the electrolysis of water: an economic and adaptable approach to device manufacture.* Energy & Environmental Science, 2014. **7**(9): p. 3026-3032.

[47] G. Scotti, P. Kanninen, V.-P. Matilainen, A. Salminen, and T. Kallio, *Stainless steel micro fuel cells with enclosed channels by laser additive manufacturing.* Energy, 2016. **106**: p. 475-481.

[48] G. Yang, J. Mo, Z. Kang, F.A. List III, J.B. Green Jr, S.S. Babu, and F.-Y. Zhang, *Additive manufactured bipolar plate for high-efficiency hydrogen production in proton exchange membrane electrolyzer cells.* international journal of hydrogen energy, 2017. **42**(21): p. 14734-14740.

[49] O. Panchenko, E. Borgardt, W. Zwaygardt, F.J. Hackemuller, M. Bram, N. Kardjilov, T. Arlt, I. Manke, M. Muller, D. Stolten, and W. Lehnert, *In-situ two-phase flow investigation of different porous transport layer for a polymer electrolyte membrane (PEM) electrolyzer with neutron spectroscopy.* Journal of Power Sources, 2018. **390**: p. 108-115.

[50] C.Y. Liu, L.H. Hu, and C.C. Sung, *Micro-protective layer for lifetime extension of solid polymer electrolyte water electrolysis.* Journal of Power Sources, 2012. **207**: p. 81-85.

[51] J.K. Mo, S.M. Steen, F.Y. Zhang, T.J. Toops, M.P. Brady, and J.B. Green, *Electrochemical investigation of stainless steel corrosion in a proton exchange membrane electrolyzer cell.* International Journal of Hydrogen Energy, 2015. **40**(36): p. 12506-12511.

[52] Z.Y. Kang, S.L. Yu, G.Q. Yang, Y.F. Li, G. Bender, B.S. Pivovar, J.B. Green, and F.Y. Zhang, *Performance improvement of proton exchange membrane electrolyzer cells by introducing in-plane transport enhancement layers.* Electrochimica Acta, 2019. **316**: p. 43-51.

[53] T. Schuler, R. De Bruycker, T.J. Schmidt, and F.N. Buchi, *Polymer Electrolyte Water Electrolysis: Correlating Porous Transport Layer Structural Properties and Performance: Part I. Tomographic Analysis of Morphology and Topology.* Journal of the Electrochemical Society, 2019. **166**(4): p. F270-F281.

[54] H. Ito, T. Maeda, A. Nakano, A. Kato, and T. Yoshida, *Influence of pore structural properties of current collectors on the performance of proton exchange membrane electrolyzer.* Electrochimica Acta, 2013. **100**: p. 242-248.

[55] T. Schuler, T.J. Schmidt, and F.N. Buchi, *Polymer Electrolyte Water Electrolysis: Correlating Performance and Porous Transport Layer Structure: Part II. Electrochemical Performance Analysis.* Journal of the Electrochemical Society, 2019. **166**(10): p. F555-F565.

[56] S. Siracusano, V. Baglio, A. Di Blasi, N. Briguglio, A. Stassi, R. Ornelas, E. Trifoni, V. Antonucci, and A. Arico, *Electrochemical characterization of single cell and short stack PEM electrolyzers based on a nanosized IrO2 anode electrocatalyst.* International journal of hydrogen energy, 2010. **35**(11): p. 5558-5568.

[57] E. Borgardt, L. Giesenberg, M. Reska, M. Müller, K. Wippermann, M. Langemann, W. Lehnert, and D. Stolten, *Impact of clamping pressure and stress relaxation on the performance of different polymer electrolyte membrane water electrolysis cell designs.* International Journal of Hydrogen Energy, 2019. **44**(42): p. 23556-23567.

[58] Z.Y. Kang, J.K. Mo, G.Q. Yang, S.T. Retterer, D.A. Cullen, T.J. Toops, J.B. Green, M.M. Mench, and F.Y. Zhang, *Investigation of thin/well-tunable liquid/gas diffusion layers exhibiting superior multifunctional performance in low-temperature electrolytic water splitting.* Energy & Environmental Science, 2017. **10**(1): p. 166-175.

[59] S.A. Grigoriev, P. Millet, S.A. Volobuev, and V.N. Fateev, *Optimization of porous current collectors for PEM water electrolysers.* International Journal of Hydrogen Energy, 2009. **34**(11): p. 4968-4973.

[60] F.J. Hackemüller, E. Borgardt, O. Panchenko, M. Müller, and M. Bram, *Manufacturing of Large-Scale Titanium-Based Porous Transport Layers for Polymer Electrolyte Membrane Electrolysis by Tape Casting.* Advanced Engineering Materials, 2019: p. 1801201.

[61] E. Borgardt, O. Panchenko, F.J. Hackemuller, J. Giffin, M. Bram, M. Muller, W. Lehnert, and D. Stolten, *Mechanical characterization and durability of sintered porous transport layers for polymer electrolyte membrane electrolysis.* Journal of Power Sources, 2018. **374**: p. 84-91.

[62] H. Ito, T. Maeda, A. Nakano, C.M. Hwang, M. Ishida, A. Kato, and T. Yoshida, *Experimental study on porous current collectors of PEM electrolyzers.* International Journal of Hydrogen Energy, 2012. **37**(9): p. 7418-7428.

[63] P. Lettenmeier, S. Kolb, N. Sata, A. Fallisch, L. Zielke, S. Thiele, A.S. Gago, and K.A. Friedrich, *Comprehensive investigation of novel pore-graded gas diffusion layers for high-performance and cost-effective proton exchange membrane electrolyzers.* Energy & Environmental Science, 2017. **10**(12): p. 2521-2533.

[64] X. Wang, W. Li, D. Xiong, D.Y. Petrovykh, and L. Liu, *Bifunctional nickel phosphide nanocatalysts supported on carbon fiber paper for highly efficient and stable overall water splitting.* Advanced Functional Materials, 2016. **26**(23): p. 4067-4077.

[65] https://www.sintef.no/globalassets/project/nexpel/pdf/hp-3d_pem-electrolysis_smo1.pdf.

[66] J. Mo, S. Steen, B. Han, Z. Kang, A. Terekhov, F.-Y. Zhang, S.T. Retterer, and D.A. Cullen. *Investigation of titanium felt transport parameters for energy storage and hydrogen/oxygen production*. in *13th international energy conversion engineering conference*. 2015.

[67] L.R. Ma, S. Sui, and Y.C. Zhai, *Investigations on high performance proton exchange membrane water electrolyzer.* International Journal of Hydrogen Energy, 2009. **34**(2): p. 678-684.

[68] Z.Y. Kang, G.Q. Yang, J.K. Mo, Y.F. Li, S.L. Yu, D.A. Cullen, S.T. Retterer, T.J. Toops, G. Bender, B.S. Pivovar, J.B. Green, and F.Y. Zhang, *Novel thin/tunable gas diffusion electrodes with ultra-low catalyst loading for hydrogen evolution reactions in proton exchange membrane electrolyzer cells.* Nano Energy, 2018. **47**: p. 434-441.

[69] Y. Li, Z. Kang, X. Deng, G. Yang, S. Yu, J. Mo, D.A. Talley, G.K. Jennings, and F.-Y. Zhang, *Wettability effects of thin titanium liquid/gas diffusion layers in proton exchange membrane electrolyzer cells.* Electrochimica Acta, 2019. **298**: p. 704-708.

[70] E. Leonard, A.D. Shum, N. Danilovic, C. Capuano, K.E. Ayers, L.M. Pant, A.Z. Weber, X. Xiao, D.Y. Parkinson, and I.V. Zenyuk, *Interfacial analysis of a PEM electrolyzer using X-ray computed tomography.* Sustainable Energy & Fuels, 2020.

[71] C. Spori, J.T.H. Kwan, A. Bonakdarpour, D.P. Wilkinson, and P. Strasser, *The Stability Challenges of Oxygen Evolving Catalysts: Towards a Common Fundamental Understanding and Mitigation of Catalyst Degradation.* Angewandte Chemie-International Edition, 2017. **56**(22): p. 5994-6021.

[72] J.W. Park, K. Jiao, and X. Li, *Numerical investigations on liquid water removal from the porous gas diffusion layer by reactant flow.* Applied Energy, 2010. **87**(7): p. 2180-2186.

[73] T.J. Mason, J. Millichamp, P.R. Shearing, and D.J. Brett, *A study of the effect of compression on the performance of polymer electrolyte fuel cells using electrochemical impedance spectroscopy and dimensional change analysis.* International journal of hydrogen energy, 2013. **38**(18): p. 7414-7422.

[74] D. Cha, J.H. Ahn, H.S. Kim, and Y. Kim, *Effects of clamping force on the water transport and performance of a PEM (proton electrolyte membrane) fuel cell with relative humidity and current density.* Energy, 2015. **93**: p. 1338-1344.

[75] O.F. Selamet and M.S. Ergoktas, *Effects of bolt torque and contact resistance on the performance of the polymer electrolyte membrane electrolyzers.* Journal of Power Sources, 2015. **281**: p. 103-113.

[76] F. Lapicque, M. Belhadj, C. Bonnet, J. Pauchet, and Y. Thomas, *A critical review on gas diffusion micro and macroporous layers degradations for improved membrane fuel cell durability.* Journal of Power Sources, 2016. **336**: p. 40-53.

[77] M. Langemann, D.L. Fritz, M. Muller, and D. Stolten, *Validation and characterization of suitable materials for bipolar plates in PEM water electrolysis.* International Journal of Hydrogen Energy, 2015. **40**(35): p. 11385-11391.

[78] D. Bessarabov, H. Wang, H. Li, and N. Zhao, *PEM electrolysis for hydrogen production: principles and applications*. 2016: CRC press.

[79] D.M. Brunette, P. Tengvall, M. Textor, and P. Thomsen, *Titanium in medicine: material science, surface science, engineering, biological responses and medical applications*. 2012: Springer Science & Business Media.

[80] R.G. Breckenridge and W.R. Hosler, *Electrical properties of titanium dioxide semiconductors.* Physical Review, 1953. **91**(4): p. 793.

[81] G. Lu, S.L. Bernasek, and J. Schwartz, *Oxidation of a polycrystalline titanium surface by oxygen and water.* Surface Science, 2000. **458**(1-3): p. 80-90.

[82] T. Bystron, M. Vesely, M. Paidar, G. Papakonstantinou, K. Sundmacher, B. Bensmann, R. Hanke-Rauschenbach, and K. Bouzek, *Enhancing PEM water electrolysis efficiency by reducing the extent of Ti gas diffusion layer passivation.* Journal of Applied Electrochemistry, 2018. **48**(6): p. 713-723.

[83] Z. Wang, H. Hu, C. Liu, and Y. Zheng, *The effect of fluoride ions on the corrosion behavior of pure titanium in 0.05 M sulfuric acid.* Electrochimica acta, 2014. **135**: p. 526-535.

[84] M. Nakagawa, S. Matsuya, T. Shiraishi, and M. Ohta, *Effect of fluoride concentration and pH on corrosion behavior of titanium for dental use.* Journal of dental research, 1999. **78**(9): p. 1568-1572.

[85] D.-S. Kong and Y.-Y. Feng, *Electrochemical anodic dissolution kinetics of titanium in fluoride-containing perchloric acid solutions at open-circuit potentials.* Journal of the electrochemical society, 2009. **156**(9): p. C283-C291.

[86] C. Briant, Z. Wang, and N. Chollocoop, *Hydrogen embrittlement of commercial purity titanium.* Corrosion Science, 2002. **44**(8): p. 1875-1888.

[87] F. Cardarelli, *Materials handbook*. 2018: Springer.

[88] C.M. Hwang, M. Ishida, H. Ito, T. Maeda, A. Nakano, A. Kato, and T. Yoshida, *Effect of titanium powder loading in gas diffusion layer of a polymer electrolyte unitized reversible fuel cell.* Journal of Power Sources, 2012. **202**: p. 108-113.

[89] P. Lettenmeier, S. Kolb, F. Burggraf, A.S. Gago, and K.A. Friedrich, *Towards developing a backing layer for proton exchange membrane electrolyzers.* Journal of Power Sources, 2016. **311**: p. 153-158.

[90] Z. Kang, G. Yang, J. Mo, S. Yu, D.A. Cullen, S.T. Retterer, T.J. Toops, M.P. Brady, G. Bender, and B.S. Pivovar, *Developing titanium micro/nano porous layers on planar thin/tunable LGDLs for high-efficiency hydrogen production.* International Journal of Hydrogen Energy, 2018. **43**(31): p. 14618-14628.

[91] T. Schuler, J.M. Ciccone, B. Krentscher, F. Marone, C. Peter, T.J. Schmidt, and F.N. Büchi, *Hierarchically Structured Porous Transport Layers for Polymer Electrolyte Water Electrolysis.* Advanced Energy Materials, 2020. **10**(2): p. 1903216.

[92] S. Choe, B.S. Lee, M.K. Cho, H.J. Kim, D. Henkensmeier, S.J. Yoo, J.Y. Kim, S.Y. Lee, H.S. Park, and J.H. Jang, *Electrodeposited IrO2/Ti electrodes as durable and cost-effective anodes in high-temperature polymer-membrane-electrolyte water electrolyzers.* Applied Catalysis B-Environmental, 2018. **226**: p. 289-294.

[93] S. Geiger, O. Kasian, B.R. Shrestha, A.M. Mingers, K.J.J. Mayrhofer, and S. Cherevko, *Activity and Stability of Electrochemically and Thermally Treated Iridium for the Oxygen Evolution Reaction.* Journal of the Electrochemical Society, 2016. **163**(11): p. F3132-F3138.

[94] S. Cherevko, S. Geiger, O. Kasian, A. Mingers, and K.J. Mayrhofer, *Oxygen evolution activity and stability of iridium in acidic media. Part 1.–Metallic iridium.* Journal of Electroanalytical Chemistry, 2016. **773**: p. 69-78.

[95] J. Emsley, *Nature's building blocks: an AZ guide to the elements*. 2011: Oxford University Press.

[96] E. Price, *Durability and Degradation Issues in PEM Electrolysis Cells and its Components.* Johnson Matthey Technology Review, 2017. **61**(1): p. 47-51.

[97] K. Mumtaz, J. Echigoya, T. Hirai, and Y. Shindo, *Iridium coatings on carbon-carbon composites produced by two different sputtering methods: a comparative study.* Journal of materials science letters, 1993. **12**(18): p. 1411-1412.

[98] N. Baklanova, N. Morozova, V. Kriventsov, and A. Titov, *Synthesis and microstructure of iridium coatings on carbon fibers.* Carbon, 2013. **56**: p. 243-254.

[99] J. Hagen, F. Burmeister, A. Fromm, P. Manns, and G. Kleer, *Iridium Coatings with Titanium Sub-Layer Deposited by RF Magnetron Sputtering: Mechanical Properties and Contact Behavior with RoHS-Compliant Glass Melt.* Plasma Processes and Polymers, 2009. **6**(S1): p. S678-S683.

[100] I. Igumenov, N. Gelfond, P. Galkin, N. Morozova, N. Fedotova, G. Zharkova, V. Shipachev, E. Reznikova, A. Ryabtsev, and N. Kotsupalo, *Corrosion testing of platinum metals CVD coated titanium anodes in seawater-simulated solutions.* Desalination, 2001. **136**(1-3): p. 273-280.

[101] H.K. Atiyeh, K. Karan, B. Peppley, A. Phoenix, E. Halliop, and J. Pharoah, *Experimental investigation of the role of a microporous layer on the water transport and performance of a PEM fuel cell.* Journal of Power Sources, 2007. **170**(1): p. 111-121.

[102] P. Deevanhxay, T. Sasabe, S. Tsushima, and S. Hirai, *Effect of liquid water distribution in gas diffusion media with and without microporous layer on PEM fuel cell performance.* Electrochemistry Communications, 2013. **34**: p. 239-241.

[103] C.-J. Tseng and S.-K. Lo, *Effects of microstructure characteristics of gas diffusion layer and microporous layer on the performance of PEMFC.* Energy Conversion and Management, 2010. **51**(4): p. 677-684.

[104] C. Chan, N. Zamel, X. Li, and J. Shen, *Experimental measurement of effective diffusion coefficient of gas diffusion layer/microporous layer in PEM fuel cells.* Electrochimica Acta, 2012. **65**: p. 13-21.

[105] J. Polonský, R. Kodým, P. Vágner, M. Paidar, B. Bensmann, and K. Bouzek, *Anodic microporous layer for polymer electrolyte membrane water electrolysers.* Journal of Applied Electrochemistry, 2017. **47**(10): p. 1137-1146.

[106] C.C. Sung and C.Y. Liu, *A novel micro protective layer applied on a simplified PEM water electrolyser.* International Journal of Hydrogen Energy, 2013. **38**(24): p. 10063-10067.

[107] T.J. Toops, M.P. Brady, F.Y. Zhang, H.M. Meyer, K. Ayers, A. Roemer, and L. Dalton, *Evaluation of nitrided titanium separator plates for proton exchange membrane electrolyzer cells.* Journal of Power Sources, 2014. **272**: p. 954-960.

[108] C. Liu, K. Wippermann, M. Rasinski, Y. Suo, M. Shviro, M. Carmo, and W. Lehnert, *Constructing a Multifunctional Interface between Membrane and Porous Transport Layer for Water Electrolyzers.* ACS Applied Materials & Interfaces, 2021. **13**(14): p. 16182-16196.

[109] M. Andisheh-Tadbir, F.P. Orfino, and E. Kjeang, *Three-dimensional phase segregation of micro-porous layers for fuel cells by nano-scale X-ray computed tomography.* Journal of Power Sources, 2016. **310**: p. 61-69.

[110] E. Leonard, A.D. Shum, N. Danilovic, C. Capuano, K.E. Ayers, L.M. Pant, A.Z. Weber, X. Xiao, D.Y. Parkinson, and I.V. Zenyuk, *Interfacial analysis of a PEM electrolyzer using X-ray computed tomography.* Sustainable Energy & Fuels, 2020. **4**(2): p. 921-931.

[111] S. Liu, M. Rasinski, Y. Rahim, S. Zhang, K. Wippermann, U. Reimer, and W. Lehnert, *Influence of operating conditions on the degradation mechanism in high-temperature polymer electrolyte fuel cells.* Journal of Power Sources, 2019. **439**: p. 227090.

[112] M. Bühler, F. Hegge, P. Holzapfel, M. Bierling, M. Suermann, S. Vierrath, and S. Thiele, *Optimization of anodic porous transport electrodes for proton exchange membrane water electrolyzers.* Journal of Materials Chemistry A, 2019. **7**(47): p. 26984-26995.

[113] H. Ostadi, P. Rama, Y. Liu, R. Chen, X. Zhang, and K. Jiang, *3D reconstruction of a gas diffusion layer and a microporous layer.* Journal of Membrane Science, 2010. **351**(1-2): p. 69-74.

[114] M. Kruth, D. Meertens, and K. Tillmann, *FEI Helios NanoLab 460F1 FIB-SEM.* Journal of large-scale research facilities JLSRF, 2016. **2**: p. 59.

[115] A. Kovács, R. Schierholz, and K. Tillmann, *FEI Titan G2 80-200 CREWLEY.* Journal of large-scale research facilities JLSRF, 2016. **2**: p. 43.

[116] Y. Li, J. Yang, Z. Pan, and W. Tong, *Nanoscale pore structure and mechanical property analysis of coal: An insight combining AFM and SEM images.* Fuel, 2020. **260**: p. 116352.

[117] R. Solmaz and G. Kardaş, *Electrochemical deposition and characterization of NiFe coatings as electrocatalytic materials for alkaline water electrolysis.* Electrochimica Acta, 2009. **54**(14): p. 3726-3734.

[118] A. Gulin, A. Shakhov, A. Vasin, A. Astafiev, O. Antonova, S. Kochev, Y. Kabachii, A. Golub, and V. Nadtochenko, *ToF-SIMS depth profiling of nanoparticles: Chemical structure of core-shell quantum dots.* Applied Surface Science, 2019. **481**: p. 144-150.

[119] A. Arvay, E. Yli-Rantala, C.H. Liu, X.H. Peng, P. Koski, L. Cindrella, P. Kauranen, P.M. Wilde, and A.M. Kannan, *Characterization techniques for gas diffusion layers for proton exchange membrane fuel cells - A review.* Journal of Power Sources, 2012. **213**: p. 317-337.

[120] M.S. Ismail, T. Damjanovic, D.B. Ingham, L. Ma, and M. Pourkashanian, *Effect of polytetrafluoroethylene-treatment and microporous layer-coating on the in-plane permeability of gas diffusion layers used in proton exchange membrane fuel cells.* Journal of Power Sources, 2010. **195**(19): p. 6619-6628.

[121] G. Bender, M. Carmo, T. Smolinka, A. Gago, N. Danilovic, M. Mueller, F. Ganci, A. Fallisch, P. Lettenmeier, K.A. Friedrich, K. Ayers, B. Pivovar, J. Mergel, and D. Stolten, *Initial approaches in benchmarking and round robin testing for proton exchange membrane water electrolyzers.* International Journal of Hydrogen Energy, 2019. **44**(18): p. 9174-9187.

[122] G. Brug, A. Van Den Eeden, M. Sluyters-Rehbach, and J. Sluyters, *The analysis of electrode impedances complicated by the presence of a constant phase element.* Journal of Electroanalytical Chemistry, 1984. **176**(1-2): p. 275-295.

[123] B. Hirschorn, M.E. Orazem, B. Tribollet, V. Vivier, I. Frateur, and M. Musiani, *Determination of effective capacitance and film thickness from constant-phase-element parameters.* Electrochimica acta, 2010. **55**(21): p. 6218-6227.

[124] B.E. Conway and T. Liu, *Characterization of electrocatalysis in the oxygen evolution reaction at platinum by evaluation of behavior of surface intermediate states at the oxide film.* Langmuir, 1990. **6**(1): p. 268-276.

[125] C. Liu, K. Wippermann, M. Rasinski, Y. Suo, M. Shviro, M. Carmo, and W. Lehnert, *Constructing a Multifunctional Interface between a Membrane and a Porous Transport Layer for Water Electrolyzers.* Acs Applied Materials & Interfaces, 2021.

[126] C. Liu, M. Shviro, A.S. Gago, S.F. Zaccarine, G. Bender, P. Gazdzicki, T. Morawietz, I. Biswas, M. Rasinski, and A. Everwand, *Exploring the Interface of Skin-Layered Titanium Fibers for Electrochemical Water Splitting.* Advanced Energy Materials, 2021: p. 2002926.

[127] L.D. Burke and P.F. Nugent, *The Electrochemistry of Gold: I The Redox Behaviour of the Metal in Aqueous Media.* Gold Bulletin, 1997. **30**(2): p. 43-53.

[128] https://en.wikipedia.org/wiki/List_of_thermal_conductivities.

[129] P. Lettenmeier, J. Majchel, L. Wang, V.A. Saveleva, S. Zafeiratos, E.R. Savinova, J.J. Gallet, F. Bournel, A.S. Gago, and K.A. Friedrich, *Highly active nano-sized iridium catalysts: synthesis and operando spectroscopy in a proton exchange membrane electrolyzer.* Chemical Science, 2018. **9**(14): p. 3570-3579.

[130] V.A. Saveleva, L. Wang, D. Teschner, T. Jones, A.S. Gago, K.A. Friedrich, S. Zafeiratos, R. Schlogl, and E.R. Savinova, *Operando Evidence for a Universal Oxygen Evolution Mechanism on Thermal and Electrochemical Iridium Oxides.* Journal of Physical Chemistry Letters, 2018. **9**(11): p. 3154-3160.

[131] L.P. Buchwalter, *Adhesion of polyimides to metals and metal oxides.* Journal of Adhesion Science and Technology, 1987. **1**(1): p. 341-347.

[132] M. Ulsh, A. DeBari, J.M. Berliner, I.V. Zenyuk, P. Rupnowski, L. Matvichuk, A.Z. Weber, and G. Bender, *The development of a through-plane reactive excitation technique for detection of pinholes in membrane-containing MEA sub-assemblies.* International Journal of Hydrogen Energy, 2019. **44**(16): p. 8533-8547.

[133] S. Kundu, M.W. Fowler, L.C. Simon, and S. Grot, *Morphological features (defects) in fuel cell membrane electrode assemblies.* Journal of Power Sources, 2006. **157**(2): p. 650-656.

[134] K. Panha, M. Fowler, X.Z. Yuan, and H.J. Wang, *Accelerated durability testing via reactants relative humidity cycling on PEM fuel cells.* Applied Energy, 2012. **93**: p. 90-97.

[135] N. Danilovic, K. Ayers, C. Capuano, J. Renner, L. Wiles, and M. Pertoso, *Challenges In Going from Laboratory to Megawatt Scale PEM Electrolysis*, in *Polymer Electrolyte Fuel Cells 16*, D.J. Jones, et al., Editors. 2016, Electrochemical Soc Inc: Pennington. p. 395-402.

12. Appendix

12.1 Image of flow fields

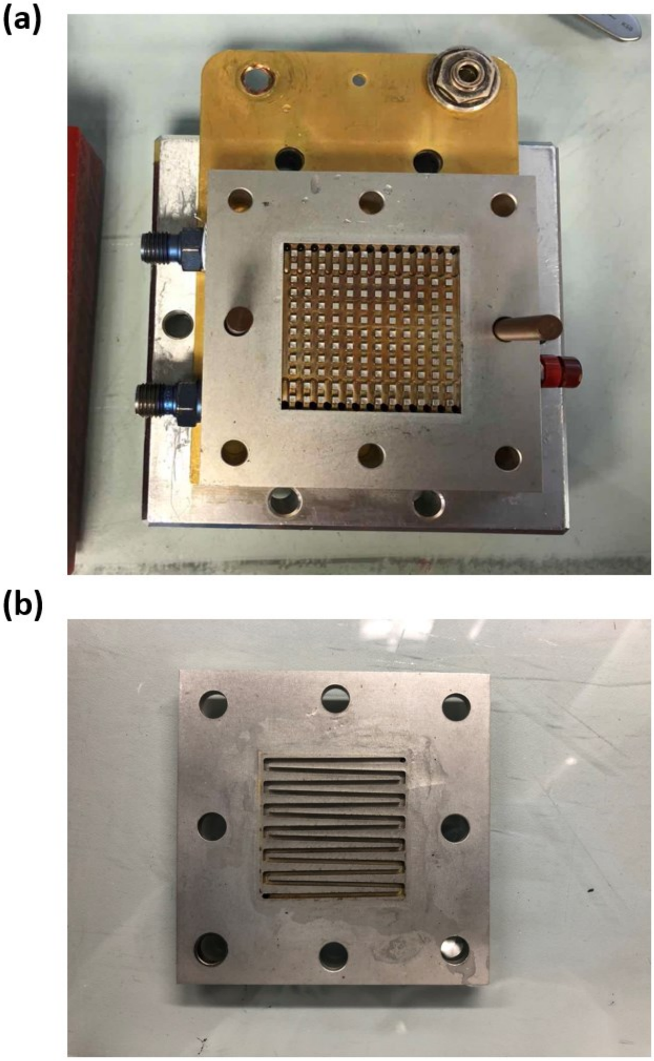

Figure 12.1 ***(a)*** *Image of pin-type flow field used in chapter 4 and 5 (active area: 25 cm^2);* ***(b)*** *Image of single serpentine type flow field used in chapter 6, 7 and 8 (active area: 17.64 cm^2).*

12.2 Pin-hole test of catalyst coated membrane (CCM)

Figure 12 shows the schematic diagram of pinhole detection device adapted from Ulsch et al. [132]. A nitrogen gas was flowed past the CCM, which was mounted in a sample holder. The anode was in contact with the nitrogen gas flow and the cathode was in contact with ambient air. The nitrogen was replaced for a short period with a hydrogen pulse. The hydrogen that permeates or diffuses to the cathode will be in contact with oxygen and react with Pt catalyst. The resulting heat signature was recorded with an infrared thermal detector. An apparent local heat signature with a temperature rise of more than 1°C indicates the loss of membrane integrity at this location.

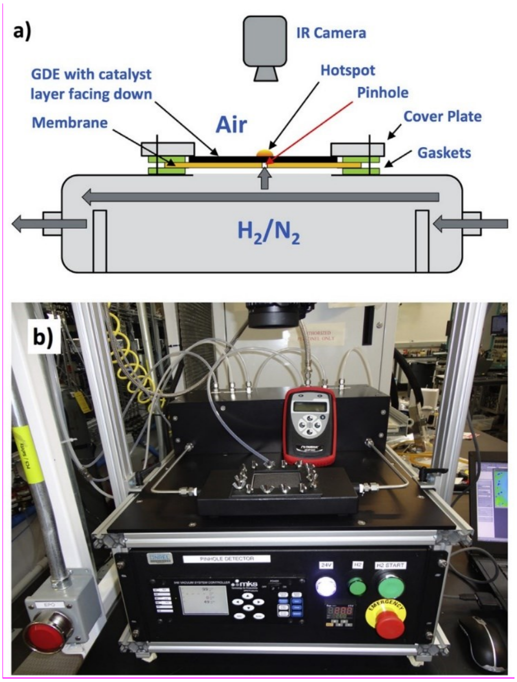

Figure 12.2 ***(a)*** *Schematic diagram of the pinhole detection apparatus depicting flow configuration through the sample hardware and mounting of the sample;* ***(b)*** *image of the pinhole detection apparatus [132].*

The high local interface resistance spots identified on our Au-coated and uncoated PTLs raised the question as to whether pinhole formation could be found on the membranes following the long-term experiment. Pinhole formation over PFSA (perfluorosulfonic acid) membranes such as

Nafion® has been extensively reported in PEM fuel cells [133, 134]. However, this topic has not been well explored in relation to PEM water electrolyzers [132]. The reason for this lies in the fact that well-hydrated conditions and cell voltages that are always above 1.23 V, which ensure the stable conditions for these membranes. The durability profiles longer than 50,000 hours have already been reported for the electrochemical systems [135]. The high local interface resistance spots identified on Au-coated and uncoated PTLs raise the question as to whether pinhole formation could be found on the CCMs that we used after the long-term operation. Subsequent to the durability tests the CCMs were interrogated for failure point development using an ex-situ infrared (IR) thermography technique. The thermal response of hydrogen gas flowing from underneath the CCM was used to identify the pinhole formation within PFSA membranes. The design and operation of pinhole detection apparatus was presented in Chapter 3 and a literature [132].

Figure 12.3 shows that no pinhole was detected for all the CCMs that after 4000 hours of operation. This does not exclude further degradation and pinhole formation on the Nafion® 117 membranes used in this study, but it does show that one should not expect pinholes before 4000 hours under the operating conditions and cell configuration employed in this study.

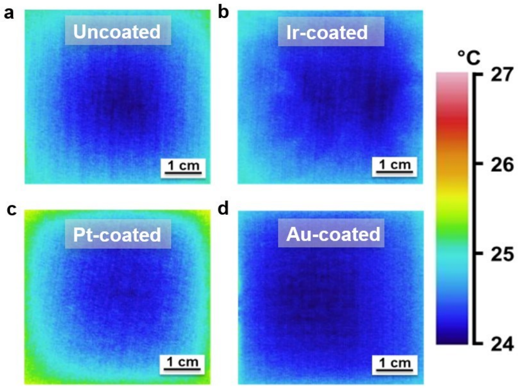

Figure 12.3 *Thermal response for the* ***(a)*** *uncoated PTL;* ***(b)*** *Ir-coated PTL;* ***(c)*** *Pt-coated PTL;* ***(d)*** *Au-coated PTL [28].*

12.3 XPS depth profiles

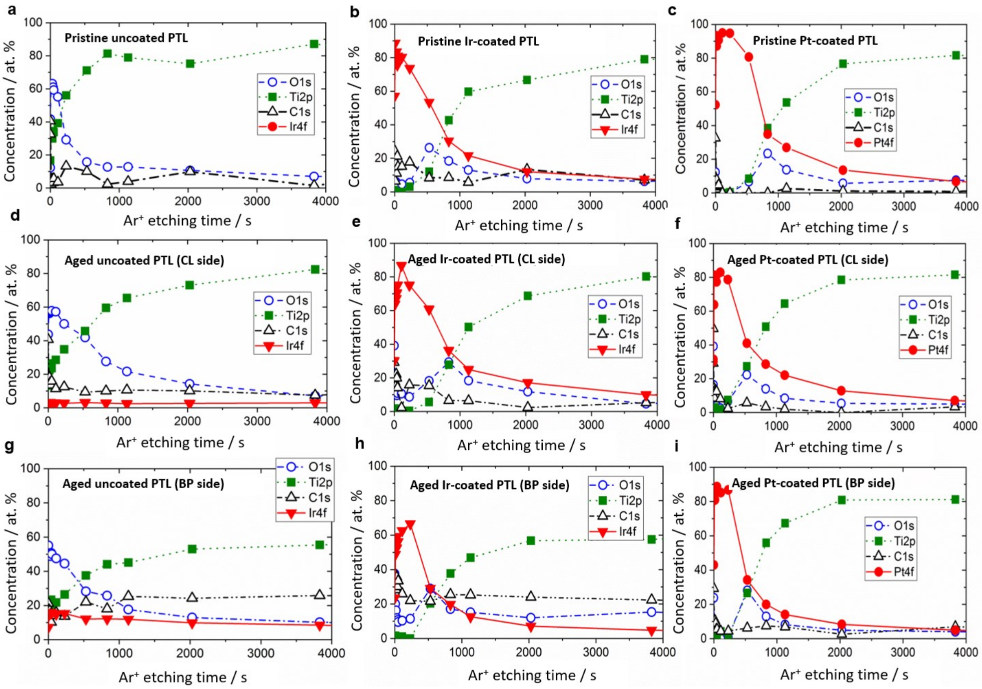

Figure 12.4 *XPS depth profiles of pristine and aged (faces CL side, bipolar plate side) PTLs showing the concentration of analyzed elements versus the ion etching time.* ***(a, b, c)*** *depth profiles of pristine uncoated PTL, Ir-coated PTL, Pt-coated PTL;* ***(d, e, f)*** *depth profiles of aged uncoated PTL, Ir-coated PTL, Pt-coated PTL that faces CL side;* ***(g ,h, i)*** *depth profiles of aged uncoated PTL, Ir-coated PTL, Pt-coated PTL that faces BP side [28].*

List of Abbreviations

AEM	anion exchange membrane
AFM	Atomic Force Microscope
CCM	catalyst coated membrane
CL	catalyst layer
CT	computed tomography
EDX	Energy Dispersive X-ray Spectroscopy
EIS	Electrochemical impedance spectroscopy
FIB-SEM	Focused ion beam - Scanning Electron Microscopy
GDL	gas diffusion layer
HER	hydrogen evolution reaction
HMVS	high-speed and micro-scale visualization system
ICR	Interfacial contact resistance
MEA	membrane electrode assembly
MPL	Micro porous layer
OER	oxygen evolution reaction
PEM	Polymer electrolyte membrane
PGM	platinum group metal
PTL	porous transport layer
PVD	physical vapor deposition
RHE	reversible hydrogen electrode
SEM	scanning electron microscopy

SHE	standard hydrogen electrode
SOEC	solid oxide electrolysis
SPE	solid polymer membrane
ToF-SIMS	Time-of-Flight secondary-ion mass spectrometry
XPS	X-ray photoelectron spectroscopy
XTM	X-ray tomographic microscopy

List of Figures

List of Tables

Acknowledgements

First and foremost, I would like to express my deepest appreciation to my Doktorvator, my supervisor Prof. Werner Lehnert for offering such a good chance to finish my PhD thesis in IEK-14 at Forschungszentrum Jülich and RWTH Aachen University in Germany. This PhD thesis was fully under his supervision and guidance. I am very grateful for all his guidance, support, and patience throughout my entire doctoral study here.

I would like to acknowledge the supervisor Dr. Marcelo Carmo for offering me the opportunity to study in his group, to benefit from such as his experimental guidance, expertise, and fruitful discussion.

I also want to express my sincere and special gratitude to Dr. Klaus Wippermann for offering significant professional guidance and discussion on electrochemical analysis and discussion. I greatly appreciate his patience and his passion for science, giving me a huge motivation to continue my scientific research in the future. Thank you very much Klaus!

Meanwhile, I would like to appreciate my best friend Yanpeng Suo, and other colleagues in IEK-14: Daniel Holtz, Stefanie Fisher, Lu Xia, Wulv Jiang, Denise Beate Günther, Andreas Everwand, Dr. Shidong Zhang, Elena Borgardt, Eugen Hoppe, Florian Berg, and Katja Klafik for their support and help during my PhD study here.

A special thanks to my working partners in other places, Dr. Guido Bender and Dr. Zhenye (Allen) Kang in National Renewable Energy Laboratory (NREL), Dr. Aldo S. Gago, Dr. Pawel Gazdzicki, Dr. Indro Biswas and Dr. Tobias Morawietz in Deutsches Zentrum für Luft und Raumfahrt (DLR), Sarah F. Zaccarine and Prof. Svitlana Pylypenko in Colorado School of Mines, Dr. Marcin Rasinski in IEK-4 (FZJ), Dr. Heinrich Hartmann in ZEA-3 (FZJ). A big thank you for their cooperation and great support for my experiments and publications. Additionally, I am very grateful to the China Scholarship Council (CSC) for the financial support for my PhD study in Germany.

I also express my gratitude to my husband Dr. Yu Lin, who supported and took care of my daily life for my entire PhD study. Thanks for his encouragement, patience, love and most importantly, accompanying me all the time. Also, I would like to express my heartfelt appreciation to my parents, especially my mom, for their support and love.

Last but not the least, I want to say thanks a lot to myself. We are experiencing a global Corona pandemic, which makes everything much slower, difficult and challenging than ever. Thanks for my strong perseverance and faith during the PhD studies, especially during this special and challenging period. Though there are so many things to struggle with in life, I overcame them and would never give up.

Band / Volume 549
Gravity waves resolved in Numerical Weather Prediction products
C. Strube (2021), iii, 139 pp
ISBN: 978-3-95806-567-3

Band / Volume 550
Experimental study of the chemical degradation of biogenic volatile organic compounds by atmospheric OH radicals
M. Rolletter (2021), XIII, 199 pp
ISBN: 978-3-95806-568-0

Band / Volume 551
Infiltrated Positive Electrodes for All-Solid-State Sodium Batteries
T. Lan (2021), vi, 104 pp
ISBN: 978-3-95806-576-5

Band / Volume 552
Trajectory Analysis on the Asian Tropopause Aerosol Layer (ATAL) based on Balloon Measurements at the Foothills of the Himalayas
S. Hanumanthu (2021), xiv, 147 pp
ISBN: 978-3-95806-578-9

Band / Volume 553
Field assisted sintering of yttria ceramics for plasma etching applications
M. Kindelmann (2021), VI, 122, XXX pp
ISBN: 978-3-95806-579-6

Band / Volume 554
Characterisation of the effect of redox potential on the emission of greenhouse gases using wireless sensing techniques
J. Wang (2021), XIV, 104 pp
ISBN: 978-3-95806-581-9

Band / Volume 555
Stability assessment of variably saturated hillslopes using coupled hydromechanical models
S. Moradi (2021), xxxii, 123 pp
ISBN: 978-3-95806-583-3

Band / Volume 556
Catalytic-doping of Silicon Alloys for the Use in Silicon Heterojunction Solar Cells
Y. Liu (2021), 126 pp
ISBN: 978-3-95806-591-8

Schriften des Forschungszentrums Jülich
Reihe Energie & Umwelt / Energy & Environment

Band / Volume 557
Formation of highly oxygenated organic molecules from α-pinene photochemistry
S. Kang (2021), xvii, 156 pp
ISBN: 978-3-95806-596-3

Band / Volume 558
Synthese von Cr_2AlC MAX-Phasen Kompositen und Bestimmung ihrer oxidativen Eigenschaften
T. Go (2021), ii, 119 pp
ISBN: 978-3-95806-598-7

Band / Volume 559
Distribution of Relaxation Times for Analysis of Solid Oxide Fuel Cell Stacks
K. Fitzek (2021), 237 pp
ISBN: 978-3-95806-599-4

Band / Volume 560
Machine Learning in Modeling of the Dynamics of Polymer Electrolyte Fuel Cells
W. Zou (2021), vii, 139 pp
ISBN: 978-3-95806-601-4

Band / Volume 561
Introduction Strategies for Hydrogen Infrastructure
S. Cerniauskas (2021), viii, 179 pp
ISBN: 978-3-95806-602-1

Band / Volume 562
Noble Metal Coated Porous Transport Layers for Polymer Electrolyte Membrane Water Electrolysis
C. Liu (2021), 139 pp
ISBN: 978-3-95806-603-8

Weitere ***Schriften des Verlags im Forschungszentrum Jülich*** unter
http://wwwzb1.fz-juelich.de/verlagextern1/index.asp

Energie & Umwelt / Energy & Environment
Band / Volume 562
ISBN 978-3-95806-603-8

Mitglied der Helmholtz-Gemeinschaft

JÜLICH
Forschungszentrum